2004

OPTIMIZATION OF BLOWING AND SUCTION CONTROL ON NACA0012 AIRFOIL USING GENETIC ALGORITHM WITH DIVERSITY CONTROL

Liang Huang
University of Kentucky, hlihng@engr.uky.edu

ABSTRACT OF DISSERTATION

Liang Huang

The Graduate School

University of Kentucky

2004

OPTIMIZATION OF BLOWING AND SUCTION CONTROL ON NACA0012 AIRFOIL USING GENETIC ALGORITHM WITH DIVERSITY CONTROL

ABSTRACT OF DISSERTATION

A dissertation submitted in partial fulfillment of the
requirements for the degree of Doctor of Philosophy in the
College of Engineering
at the University of Kentucky

By

Liang Huang

Lexington, Kentucky

Co-Director: Dr. Raymond P. Lebeau, Assistant Professor of Mechanical Engineering
Dr. George P. Huang, Professor of Mechanical Engineering
and Dr. Thomas Hauser, Assistant Professor of Aerospace & Mechanical Engineering, Utah State University

Lexington, Kentucky

2004

ABSTRACT OF DISSERTATION

OPTIMIZATION OF BLOWING AND SUCTION CONTROL ON NACA0012 AIRFOIL USING GENETIC ALGORITHM WITH DIVERSITY CONTROL

Active control of the flow over an airfoil is an area of heightened interest in the aerospace community. Previous research on flow control design processes heavily depended on trial and error and the designers' knowledge and intuition. Such an approach cannot always meet the growing demands of higher design quality in less time. Successful application of computational fluid dynamics (CFD) to this kind of control problem critically depends on an efficient searching algorithm for design optimization.

CFD in conjunction with Genetic Algorithms (GA) potentially offers an efficient and robust optimization method and is a promising solution for current flow control designs. But the traditional binary GA and its operators need to be transformed or re-defined to meet the requirements of real world engineering problems.

Current research has combined different existing GA techniques and proposed a real-coded "Explicit Adaptive Range Normal Distribution" (EARND) genetic algorithm with diversity control to solve the convergence problems. First, a traditional binary-coded GA is replaced by a real-coded algorithm in which the corresponding design variables are encoded into a vector of real numbers that is conceptually closest to the real design space. Second, to address the convergence speed problem, an additional normal distribution scheme is added into the basic GA in order to monitor the global optimization process;

meanwhile, design parameters' boundaries are explicitly updated to eliminate unnecessary evaluations (computation) in un-promising areas to balance the workload between the global and local searching process. Third, during the initial 20% evolution (search process), the diversity of the individuals within each generation are controlled by a formula in order to conquer the problem of preliminary convergence to the local optimum.

In order to better understand the two-jet control optimization results and process, at first, a single jet with a width of 2.5% the chord length is placed on a NACA 0012 airfoil's upper surface simulating the blowing and suction control under Re=500,000 and angle of attack 18 degree. Nearly 300 numerical simulations are conducted over a range of parameters (jet location, amplitude and angle). The physical mechanisms that govern suction and blowing flow control are determined and analyzed, and the critical values of suction and blowing locations, amplitudes, and angles are discussed. Moreover, based on the results of single suction/blowing jet control on a NACA 0012 airfoil, the design parameters of a two-jet system are proposed. Our proposed algorithm is built on top of the CFD code, guiding the movement of two jets along the airfoil's upper surface. The reasonable optimum control values are determined within the control parameter range. The current study of Genetic Algorithms on airfoil flow control has been demonstrated to be a successful optimization application.

KEYWORDS: Flow Control, Genetic Algorithm, Non-forcing Jets, Blowing / Suction

Liang Huang

04/28/2004

OPTIMIZATION OF BLOWING AND SUCTION CONTROL ON NACA0012 AIRFOIL USING GENETIC ALGORITHM WITH DIVERSITY CONTROL

By

Liang Huang

George Huang

Co-Director of Dissertation

Raymond P. LeBeau

Co-Director of Dissertation

Thomas Hauser

Co-Director of Dissertation

George Huang

Director of Graduate Studies

04/28/2004

RULES FOR THE USE OF DISSERTATIONS

Unpublished dissertations submitted for the Doctor's degree and deposited in the University of Kentucky Library are as a rule open for inspection, but are to be used only with due regard to the rights of the authors. Bibliographical references may be noted, but quotations or summaries of parts may be published only with the permission of the author, and with the usual scholarly acknowledgments.

Extensive copying or publication of the dissertation in whole or in part also requires the consent of the Dean of the Graduate School of the University of Kentucky.

DISSERTATION

Liang Huang

The Graduate School

University of Kentucky

2004

OPTIMIZATION OF BLOWING AND SUCTION CONTROL ON NACA0012 AIRFOIL USING GENETIC ALGORITHM WITH DIVERSITY CONTROL

DISSERTATION

A dissertation submitted in partial fulfillment of the
requirements for the degree of Doctor of Philosophy in the
College of Engineering
at the University of Kentucky

By

Liang Huang

Lexington, Kentucky

Co-Director: Dr. Raymond P. Lebeau, Assistant Professor of Mechanical Engineering
Dr. George P. Huang, Professor of Mechanical Engineering
and Dr. Thomas Hauser, Assistant Professor of Aerospace & Mechanical Engineering, Utah State University

Lexington, Kentucky

2004

TO MY PARENTS AND MY WIFE, XINLI

ACKNOWLEDGEMENTS

Throughout the endeavor that resulted in the thesis, I am indebted to so many people for their assistance, ideas and support. I would like to express my sincere gratitude to my family, committee members, friends and those who inspired my curiosity and helped me to acquire a doctoral degree during the entire process of this study.

Special thanks should go to Dr. George P. Huang, Dr. Raymond P. Lebeau and Dr. Thomas Hauser, three co-directors of my thesis, for their continuous support and encouragement, insightful advice, and constructive comments on this dissertation. At the same time, I'd like to extend my sincere thanks to Dr. Hank Dietz, Dr. J. D. Jacob and Dr. Dayong Gao for their continuous service on the advisory committee.

I would like to acknowledge the financial supports from Department of Mechanical Engineering at University of Kentucky, Kentucky NASA EPSCoR and Kentucky Science and Engineering Foundation.

Last, but not the least, I must thank my beautiful wife, Dr. Xinli Liu, for her patience, support, and understanding.

TABLE OF CONTENTS

Acknowledgements iii

List of Tables vii

List of Figures viii

List of Files xii

Chapter 1 Introduction 1

1.1 Overview 1

1.2 Background 1

1.2.1 Flow Control 2

1.2.2 Flow Control Study through CFD 3

1.2.3 Optimization Algorithms 5

1.3 Motivations and Objectives 7

1.4 Organization of the Dissertation 9

Chapter 2 Literature Survey 10

2.1 Survey of Flow Control Theory and Experiments 10

2.2 Survey of Flow Control Study Using CFD 13

2.3 Survey of Genetic Algorithm on Optimization 15

Chapter 3 Genetic Algorithm 19

3.1 Definition, Terminology and Genetic Coefficients 20

3.1.1 Definition 20

3.1.2 Terminology 20

3.1.3 Major Genetic Coefficients 20

3.2 Basic Algorithm and Minor Improvements 21

3.2.1 Binary String Representation Limitation 21
3.2.2 Roulette Wheel Selection Operator and Its Improvement 24
3.2.3 Crossover Operator 27
3.2.4 Mutation Operator 28
3.3 Improved Algorithm 29
3.3.1 Normal distribution 29
3.3.2 Explicit updated boundary 30
3.3.3 Diversity control 31
3.4 Algorithm Performance Test and Case Study 32
Chapter 4 Single Suction/Blowing Jet Study 40
4.1 Case Setup 40
4.1.1 Numerical Scheme 40
4.1.2 Grid Setup 42
4.1.3 Parameter Selection 50
4.2 Computation Results and Analysis 52
4.2.1 Suction Jet Study 52
4.2.2 Blowing Jet Study 56
4.2.3 Conclusions of Single Suction/Blowing Jet Study 65
Chapter 5 Two Jet System Optimization (I) 67
5.1 One Suction Jet and One Blowing Jet Case Setup 67
5.1.1 Control Parameters Selection 67
5.1.2 Genetic Algorithm Coefficients and Programming Model 69
5.2 Optimization Process of One Suction Jet and One Blowing Jet System 70

5.2.1 Understanding of the optimization process 70
5.2.2 Improved algorithm with/without diversity control comparison 74
5.3 Flow Control Physics 79
5.3.1 Suction Control 79
5.3.2 Blowing Control 85
5.3.3 Two Jet Control 87
Chapter 6 Two Jet System Optimization (II) 91
6.1 Two Suction Jet Case Setup 91
6.1.1 Control Parameters Selection 91
6.1.2 Genetic Algorithm Coefficients and Programming Model 92
6.2 Optimization Process of Two Suction Jets System 93
6.3 Discussion of Optimized Results 96
Chapter 7 Conclusions and Discussions 99
7.1 Genetic Algorithm in current work 99
7.2 Conclusions of Blowing and Suction Jet Control 100
7.3 Future Work and Other Potential Applications 100
References 102
Vita 113

LIST OF TABLES

Table 4.1, Coarse grid and dense grid comparison 44

Table 4.2, Coarse and dense grid C_l and C_d comparison 45

Table 4.3, Comparison of computation results and experiment at $\alpha \leq 10^0$ 46

Table 4.4, Parameters of the four series of numerical simulations 51

Table 5.1, Run 1 (Without Diversity Control) 80

Table 5.2, Run 2 (Without Diversity Control) 80

Table 5.3, Run 3 (With Diversity Control) 81

Table 5.4, Two jet study 90

Table 6.1, 10 best fit individuals of two suction jets system 98

Table 6.2, Comparison between different cases 98

LIST OF FIGURES

Figure 1.1, Multi-discipline research 2

Figure 1.2, Flow control classification 3

Figure 1.3, Computational Fluid Dynamics (CFD) through network computing 4

Figure 3.1, Process of Genetic Algorithm -- the basic algorithm and the improved algorithm 19

Figure 3.2, Roulette wheel selection using raw fitness 25

Figure 3.3, Roulette wheel selection using scale fitness 26

Figure 3.4, One cut point crossover 27

Figure 3.5, Mutation Operator 28

Figure 3.6, Diversity distribution within one generation 31

Figure 3.7, Object fitness comparison between basic algorithm and improved algorithm without/with diversity control, Ackley's Function: (a) basic algorithm, (b) improved algorithm without diversity control, (c) improved algorithm with diversity control 36

Figure 3.8, Diversity comparison between basic algorithm and improved algorithm without/with diversity control, Ackley's Function: (a) basic algorithm, (b) improved algorithm without diversity control, (c) improved algorithm with diversity control 37

Figure 3.9, Object fitness comparison between basic algorithm and improved algorithm without/with diversity control, Rastringin's Function: (a) basic algorithm, (b) improved algorithm without diversity control, (c) improved algorithm with diversity control 38

Figure 3.10, Diversity comparison between basic algorithm and improved algorithm without/with diversity control, Rastringin's Function: (a) basic algorithm, (b) improved algorithm without diversity control, (c) improved algorithm with diversity control..... 39

Figure 4.1, Multi-Zonal (blocks) grid, total of 15 blocks..... 41

Figure 4.2, Layout of foreground grid and background grid, where 4 foreground airfoil blocks overlap on 3 background blocks; information in the covered area of the background blocks are interpolated from the foreground blocks, adjacent block information is exchange..... 42

Figure 4.3, Grid independence study of the grids in Table 4.1 under Re=500,000 condition..... 45

Figure 4.4, Comparison between computation data and experiment data at Re=500,000..... 47

Figure 4.5, Computation results at Re=100,000, 500,000, 1000,000..... 48

Figure 4.6, Three control parameters: Jet Location (L_j), Amplitude (A), Angle (θ)..... 49

Figure 4.7, Suction computation results of initial single jet study, $0.1 \le L_j \le 0.8$, $0.01 \le A \le 0.5$, $\theta = -90^0, -30^0$..... 53

Figure 4.8, Control effects of suction at different locations , L_j=0.1, 0.333 and 0.567, A=0.173, $\theta = -90^0$..... 55

Figure 4.9, Control effects of suction at different amplitudes, L_j=0.1, $0 \le A \le 0.5$, $\theta = -90^0$..... 56

Figure 4.10, Suction computation results on leading edge, $0.05 \le L_j \le 0.125$, $0.01 \le A \le 0.2$, $\theta = -90^0, -30^0$..... 58

Figure 4.11, Computation results of initial blowing study, $0.1 \le L_j \le 0.8$, $0.01 \le A \le 0.5$, $\theta = 30^0, 90^0$ 59

Figure 4.12, Control effects of blowing at different locations, $L_j = 0.1$, 0.333 and 0.567, $A = 0.173$, $\theta = 90^0$ 60

Figure 4.13, Computation results for blowing on the leading edge, $0.2 \le L_j \le 0.8$, $0.01 \le A \le 0.2$, $\theta = 0^0, 30^0, 60^0, 90^0$ 61

Figure 4.14, Control effects of blowing at different amplitudes, $L_j = 0.1$, $0.01 \le A \le 0.5$, $\theta = 30^0$ 63

Figure 4.15, Computation results for blowing on downstream, $0.2 \le L_j \le 0.8$, $0.01 \le A \le 0.2$, $\theta = 0^0, 30^0, 60^0, 90^0$ 64

Figure 5.1, Maximum normalized lift at different amplitudes of single suction of single blowing jet control 68

Figure 5.2, Programming Model 70

Figure 5.3, Two-jet control system optimization convergence history 72

Figure 5.4, Statistic information of optimization process: mean and deviation (error bar) for every eighth generation 73

Figure 5.5, Value of five control parameters of the best 100 fit individuals 74

Figure 5.6, Fitness comparison between algorithm without and with diversity control ... 75

Figure 5.7, Comparison of fitness of the best 100 individuals between the algorithm without diversity control and the algorithm with diversity control 75

Figure 5.8, Comparison of diversity level between the algorithm with diversity control and the algorithm without diversity control 75

Figure 5.9, Values of design parameters of five control parameters of the best

100 fit individuals: (a) algorithm without diversity control (run 1),
(b) algorithm without diversity control (run 2),
(c) algorithm with diversity control(run 3) 77

Figure 5.10, Statistics information of optimization process: mean and deviation (error bar) for every eight generation: (a) algorithm without diversity control (run 1),
(b) algorithm without diversity control (run 2),
(c) algorithm with diversity control (run 3) 78

Figure 5.11, Single suction jet study..... 82

Figure 5.12, Control effects of suction at different locations , L_j=0.1, 0.333 and 0.567, A=0.173, θ=-90^0 84

Figure 5.13, Single blowing jet study 85

Figure 5.14, Flow field and C_p distribution of “Baseline” case, “Suction Only” case, “Blowing Only” case and “Optimized” case 89

Figure 6.1, Two Suction Jet Control System Optimization Convergence History..... 93

Figure 6.2, Statistic information of optimization process: mean and deviation (error bar) for every eighth generation..... 94

Figure 6.3, Value of four control parameters of the best 100 fit individuals..... 95

Figure 6.4, C_p distribution of "case *" and "case 2" 97

LIST OF FILES

LiangDis.pdf 5.2MB

Chapter 1

Introduction

1.1 Overview

This research is the first attempt to solve a large scale two-jet active flow control optimization problem on a NACA 0012 airfoil using the combination of a Genetic Algorithm and CFD. Control effects of jet locations, angles and amplitudes of both the blowing jet and suction jet are extensively studied. Their optimum conditions are searched by the proposed improved Genetic Algorithm and the end results achieve the design goal of a high lift and low drag system within the jet control parameters' range. There are in total around 12,000 numeral simulation cases and the overall computation time is around 300,000 CPU hours ~ 33years on a single processor.

1.2 Background

A stated goal of the National Aeronautics and Space Administration (NASA) is to apply flow control techniques to improve the lift-to-drag ratio (high lift and low drag system) of the commercial fleet of aircraft by a factor of two during the next two decades. This could save the aerospace industrial billions of dollars every year on less fuel consumption. Therefore, flow control methods and their applications are so important that they become the hottest research topics in the aerospace community. As technology advances and

becomes more and more mature in areas of computational fluid dynamics (CFD) and optimization algorithms, the combined application of flow control, CFD and optimization algorithms (figure 1.1) has become a research frontier.

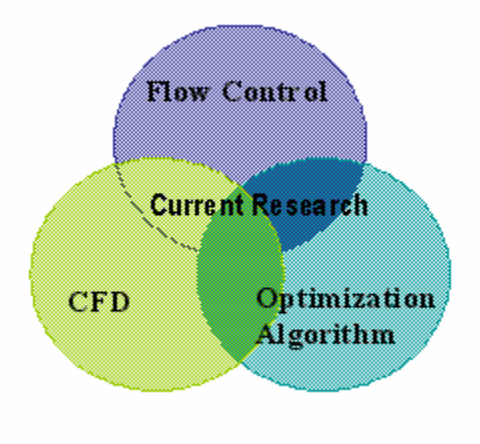

Figure 1.1 Multi-discipline research

1.2.1 Flow Control

The objective of the flow control is an attempt to manipulate a particular flow field with a small energy input typically aiming to increase the lift and reduce the drag, to enhance the mixture of momentum, energy, and species, and to suppress the flow-induced noise. Examples of techniques to obtain these outcomes are: delay or advance transition, prevent or provoke separation, and suppress or enhance turbulence.

Flow control can be divided (figure 1.2) into passive control and active control based on energy expenditure and the involved control loops. Passive control does not need an external energy expenditure and was extensively studied before 1990. During the last decade, researchers have focused on the development of active control methods in which

external power is introduced into the flow field such as blowing and suction jets. Based on the control loops, active flow control can be further classified into predetermined control and interactive control [1]. Predetermined control introduces the steady and unsteady energy inputs without consideration for the state of the flow field. The interactive control uses the controller to adjust the power by a feedback sensor. Previous research mainly focused on passive control and predetermined control methods, and current research mainly focuses on interactive control methods which seek the optimum operating conditions under a wider range of working conditions.

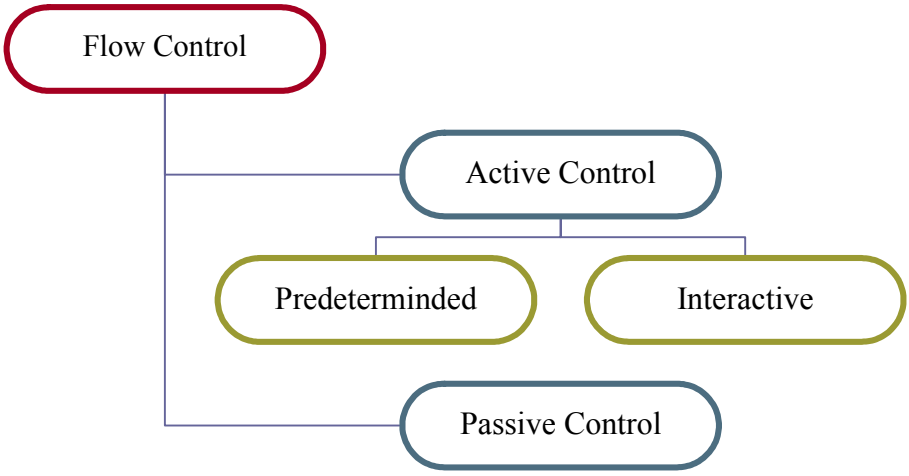

Figure 1.2 Flow control classification

1.2.2 Flow Control Study through CFD

An obvious and important question that arises from flow control applications is how to efficiently synergize all the control components to form a better system. One approach could be through experimental study. For example, in previous decades numerous

experiments were performed on the most common NACA airfoils, measuring lift and drag coefficients under different flow conditions. However, under some conditions even this type of simple measurement can yield wind tunnel data with a wide range of scatter [2] [3] [4]. In these cases, the addition of suction and blowing controls will paradoxically require finer measurements of sensitive, smaller scale flows while increasing the complexity of the overall flow, further increasing the likelihood of experimental error. Trying to repeat these experiments over a wide range of potential parameters necessary to determine the optimal performance conditions for an active flow control design would necessarily be expensive; systematically isolating the multiple factors and fine-flow structures that potentially govern the behavior of the active flow systems through experiments is nearly impossible.

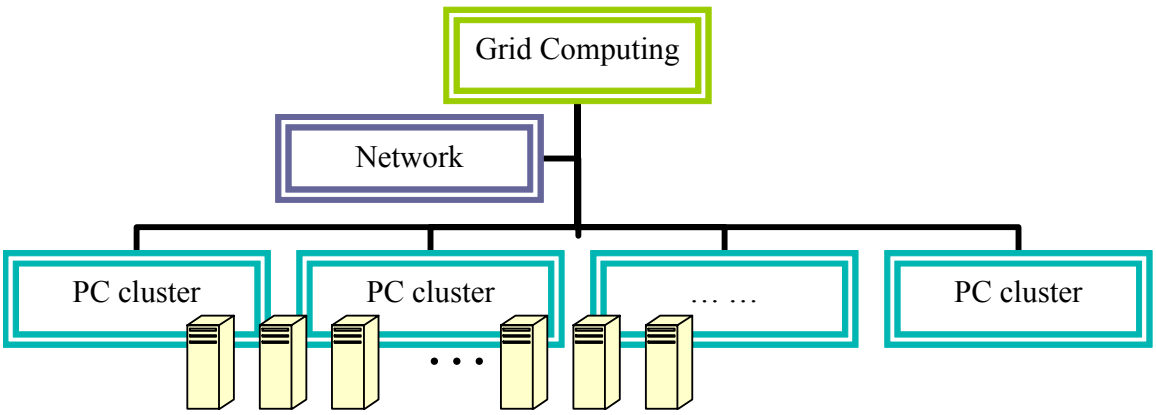

Figure 1.3 Computational Fluid Dynamics (CFD) through network computing

The alternate approach is numerical simulation, which is, in the proper context, more affordable, practical, systematic, and reliable. Numerical simulation can provide a deeper understanding inside the control mechanisms and can lead to the discovery of critical

fluid phenomena and pattern changes. At the same time, the growth of commodity computer clusters and techniques for distributed CFD such as grid computing (figure 1.3) have allowed us to transfer much of the work from traditional supercomputer mainframes to relatively inexpensive groups of personal computers linked by a dedicated network [5]. Series of numerical prototype test computations for a novel design concept and optimization can now be conducted on such a cluster, making large-scale and extensive numerical studies of active flow control prototypes increasingly practical. Therefore, this approach is adopted in the current flow control study.

1.2.3 Optimization Algorithms

The perfection of human nature leads to the studies of optimization algorithms. Over history, optimization algorithms are developed and rooted in solving engineering, economics, operation, and management problems. In recent years optimization has seen a dramatic increase in activities. This is a natural consequence of new algorithmic developments and the increased power of computers. Many of these problems can be very large, although what is large in optimization reflects not only the size but also the inherent complexity of a problem.

Evolutionary optimization algorithms are major breakthrough in the area of optimization algorithm development because of the failure of traditional gradient-based climb-hill methods for solving complex problems. The complexities of the problems exist both in search space and solution space; furthermore, because of their strong non-linearity, vigorous mathematical descriptions are hard to set up, such as with the physics phenomena.

All evolutionary algorithms have two prominent features which distinguish them from other search algorithms. First, they are all population-based methods which means they work on multiple points in the multiple directions. Second, there are communication and information exchanges among individuals in and between populations. Such communication and information exchanges are the result of selection and recombination in evolutionary algorithms.

The Genetic Algorithm is one of the most popular used evolutionary algorithms. It was developed at the University of Michigan [6] to abstract and explain the natural system and to design artificial systems software that retains the important mechanisms of nature systems. The goal is to achieve robustness, while at the same time not compromise the efficiency, on the artificial system. A Genetic Algorithm exceeds and is fundamentally different from traditional methods in three aspects: (1) it encodes the parameters, not playing with parameters themselves directly; (2) it searches and evaluates many points at the same time, not at a single point; (3) it uses stochastic methods instead of deterministic rules, and uses fitness information instead of derivatives or other similar information. The Genetic Algorithm is better than other methods for solving complicated engineering problems for the following reasons: (1) it is robust and may capture global optimal solutions; (2) it is easy to incorporate a genetic algorithm into existing evaluation software such as CFD and CEM solvers; (3) it can handle either single or multiple objective problems; (4) it is easily parallelized (different individuals can be solved concurrently on different processors).

1.3 Motivations and Objectives

In spite of popular usage in numerous areas, Genetic Algorithms have not yet been widely applied to active flow control problems through CFD study. This thesis is the first effort to solve a large scale active flow control optimization problem on a NACA 0012 airfoil. Generally, engineering design problems involve a large number of real design variables. Regarding the searching algorithm, the traditional binary GA and its operators need to be transformed or re-defined to meet the requirements of these real world engineering problems. Since traditional binary substrings representing each parameter with the desired precision are concatenated to represent an individual in the GA, the resulting string encoding of a large number of design variables yields a huge string length; therefore, traditional genetic algorithms generally perform poorly for such design problems.

Beyond this difficulty, applications of traditional Genetic Algorithms to solve engineering optimization problems face two further challenges. The first is that although a GA is good at exploring the search space globally to find promising regions, it has been found to lack fine-grained searching ability, thereby resulting in slow convergence to a precise solution. But most of the engineering optimization tasks require reasonably precise solutions within a limited time frame, so increasing the rate of convergence is vital. Second, even for a robust global optimization method like the GA, applications are sometimes trapped in local optima, which can lead to inaccurate preliminary convergence. Generally speaking, the method dealing with the first challenge and the method dealing with the second challenge are contradictory. For example, a method dealing with the

second challenge will require higher diversity among the initial 10%~20% GA evolution, which will likely slow down the initial convergence rate; therefore, the diversity control method may not be suitable for some very time-demanding engineering optimization problems although a GA with diversity control has proved to be more robust.

The approach taken in this research is to combine different existing GA techniques and proposed a real-coded "Explicit Adaptive Range Normal Distribution" (EARND) genetic algorithm with diversity control to solve the convergence problems. First, a traditional binary-coded GA is replaced by a real-coded algorithm in which the corresponding design variables are encoded into a vector of real numbers that is conceptually closest to the real design space. Second, to address the convergence speed problem, an additional normal distribution scheme is added into the basic GA in order to monitor the global optimization process; meanwhile, design parameters' boundaries are explicitly updated to eliminate unnecessary evaluations (computation) in un-promising areas to balance the workload between the global and local searching process. Third, during the initial 20% evolution (search process), the diversity of the individuals within each generation is maintained at a high level in order to conquer the problem of preliminary convergence to local optima.

In this thesis, we first perform a single jet suction/blowing study in order to better understand the two-jet control optimization process. Two two-jet control systems are then set up on a NACA 0012 airfoil. The proposed genetic algorithm is applied on this system

and the optimization results are presented and analyzed. The two two-jet control systems tested are a single suction jet and single blowing jet system, and a two suction jet system.

1.4 Organization of the Dissertation

Overview, background, motivation and objectives of this dissertation study are introduced in Chapter1. The literature survey about recent developments and achievements in CFD in combination with Genetic Algorithms will be presented in Chapter 2. The basic ideas, essential operators, and evolution (genetic algorithm) process of the Genetic Algorithm are shown in Chapter 3. Preliminary single suction/blowing jet studies and their results are included in Chapter 4. Application of a genetic algorithm on a suction/blowing jet system is demonstrated in Chapter 5 and application of a genetic algorithm on a two suction jet system is demonstrated in Chapter 6. Conclusions are provided in Chapter 7.

Chapter 2

Literature Survey

The overall goal of this thesis is to optimize the blowing and suction control on the NACA0012 airfoil, using a Genetic Algorithm with diversity control, in conjunction with Computational Fluid Dynamics as evaluator. The emphasis of the literature survey is three fold: first looking at flow control theory and experiments, especially those in relative with airfoils; second examining flow control studies using CFD; third reviewing the development of Genetic Algorithms and the combined applications of Genetic Algorithms and CFD in control studies.

2.1 Survey of Flow Control Theory and Experiments

Of all various types of flow control, separation control (historically referred as boundary layer control -- BLC) is probably the oldest and the most economically important to the aviation industry. The goal of separation control on an airfoil is to achieve high lift and low drag.

Separation flow control had long been studied both theoretically and experimentally. At the theoretical side, mathematicians and physicists tried to establish the basic separation control theories from the boundary layer equation. Many approximate methods have been devised to solve the boundary layer equations, with one of the best known solutions given

by Thwaites [7]. Simple criteria for laminar separation based on the solution are given by Stratford [8], Lighthill [9] and others. Curle et al. [10] revised the work of Thwaites, Stratford, and Lighthill by relying on the examination of a number of exact solutions in an effort to obtain a solution which best fits all of these. Then, theoretical studies shifted to turbulent boundary control because the turbulent boundary layer does not separate as easily as a laminar one. However, since turbulent mixing is much larger than laminar mixing, this delaying of separation is at the cost of a significant increase of skin friction. The criterion for transition to turbulence was studied by several researchers such as Crabtree [11]. Since turbulence was not fully understood, many approximate methods, based on semi-empirical theories for the criteria of turbulence separation, had been devised, such as the methods by Thwaites [12] and Maskell [13]. At the same time, boundary layer experimental measurement and studies on the airfoil were conducted by Brewer et al. [14] and others. The effects of compressibility on separation were also studied and tested by Reshotko et al. [15], Allen et al. [16] and Stack [17]. But all analytical studies were limited to simple conditions and assumptions; hence the predictions did not agree with the experiments in most cases.

Although vigorous theoretical formulation of separation control was still in critical need, novel experimental control methods have been proposed. Works in the early days primarily emphasized passive methods, such as modifying the surface condition [18] (smoothness and waviness) and geometric shapes [19] to maneuver the pressure gradient [20], thereby delaying turbulence [21] and preventing separation over the airfoils' upper (lower pressure) surface [22]. While these techniques seem like a sound idea, the end

results are not always adequate, for these methods are limited by the geometrical constraint of the airfoil. Therefore, other passive approaches were tried, such as passive suction and passive vortex generators. The idea of passive suction is to use a passive porous surface [23] [24] to mitigate the local pressure gradients and obviate separation to reduce drag. The vortex generators [25] use passive momentum adding to the near wall boundary to conquer the adverse pressure gradient, and this approach was widely used for airfoil flow control [26] [27] [28] during the early days.

Because passive methods are always limited to some certain working conditions, they can not be adjusted to work under wider conditions. Therefore, the active methods that can meet wider requirements started to receive a lot of interest, such as suction control, blowing control and the combination of both. As for the suction control [29] [30] [31] [32], all research pointed to leading edge suction for all kinds of airfoil, but the locations of suction being studied were selected without a systematic study. As for the blowing control [33] [34] [35], all research pointed to trailing edge tangential blowing for a number of airfoil test cases, but theoretical blowing control studies [36] were less clear than suction control.

The recent development of synthetic jets [37] combines the benefits of suction and blowing into one zero-mass compact device. The detailed physics of the formation and evolution of synthetic jets are discussed by Glezer, et al. [38]. A synthetic jet is generally considered the acoustic streaming of flow from an orifice or slot being driven by a pressure oscillation (with zero mean pressure difference) in an adjacent cavity. The

pressure oscillation is usually generated by a moving diaphragm inside the cavity. Candidate designs of synthetic jets include piezoelectric ceramics [37], fluidics [39], and linear [40] and rotary [41] electromechanical motors. Experimental studies [42] [43] [44] and designs are actively carried by the Georgia Institute of Technology and Texas A&M University.

Synthetic jets have been actively applied to separation control to generate virtual shapes on solid walls. They can efficiently provide periodic forcing for dynamic separation control and completely suppress the separation by sufficient momentum injection when oscillating at higher levels. The applications of synthetic jets are numerous, such as shear flow control using fluidic actuator technology [39] and aerodynamic flow control of bluff bodies using synthetic jet actuators [45]. The abilities of synthetic jets are so versatile that they also apply to other areas such as the mixing enhancement in combustion [46] [47].

2.2 Survey of Flow Control Study Using CFD

As the numerical methods of Computational Fluid Dynamics (CFD) become more and more mature and as computing power still follows Moore's law, CFD has become an integral part of the aircraft design process and a major tool for flow control study. In the previous section, we discussed the wide applications of blowing/suction type active flow control methods, hence, we now narrow down our interest only to this type of control study that use CFD.

Numerical studies of blowing/suction type control (including synthetic jets) [48] [49] [50] aimed at qualitatively capturing the flow physics and the underlying control mechanisms. There are several different approaches from different perspectives. From the numerical methods perspective, some use RANS, some use DNS; from the computation geometry perspective, some use 2-D grids, some use 3-D grids; from the simulation of membrane motion condition perspective, some use moving grid boundary, some directly apply velocity profiles at the boundary.

The two representative approaches are those of Kral et al [48] and Rizzetta et al [49]. Kral et al. applied a 2-D RANS approach to solve a boundary value problem for the incompressible, unsteady 2-D Reynolds Averaged Navier-Stokes equations with the Spalart-Allmaras (SA) turbulence model. Their computational domain encompassed only the region external to the jet, excluding the cavity or actuating membrane. The jet presence was simulated by forcing an analytical velocity profile on the boundary region corresponding to the jet orifice. Rizzetta et al. applied a 3-D DNS approach to solve the unsteady, compressible Navier-Stokes equations. The external region, the cavity itself and the throat were calculated on separate grids and linked through a chimera methodology. The membrane motion was represented by varying the position of appropriate boundary points. These 3-D simulations show that the internal cavity flow becomes periodic after several cycles. Therefore, it is appropriate for Kral et al. to use the velocity profile as a boundary condition to simplify the computation.

Since the above pure numerical simulations of blowing/suction type control all proved to match at least qualitatively to the experiment data, the numerical simulations promptly extended to the control application studies. Several research works with different jet locations and angles of attack are briefly mentioned here. Wu et al. [51] studied control effects on a NACA 0012 airfoil with a local unsteady forcing (2.5% chord length width) located at 5% from the leading edge at the angle of attack from 18^0 to 35^0 with a 2-D RANS (SA turbulence model) approach. Catalin [52] studied control effects on a NACA 0012 airfoil with synthetic jet array (10% width) located at 10% from the leading edge at the angle of attack 13^0 with a 2-D RANS (modified $\kappa - \varepsilon$ turbulence model) approach. Hassan et al [53] studied a synthetic jet located at 13% from the leading edge at the angle of attack of 0^0 and 5^0 with a 2-D RANS (Baldwin-Lomax turbulence model) approach.

All the above studies find that the synthetic jet and forcing/non-forcing (oscillatory/ steady) suction/blowing on the airfoil leading edge can increase lift and decrease drag at certain angles of attack, but systematic studies of the best location and other control parameters, such as blowing/suction angle and amplitude, have not been performed.

2.3 Survey of Genetic Algorithm on Optimization

Our survey of Genetic Algorithms mainly focuses on two aspects. One is the algorithm itself; the other is the application of genetic algorithms to optimization, especially coupling with CFD on design and control problems.

From the algorithm perspective, the Genetic Algorithm (GA) emerges from the goal of developing a general canonical search and learning procedure. It starts from the less knowledge-specific position to solve a wide range of optimization problems. In the optimization process, a Genetic Algorithm aims to locate highly fit similarities in the global region and to experiment with combinations of these highly fit similarities in order to find the best fit individual (solution). In recent years, the applications of Genetic Algorithms is soaring in many areas such as machine learning [54], real time trading models [55], logistics [56], and biology [57], but GA has not frequently been applied to active flow control optimization on an airfoil.

There are a variety of techniques used for Genetic Algorithm representations, selection methods, crossover methods, and mutation methods. In the original work of Holland [6], binary-strings are used to form chromosomes to represent each individual (candidate solution). However, binary strings lack the flexibility to closely represent the real solution and also have a huge memory cost when representing a large number of parameters. Therefore, real-coded Genetic Algorithm have been more widely used by the genetic algorithm practitioners in the last several years. For example, Janikow et al. [58] and Wright [59] demonstrated that real-coded Genetic Algorithms outperformed binary-coded (binary-string representation) Genetic Algorithms in several design problems.

The selection operator is an important operator in Genetic Algorithms because selection pressure (preference) is key to a successful evolution. It is an art to chose the selection method to separate the best individuals from the worst individuals, while at the same time

maintain a certain level of diversity to maintain the robustness of the algorithm. There are two main selection strategies: one is fitness (raw or scale fitness) based proportional selection, like roulette-wheel selection [60], the other is non fitness based selection, such as ranking selection [61] and tournament selection [62].

The crossover operator is a recombination operator in Genetic Algorithms for parents to generate children. Traditional binary-coded algorithms [60] have one-cut point crossover, two-cut point crossover, and multiple-cut point crossover. For the real-coded algorithm, there are Blend Crossover methods [63] and Simulated Binary Crossover [64] methods.

The mutation operator brings random mutation into the generation. For a binary-coded algorithm, the mutation [60] is performed by randomly selecting a bit and flipping it ("1" to "0" or "0" to 1). The corresponding approach in a real-coded algorithm is to randomly generate a value and add/subtract from randomly selected individuals [65].

Regarding the applications, before we look at the applications of Genetic Algorithms in the aerospace industry using CFD, we need to mention the failure of Gradient Based methods. Although Gradient Base method [66] [67] [68] coupling with CFD came before Genetic Algorithms, researchers soon realized that in order to find a global optimum using Gradient Base method, one must start the optimization process repeatedly from a number of initial points and check for consistency of the optima obtained. Therefore, the Gradient Base method is not a candidate for an efficient and robust algorithm.

Because of its efficiency and robustness, Genetic Algorithms and closely related evolution algorithms had been successfully applied to conceptual design of aircraft [69] [70] and the preliminary design of turbines [71]. In addition, since it is easily implemented and coupled with CFD codes, Genetic Algorithms have been applied to optimization problems using CFD as a means for evaluation and simulation. Quagliarella et al. [72] used the Genetic Algorithm and a potential solver to design an airfoil shape, Yamamoto et al. [73], Obayashi et al. [74] and Holst et al. [75] also used the Genetic Algorithm and a Navier-Stokes solver to design an airfoil shape.

There are two common issues in the above applications of genetic algorithms coupling with CFD. First is that the CFD computation time for each single individual (candidate solution) of all the above applications was small, ranging from minutes to several hours on a single processor. Second, they all studied passive flow control problems (airfoil shape design) because active flow control such as jet control requires a large amount of computation time which makes the application of a Genetic Algorithm on active flow control costly. Therefore, how to design an efficient and robust Genetic Algorithm to cut down the computation cost is an important issue.

Chapter 3

Genetic Algorithm

In this chapter, we start by examining the basic genetic algorithm (figure 3.1, left) with its genetic coefficients and operators, the specific details about which can be found in reference [60] and [65]. Subsequently, the modifications (figure 3.1, right) added to improve convergence are discussed. Convergence issues between the basic algorithm and the proposed improved algorithm are compared and validated by two test-bed functions.

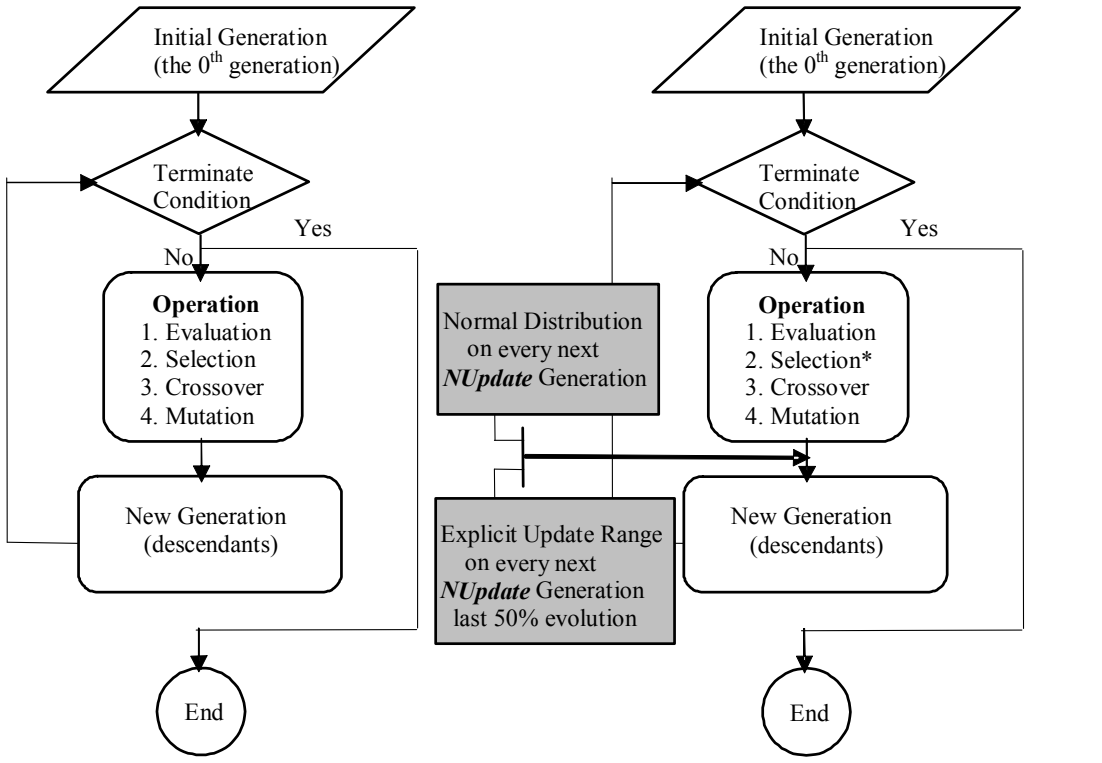

Figure 3.1 Process of Genetic Algorithm -- the basic algorithm and the improved algorithm

3.1 Definition, Terminology and Genetic Coefficients

3.1.1 Definition

A Genetic Algorithm (GA) uses genetic concepts to encode the problems into a generation (a group of individuals) and then simulates the generation evolution by applying mathematic genetic operators (selection, crossover and mutation) to determine the best solution (individual) over multiple iterations of a finite number of generations. The definition of "best" comes from a fitness function that defines whether a given individual is better or worse than other individuals.

3.1.2 Terminology

The Genetic Algorithm concept is borrowed from genetic engineering, so the terminology is similar. Some critical terms are:

- *Chromosome (binary string, individual)* means *candidate solution*.
- *Genes (bits of binary string)* means *part of solution* or *a parameter*.
- *Locus* means *position of gene*.
- *Alleles* means *values of gene*.
- *Phenotype* means *decoded solution*.
- *Genotype* means *encoded solution*.

3.1.3 Major Genetic Coefficients

Genetic coefficients play important roles in the optimization process, for every specific problem, coefficients can be fine tuned to get the best convergence speed and results. The most important coefficients are:

- Number of total generations, *NGeneration*
- Number of individuals (population size) per generation, *NPopSize*
- Number of function variables (design parameters), *NVariable*
- Crossover percentage, P_c
- Mutation percentage, P_m

3.2 Basic Algorithm and Minor Improvements

Traditional Genetic Algorithms use the binary strings to represent solutions. But given a relatively precise resolution requirement of the design parameter, for example 10^{-6}, this method will result in a large string length for most of the engineering design problems. Therefore, the traditional binary string needs to be transformed and re-defined to conqueror this challenge.

In the following sections, we will walk through the typical optimization process of a genetic algorithm, and re-define the traditional binary string representation and operators into the real-coded representation. In addition, we will make some minor improvements to the basic algorithm. Further information on these topics may be founded in reference [60] and [65].

3.2.1 Binary String Representation Limitation

Though the original work of Genetic Algorithm used binary string representation, it has two major limitations, one is the solution resolution and memory problem, and the other

is the representation problem. Therefore, the binary string has almost been replaced by real-coded representation in recent years, especially in the engineering optimization field. The following five-variable example demonstrates two limitations of traditional binary string representation.

Example:

$$f_{\max}(x_i) = -\sum_{i=1}^{n}(x_i - 0.5)^2 \ , \ 0 \le x_i \le 1, \ n = 5$$

if we use only use 3 bits to represent each variable for a candidate solution

$$\{x_1, x_2, x_3, x_4, x_5\} = \{1/7,\ 2/7,\ 3/7,\ 0,\ 6/7\},$$

then the resolution of each variable is only

$$\frac{1}{2^3 - 1} = \frac{1}{7} = 0.142857\,,$$

and the corresponding binary representation is:

$$\{x_1, x_2, x_3, x_4, x_5\} = \{001,010,011,000,110\}$$

For this candidate solution, its raw fitness (function evaluation results) is:

$$fit_{raw} = -\left[(\frac{1}{7} - 0.5)^2 + (\frac{2}{7} - 0.5)^2 + (\frac{3}{7} - 0.5)^2 + (0 - 0.5)^2 + (\frac{6}{7} - 0.5)^2\right] = -0.556122$$

If we require a resolution of 10^{-6} in solution space, then we need to use 20 bits to encode each variable, as $10^{-6} \approx \frac{1}{2^{20} - 1}$; hence, each candidate solution (binary string) of this five-variable function will require a total 100 bits. Most of the engineering design problems have more design variables than five which will lead to an extremely long binary string for each candidate solution and excessive memory usage.

Beyond the memory storage problem, there is another obvious problem in the above example. The optimum solution should be:

$$\{x_1, x_2, x_3, x_4, x_5\} = \{0.5, 0.5, 0.5, 0.5, 0.5\},$$

but our binary string (3-bit for each variable) can not represent this candidate solution. Ways to solve this problem are either through dynamically updating variable boundaries or through dynamically increasing the bit length, or through both methods. But this approach would add tremendous management efforts to the programs.

Due to these limitations, in the recent years, traditional binary-coded (binary string represented) algorithms have been replaced by real-coded algorithms in which the corresponding design variables are encoded into a vector of real numbers that is conceptually closest to the real design space. On all modern IA-32 personal computers, the default real (double) number precision is 10^{-16}, which is generally sufficient to represent any solution accurately. Therefore, in a real-coded algorithm, there is no string length issue, and the candidate solution of the above example can be represented as following (use C++ notation):

```
struct myChromosome{
   double genes[NVariable]; // NVariable =5
   double rawFitness; // function evaluation results
   double scaleFitness; // fitness after scale
}
myChromosome X;
X.genes[0]=0.142857;
X.genes[1]=0.285714;
X.genes[2]=0.428571;
X.genes[3]=0;
X.genes[4]=0.714286;
```

3.2.2 Roulette Wheel Selection Operator and Its Improvement

In this section, we first introduce the idea and basic procedures of roulette wheel selection, with an example that demonstrates the insufficiency of raw fitness in basic wheel selection. Then, we use the same example to demonstrate the better performance of improved roulette wheel selection in which raw fitness is replaced by scale fitness.

A simple roulette wheel selection process follows two steps. The first step is to use raw fitness of each individual in the parent generation to form the cumulative selection space.

$$cul_j = \frac{\sum_{i=1}^{j} fit_{raw}}{\sum_{i=1}^{NPopSize} fit_{raw}}, 1 \le j \le NPopSize \qquad (1)$$

Then in the selection process, randomly generate a value that simulates the spinning wheel process:

$$r_k \in [0,1],\ 1 \le k \le NPopSize$$

individual $\vec{X}_n$ will be selected into the new generation if it satisfies

$$cul_{n-1} \le r_k \le cul_n,\ 1 \le n \le NPopSize$$

But under most circumstances, using raw fitness will not generate a proper cumulative selection space as can be seen in figure 3.2. This example case assumes that there are 5 individuals within one generation. In the figure, it can be seen that the relative best solution $\vec{X}_1$ is assigned the smallest selection space by using raw fitness. Therefore, in the selection process, it has the least chance to survive into the children generation which is in the opposite direction of our goal that a better fit individual should get larger chance to survive into the children generation.

Individual	Raw fitness $f(x_i)$	Cumulative fitness space	Random Number	Selection Individual
$\vec{X}_1$	-0.11	-0.11/(-0.11-0.12-0.13-0.14-0.15)=0.169230	0.489761	$\vec{X}_3$
$\vec{X}_2$	-0.12	(-0.11-0.12)/(-0.11-0.12-0.13-0.14-0.15)=0.353846	0.069876	$\vec{X}_1$
$\vec{X}_3$	-0.13	(-0.11-0.12-0.13)/(-0.11-0.12-0.13-0.14-0.15)=0.553846	0.559043	$\vec{X}_4$
$\vec{X}_4$	-0.14	(-0.11-0.12-0.13)/(-0.11-0.12-0.13-0.14-0.15)=0.769231	0.979265	$\vec{X}_4$
$\vec{X}_5$	-0.15	(-0.11-0.12-0.13-0.14-0.15)/(-0.11-0.12-0.13-0.14-0.15)=1	0.274654	$\vec{X}_2$

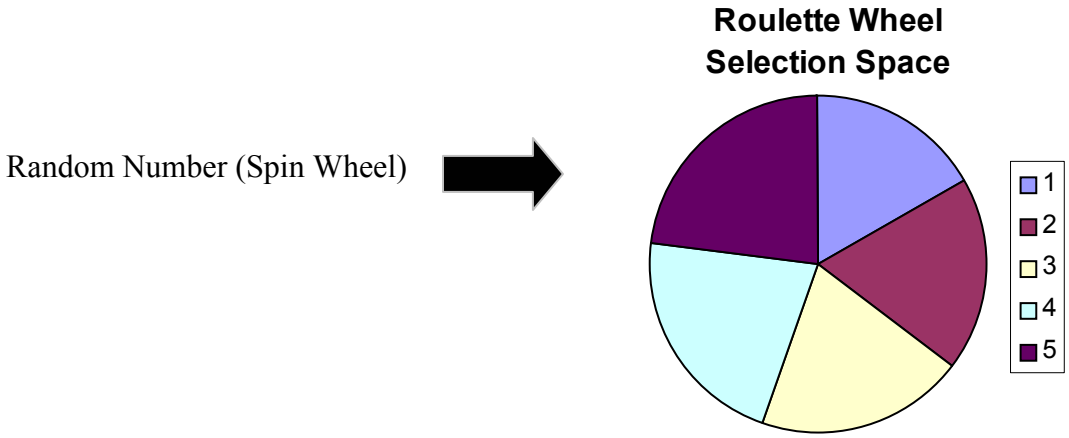

Figure 3.2 Roulette wheel selection using raw fitness

To correct this, generation-adaptive coefficient is added to the simple roulette wheel selection, to address the different selection pressure among individuals within one generation, according to their scale fitness fit_{scale}. Assume $fit_{\max}$ represents the maximum fitness within one generation and $fit_{\min}$ represent the minimum fitness within one generation. In this case, each individual's corresponding fitness value can be calculated as

$$fit_{scale} = \frac{fit - fit_{\min} + \gamma}{fit_{\max} - fit_{\min} + \gamma}, \quad (2a)$$

for $f_{\max}(\vec{X})$ function optimization, or

$$fit_{scale} = \frac{fit_{\max} - fit + \gamma}{fit_{\max} - fit_{\min} + \gamma}, \qquad (2b)$$

Individual	Raw fitness $f(x_i)$	Scale fitness f_{scale}	Cumulative fitness space	Random Number	Selection Individual
$\vec{X}_1$	-0.11	1	0.3	0.489761	$\vec{X}_2$
$\vec{X}_2$	-0.12	0.833333333	0.55	0.069876	$\vec{X}_1$
$\vec{X}_3$	-0.13	0.666666667	0.75	0.559043	$\vec{X}_3$
$\vec{X}_4$	-0.14	0.5	0.9	0.979265	$\vec{X}_5$
$\vec{X}_5$	-0.15	0.333333333	1	0.274654	$\vec{X}_1$

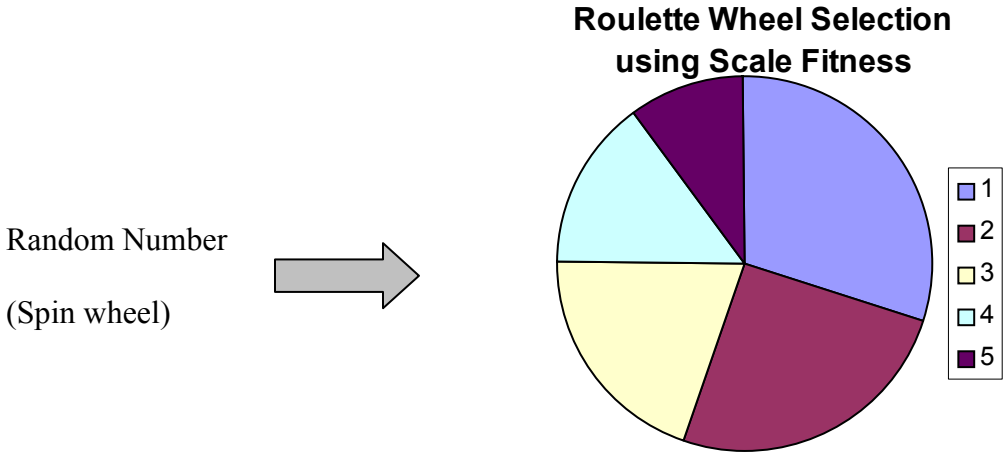

Figure 3.3 Roulette wheel selection using scale fitness

for $f_{\min}(\vec{X})$ function optimization. In current research, γ will range from $2.5 \cdot (fit_{\max} - fit_{\min})$ to $0.25 \cdot (fit_{\max} - fit_{\min})$ as cur_gen (current generation) changes from 0 to $NGeneration$, in order to increase the selection pressure (preference) between the best fit and least fit individual within one generation during the evolution. The benefit

of using scale fitness to form a better selection space instead of using raw fitness can be seen in figure 3.3, defining γ as $0.5 \cdot (fit_{\max} - fit_{\min})$ in this example. Then, the raw fitness in equation (1) will be replaced by scale fitness in order to calculate the accumulative selection space.

3.2.3 Crossover Operator

The idea behind the crossover operator is to generate children individuals by recombining characteristics of the parent individuals. Figure 3.4 shows a one-cut point crossover in a binary string representation.

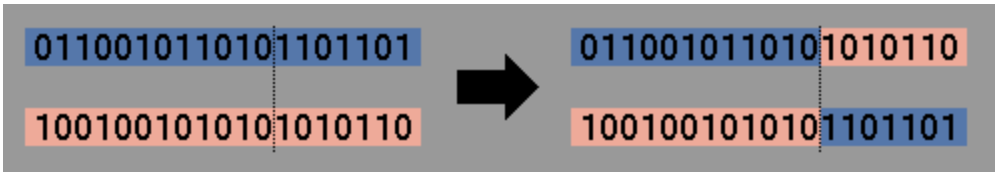

Figure 3.4 One cut point crossover

Following the crossover idea, one way to do it in a real-coded manner is to first randomly generate a value

$$r_k \in [0,1],\ 1 \le k \le NPopSize\ .$$

If $r_k < P_c$ (crossover percentage), then for any given pair of parent individuals, their children give birth as following:

$$\vec{X}_{child1} = C_1 \cdot \vec{X}_{parent1} + C_2 \cdot \vec{X}_{parent2}\ ,$$

$$\vec{X}_{child2} = C_2 \cdot \vec{X}_{parent1} + C_1 \cdot \vec{X}_{parent2}\ , \qquad (3)$$

and the values of the two crossover coefficients are the golden section numbers of

$$C_1 = 0.38197\ , C_2 = 0.61803$$

It had been proved in reference [76] that the golden section numbers are the appropriate values in a one dimension searching process.

3.2.4 Mutation Operator

The idea behind the mutation is to add random variation to individuals among one generation, and a binary string representation can be seen in figure 3.5.

Figure 3.5 Mutation Operator

This idea can be re-defined in a real-coded manner as follows. In the mutation process, randomly generate a value

$$r_k \in [0,1],\ 1 \le k \le NPopSize$$

If $r_k < P_m$ (mutation percentage), then it performs the random mutation. A generation-adaptive random mutation value δ is generated and added/subtracted from the individuals after the selection and crossover operation. If the variables' value of the mutated individuals is out of range, it will be set to the nearest boundary. δ is calculated using the following steps:

$$\tau = (1.0 - 0.99 \cdot \frac{cur\_gen}{NGeneration})^s, \qquad (4)$$

s is a scale up factor. x_i^{Upper} and x_i^{Lower} represent the upper and lower boundary value of variable x_i.

$$dif_1 = \max(x_i^{Upper} - x_i, x_i - x_i^{Lower}),$$

$$dif_2 = \min(x_i^{Upper} - x_i, x_i - x_i^{Lower}). \quad (5)$$

If cur_gen is an even generation, then

$$\zeta = dif_1, \quad (6a)$$

or if cur_gen is odd generation, then

$$\zeta = dif_2. \quad (6b)$$

The random mutation value is

$$\delta = \tau \cdot \varsigma \cdot rand[0,1]. \quad (7)$$

3.3 Improved Algorithm

3.3.1 Normal distribution

Based on the above basic algorithm, we add a normal distribution function [77] in order to act as a global optimization monitor and to speed up the search convergence. In every $NUpdate$ generation, the new generation will give birth according to the normal distribution rule based on the statistic information of the best up to current $NUpdate \cdot NPopSize$ individuals. For example, the i^{th} individual in the new generation is generated as follows. First randomly generate a value:

$$r_j^i \in [0,1],\ 1 \le i \le NPopSize,\ 1 \le j \le NVariable.$$

Find the corresponding p_j^i [78] which makes

$$r_j^i = \int_{-\infty}^{p_j^i} N(0,1)(z)dz, \quad (8)$$

$$1 \le i \le NPopSize,\ 1 \le j \le NVariable$$

Suppose μ_j and σ_j are the j^{th} variable's statistical mean and deviation of the $NUpdate \cdot NPopSize$ best individuals. Then, the i^{th} new individual's j^{th} variable value can be calculated as

$$x_j^{\,i} = \mu_j + \sigma_j \cdot p_j^{\,i}. \qquad (9)$$

In general, this normal distribution is applied 10~20 times during the total evolution, so the genetic coefficient $NUpdate$ is set at 1/20 ~ 1/10 of total number of generations.

3.3.2 Explicit updated boundary

Building on the previous step, when an evolution passes half of the total generations (50% evolution), then in every next $NUpdate$ generation the variables' design space (upper and lower boundary) will also be explicitly updated according to the $NUpdate \cdot NPopSize$ best individuals statistical information. The new ranges are chosen as:

$$x_j^{Upper} = \min(x_j^{oldUpper}, \mu_j + \kappa\sigma_j)$$

$$x_j^{Lower} = \max(x_j^{oldLower}, \mu_j - \kappa\sigma_j) \qquad (10)$$

In the current paper, we choose coefficient κ as 5.0 which is conservative but robust; reducing the coefficient κ can make the searching process advance in a more aggressive and deterministic direction,

The scale up factor s in equation (4) is also updated to maintain the resolution.

$$s_j = s_j^{\,old} - 0.5 \cdot \log_{10}\left(\frac{x_j^{\,oldUpper} - x_j^{\,oldLower}}{x_j^{\,Upper} - x_j^{\,Lower}}\right) \qquad (11)$$

3.3.3 Diversity control

In the literature survey, we can see that there are several existing techniques to control the diversity of the evolution (optimization) process to increase the robustness, especially for the initial 10%~20% of the process. In the current paper, we present a simple and novel diversity control technique which will suppress the reproduction of the super fit individuals at the selection process. We add a denominator d to the scale fitness equation, which means that each individual's corresponding fitness value can be calculated as

$$fit_{scale} = \frac{fit - fit_{\min} + \gamma}{fit_{\max} - fit_{\min} + \gamma} \cdot \frac{1}{d}, \qquad (12a)$$

for $f_{\max}(\vec{X})$ function optimization, or

$$fit_{scale} = \frac{fit_{\max} - fit + \gamma}{fit_{\max} - fit_{\min} + \gamma} \cdot \frac{1}{d}, \qquad (12b)$$

for $f_{\min}(\vec{X})$ function optimization. The value d is how many similar individuals fall in the same category for each corresponding individuals.

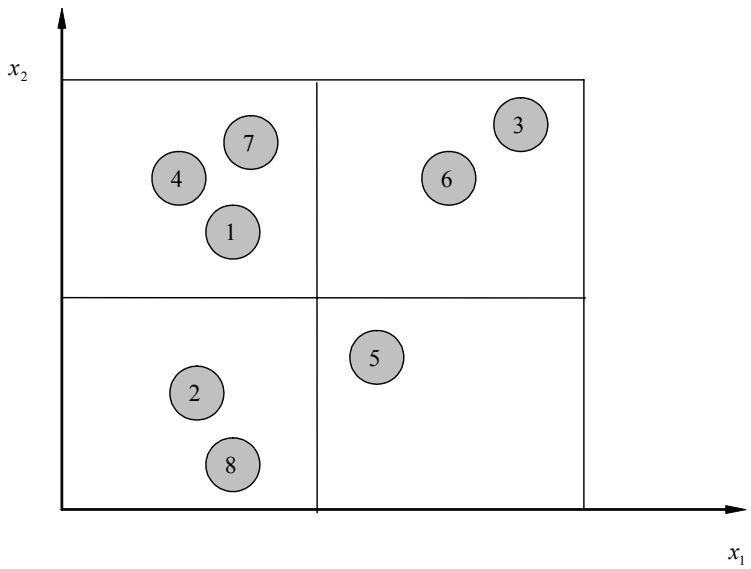

Figure 3.6 Diversity distribution within one generation

For example, there are 8 individuals within one generation for a 2-variable (x_1 , x_2) problem. Figure 3.6 shows the distribution of these 8 individuals in the 2-D space. From this figure we can see that, for individual "1", there are three individuals that fall in the same category, so the denominator value d for individual "1" is 3; for individual "2", there are two individuals in the same category, so the denominator value d for individual "2" is 2.

The diversity value of each generation can be measured in the following equation,

$$\Xi = -\sum_{i=1}^{NPopSize} \frac{d_i}{NPopSize} \cdot \log_{10} \frac{d_i}{NPopSize} \quad (13)$$

and we can call Ξ "entropy" which reflects the diversity level of one generation. In order to compare the entropy between different systems, we can further normalized Ξ divided by $\Xi_{\max}$, which is

$$\Xi_{\max} = -NPopSize \cdot \frac{1}{NPopSize} \cdot \log_{10} \frac{1}{NPopSize} = \log_{10} NPopSize .$$

Of course, the diversity level is also determined by the way that solution space is classified.

3.4 Algorithm Performance Test and Case Study

Two representative genetic algorithm test bed functions are chosen to validate our genetic algorithm. Three algorithms, namely the basic algorithm, the improved algorithm without diversity control and the improved algorithm with diversity controls, are tested. The corresponding results of object fitness and diversity for test functions 1 and 2 for both

algorithms are compared in figures 3.7, 8 and 3.9, 10, respectively. Each algorithm is tested by five sets of randomly generated initial (0^{th}) generations. For every data set, each algorithm runs 10 times and the averages are measured. In order to demonstrate the convergence more clearly, in test function 1 the absolute value of the function object fitness is plotted when it becomes smaller than zero.

Test Function 1: Ackley's Function:

The Ackley's function is written as:

$$\min f(x_1, x_2) = -c_1 \cdot \exp\left(-c_2 \sqrt{\frac{1}{2}\sum_{j=1}^{2} x_j^{\,2}}\right) - \exp\left(\frac{1}{2}\sum_{j=1}^{2} \cos(c_3 \cdot x_j)\right) + c_1 + e$$

$$-5.0 \le x_1 \le 5.0, -5.0 \le x_2 \le 5.0,$$

$$c_1 = 20, c_2 = 0.2, c_3 = 2\pi, e = 2.71282$$

The known best solution is:

$$f_{\min}(v) = f_{\min}(x_1, x_2) = f(1.96370 \times 10^{-6}, 5.71207 \times 10^{-7}) = -5.45604 \times 10^{-3}$$

The genetic coefficients are chosen as followings:

$$NGeneration = 1000,$$

$$NPopSize = 16,$$

$$NVariable = 2,$$

$$NUpdate = 50,$$

$$P_c = 0.2, P_m = 0.1, \; s = 3.0$$

From figure 3.7, it can be seen that for the improved algorithm (with-a, without-b diversity control), all object fitnesses converge to a global optimum before 650 generations; but for the basic algorithm, complete converge occurs after 900 generations.

Comparing between improved algorithm with and without diversity control, it can be seen that the addition of diversity control may cause the convergence rate to slow over the first 20% of the evolution. However, the overall convergence rate is essentially unchanged (650 generations), and because diversity control forces the algorithm to more widely explore the global search space, the result is a more robust solution. From figure 3.8, it can be validated that the improved algorithm with diversity control maintain a high diversity level during the initial 20% of the evolution (the first 200 generations); the abrupt drop of the diversity level in figure 3.8(c) after 200 generations is due to the algorithm having collected enough global information to move on in the optimum direction very deterministically.

Test Function 2: Rastringin's function:

The Rastringin's function is written as:

$$f_{\min}(\vec{x}) = \frac{1}{n}\sum_{i=1}^{n}\left[x_i^{\,2} - 10\cos(2\pi x_i) + 10\right]$$

given condition $n = 5$, and

$x_i \in [-0.12, 0.12]$, $i = 1,2,3$;

$x_j \in [-1.12, 1.12]$, $j = 4,5$.

The known best solution is:

$$f_{\min}(v) = f(\vec{0}) = 0$$

The genetic coefficients are chosen as following:

$NGeneration = 1000$,

$NPopSize = 32$,

$NVariable = 5$,

$NUpdate = 50$

$P_c = 0.2$, $P_m = 0.1$, $s = 3.0$

From figure 3.9, comparing the average object fitness performance, the improved algorithm with diversity control approaches zero more rapidly than the algorithm without diversity control. Likewise, the improved algorithm without diversity control is better than the basic algorithm. Also, comparing with 3.9 (a) and (b), it can be easily seen that the improved algorithm without diversity control converges more rapidly than the basic algorithm if does not get trapped into the local optimum (a robustness issue). Comparing 3.9 (b) and (c), it can be seen that improved algorithm with diversity control makes the algorithm more robust as it is not trapped easily into the local optimum. The high diversity level can be further confirmed in figure 3.10.

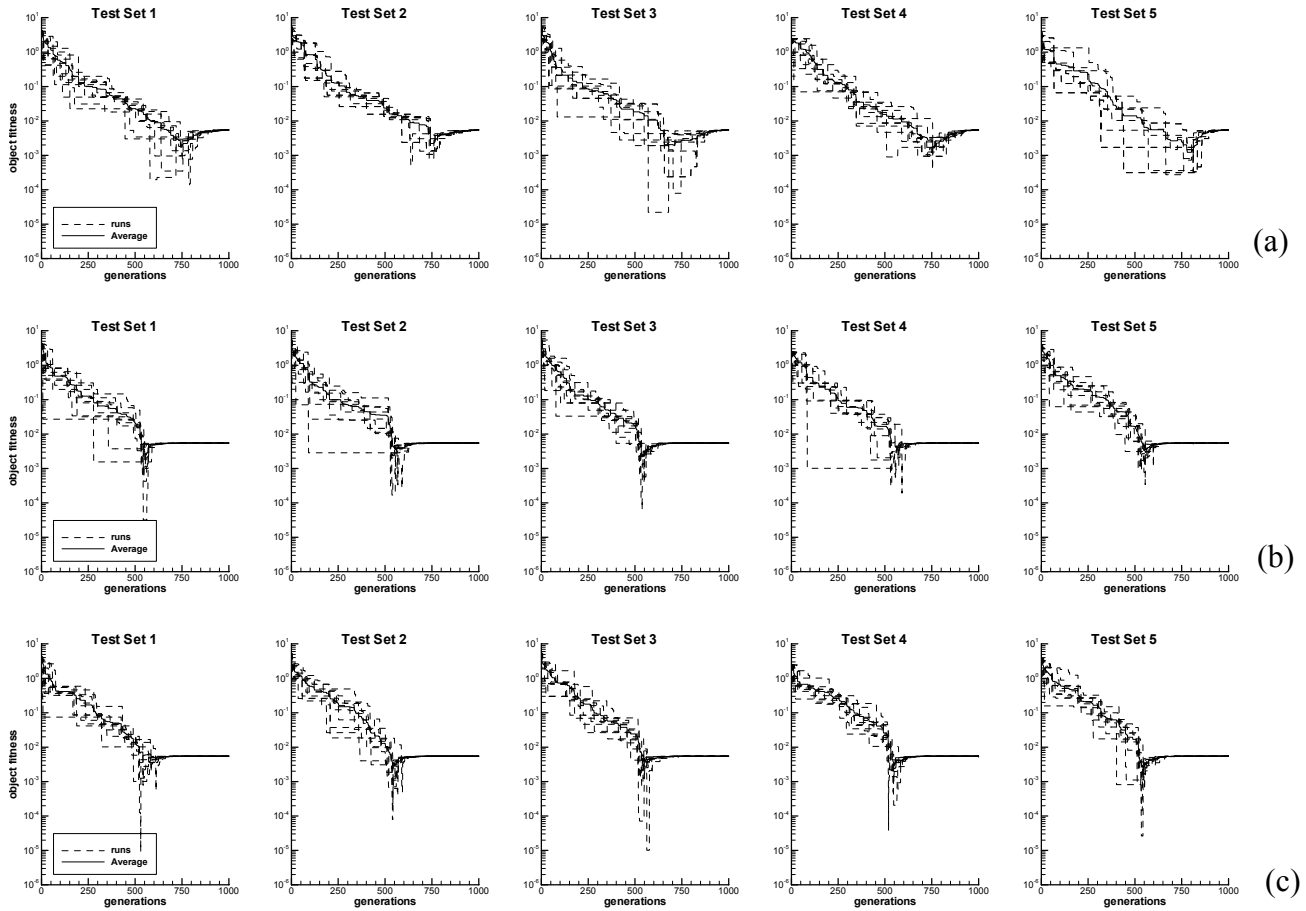

Figure 3.7 Object fitness comparison between basic algorithm and improved algorithm without/with diversity control, Ackley's Function: (a) basic algorithm, (b) improved algorithm without diversity control, (c) improved algorithm with diversity control

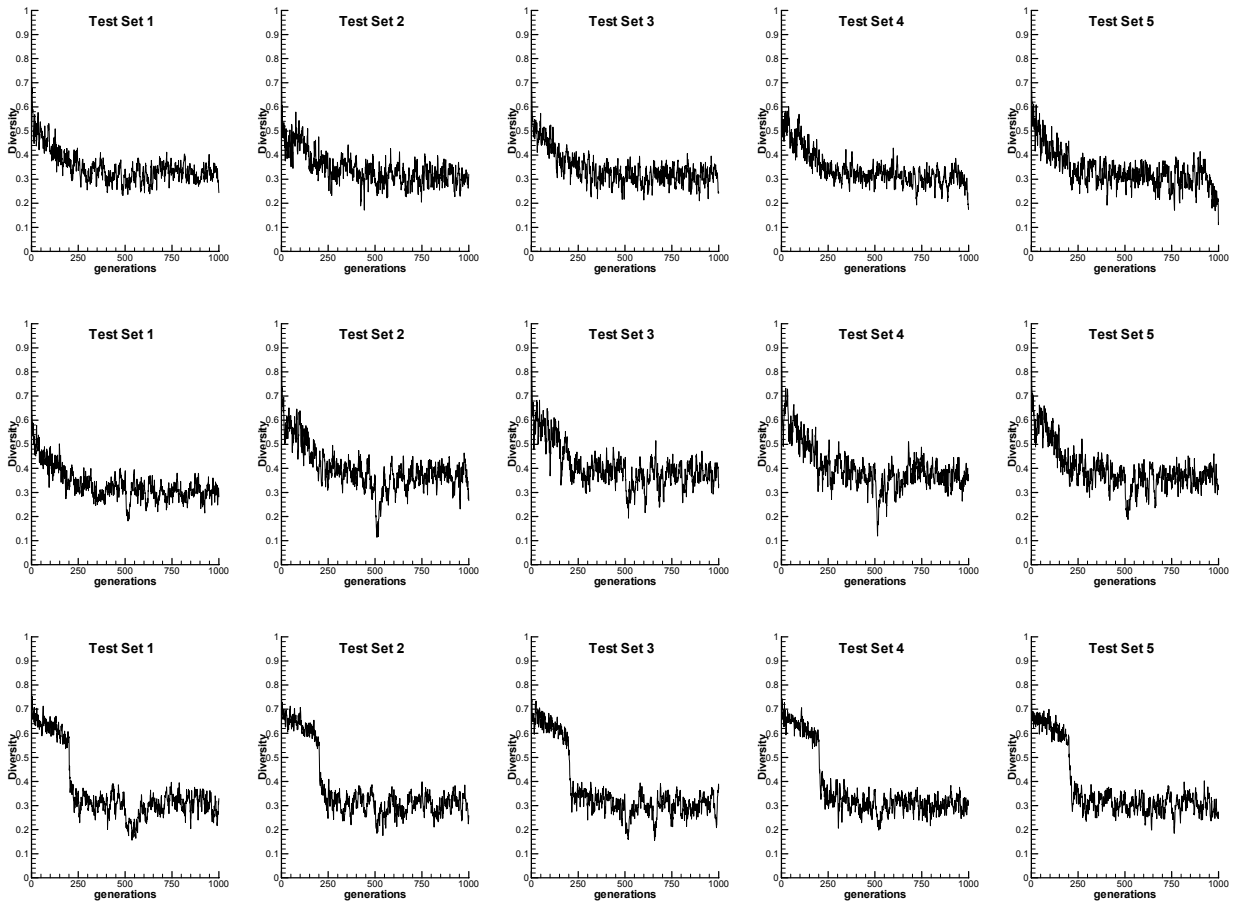

Figure 3.8 Diversity comparison between basic algorithm and improved algorithm without/with diversity control, Ackley's Function: (a) basic algorithm, (b) improved algorithm without diversity control, (c) improved algorithm with diversity control

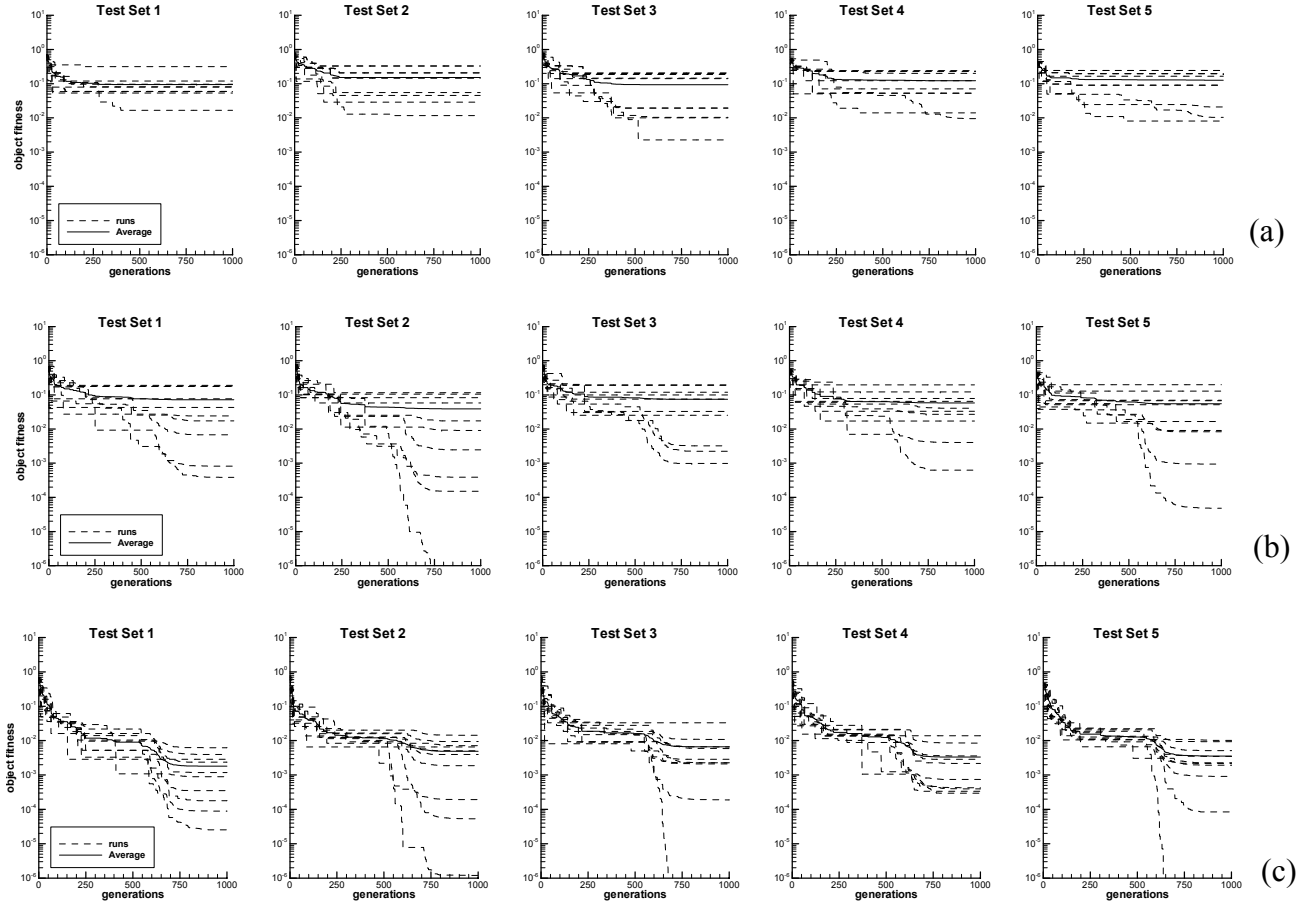

Figure 3.9 Object fitness comparison between basic algorithm and improved algorithm without/with diversity control, Rastringin's Function: (a) basic algorithm, (b) improved algorithm without diversity control, (c) improved algorithm with diversity control

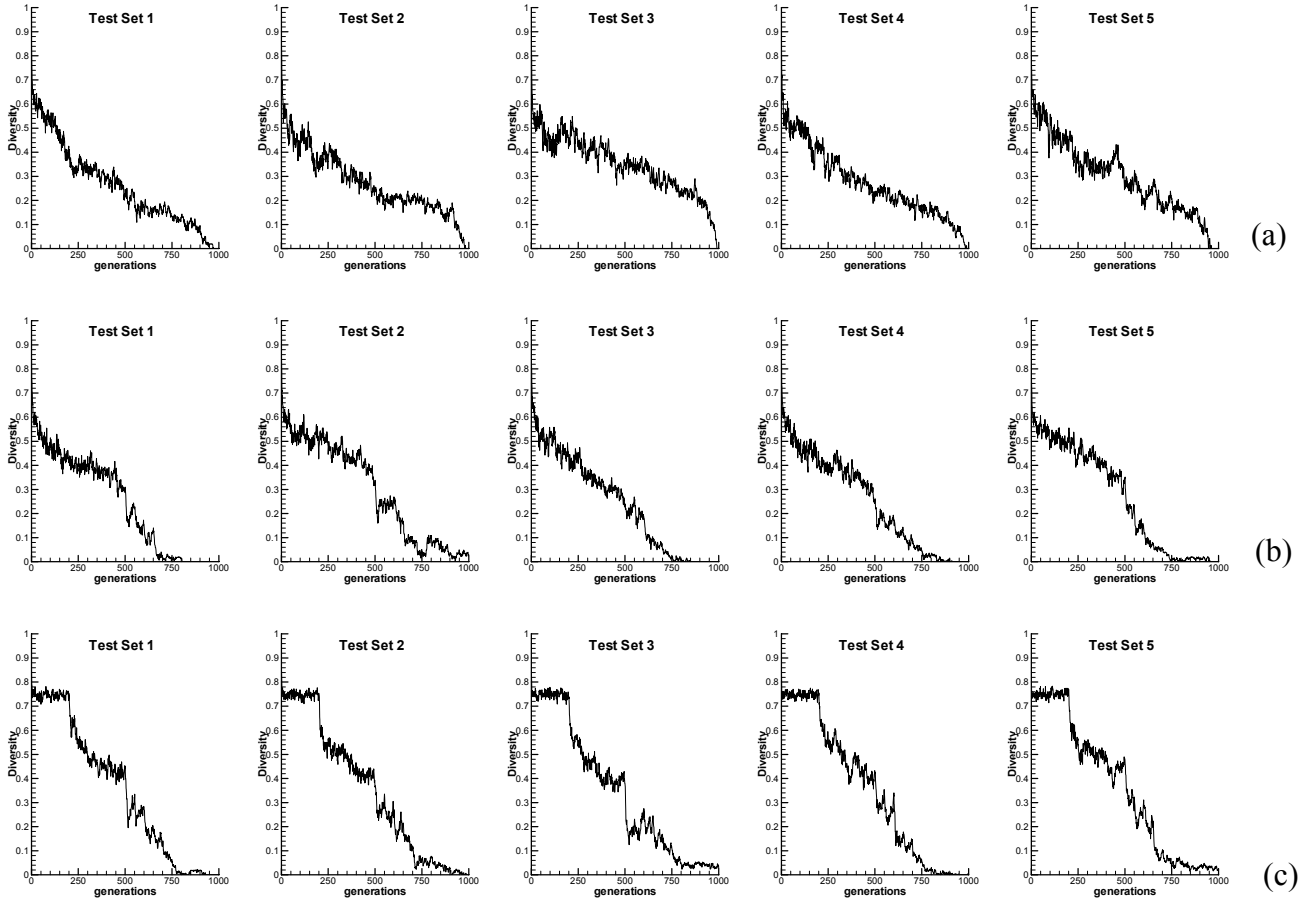

Figure 3.10 Diversity comparison between basic algorithm and improved algorithm without/with diversity control, Rastringin's Function: (a) basic algorithm, (b) improved algorithm without diversity control, (c) improved algorithm with diversity control

Chapter 4

Single Suction/Blowing Jet Study

In order to design a two jet control system and understand the optimization process, we first study the single Suction/Blowing Jet system.

4.1 Case Setup

4.1.1 Numerical Scheme

All computations in the present paper were performed with the CFD code, GHOST. GHOST is an in-house CFD code developed at the University of Kentucky by P. G. Huang. The code is based on a finite volume structured formulation with chimera overset grids. The QUICK and Total Variation Diminishing (TVD) schemes are applied to discretize the convective terms in the momentum and turbulence equations, respectively. The central difference scheme is used for the diffusive terms and the second order upwind time discretization is employed for the temporal terms. This code has been tested extensively and is routinely used for turbulence model validation [79] [80] [81]. The turbulence model used in the present computation is Menter's Shear Stress Transport (SST) two equation model [82], which provides excellent predictive capability for flows with separation [83]. The multi-block and chimera features of the code allow the use of

fine gird patches near the jet entrance and in regions of highly active flow. The code also employs MPI parallelization to allow different computational zones to be solved on different processors. The single blowing/suction jet studies are performed on the PC cluster KFC2 (48 Athlon 2000+ XP CPU), constructed by the CFD group at the University of Kentucky. Each case requires 15 processors, so three cases can be evaluated at the same time on the cluster.

The Reynolds number being investigated in the present computations is 500,000; therefore, a fully turbulent flow is reasonably assumed and no transition is involved in the computation. Because the focus of the current investigation is the control of the flow separation through blowing and suction jets, an incompressible Navier-Stokes solver is used to eliminate additional uncertainties caused by compressibility effects.

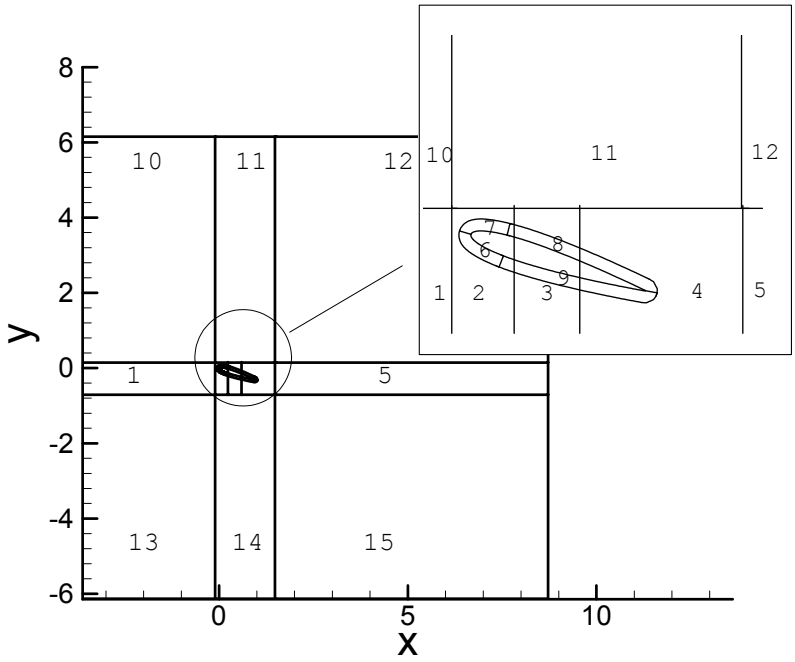

Figure 4.1 Multi-Zonal (blocks) grid, total of 15 blocks

4.1.2 Grid Setup

The basic grid without jets implemented on the airfoil is set up as 15, two-dimensional multi-zonal blocks (figure 4.1). The grid of the NACA0012 airfoil is decomposed into 4 blocks (blocks 6-9), overlapping on 3 background blocks; another 8 peripheral blocks surround the 3 background blocks. The dimensionless outer boundary of the computational area is chosen as $A_H \times A_W = 12c \times 12c = 12.0 \times 12.0$, large enough to prevent the outer boundary from affecting the near flow field around the airfoil.

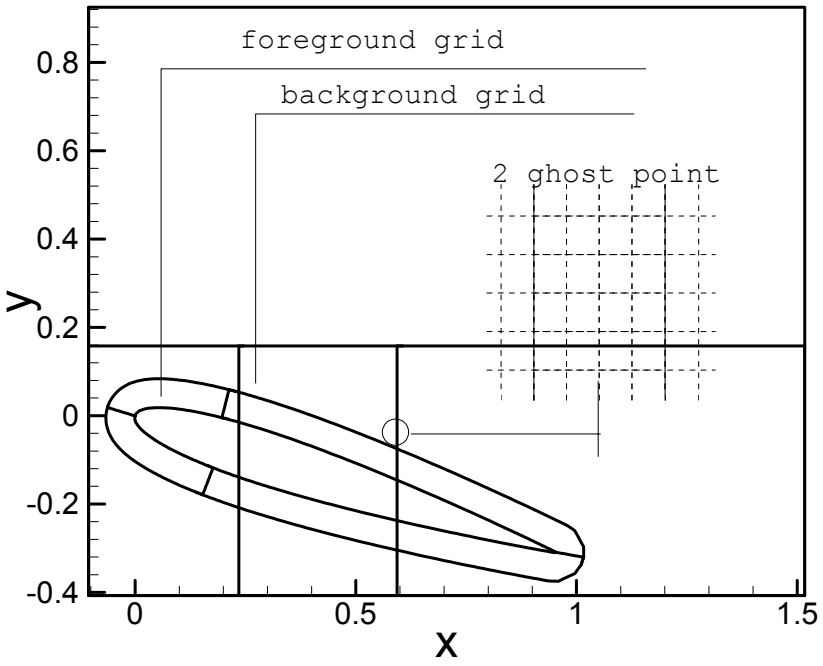

Figure 4.2 Layout of foreground grid and background grid, where 4 foreground airfoil blocks overlap on 3 background blocks; information in the covered area of the background blocks are interpolated from the foreground blocks, adjacent block information is exchange

On the outer boundary, the left (inlet) boundary is fixed with a uniform dimensionless inlet velocity $u_\infty = 1.0$, the upper and lower boundary condition are "free-stream" boundaries which satisfy the Neumann condition, and the right (outflow) boundary condition is set to a zero velocity gradient condition. For the airfoil blocks, the inner boundary condition is a no-slip wall boundary condition, and the outside boundary is set to "overlap" which allows the background grid points being overlapped by the airfoil block grid points to interpolate values from the foreground airfoil grid points. Computation information between adjacent blocks is exchanged by two ghost points (figure 4.2). All the parameters chosen in the computation are dimensionless. A special attempt was made to ensure that the near wall y+ values of the airfoil blocks were kept within 0.5.

Airfoil blocks and their background blocks are the most sensitive computation areas; hence, the number of grid points in these blocks is most critical. To test for grid independence, three sets of grids, with increasing grid density (labeled 1, 2, and 3), are studied and their results are listed in Table 4.1. These grids are studied under a Reynolds number of 500,000 and computational results for different angles of attack are compared in Table 4.2 and figure 4.3. The differences in the computational results between set 1 and set 2, and between set 2 and set 3, are less than 2%. In order to maintain grid resolution consistency at different jet locations and relatively high grid resolution at the jet (dimensionless jet width of 0.025, grid resolution of 0.001), the relatively dense grid of set 2 is adopted in the current computation.

Present over-set, multi-block grids give us the freedom to zoom into the flow field around the suction and blowing location to investigate the flow patterns and corresponding properties. The number of grid points in set 2 is about 210,000 and the computation time is around 2 hours on 15 processors for each case.

Table 4.1 Coarse grid and dense grid comparison

Block number	1 (i*j)	2 (i*j)	3 (i*j)
1	55*70	110*140	110*200
2 (background)	70*70	140*140	200*200
3 (background)	55*70	110*140	150*200
4(background)	70*70	140*140	200*200
5	55*70	110*140	110*200
6 (airfoil)	54*25	107*50	148*75
7 (airfoil)	54*25	107*50	148*75
8 (airfoil)	70*25	120*50	220*75
9 (airfoil)	70*25	120*50	220*75
10	55*70	110*140	110*140
11	70*70	140*140	140*140
12	55*70	110*140	110*140
13	70*70	110*140	110*140
14	70*70	140*140	140*140
15	55*70	110*140	110*140

Table 4.2 Coarse and dense grid C_l and C_d comparison

α	1 C_l	2 C_l	3 C_l	1 C_d	2 C_d	3 C_d
0	0.001041	0.001325	0.001044	0.015655	0.015959	0.015820
2	0.189010	0.189645	0.189743	0.017108	0.017373	0.017036
5	0.463010	0.462302	0.462325	0.024201	0.024530	0.024260
10	0.853619	0.855687	0.857277	0.052585	0.052528	0.052540
12	0.958216	0.969597	0.963591	0.071107	0.071038	0.068659
14	1.016713	1.022523	1.015824	0.095095	0.093348	0.089901
16	0.974193	0.996049	0.977925	0.124510	0.122691	0.118370
18	0.856149	0.875904	0.897605	0.168011	0.166208	0.169420

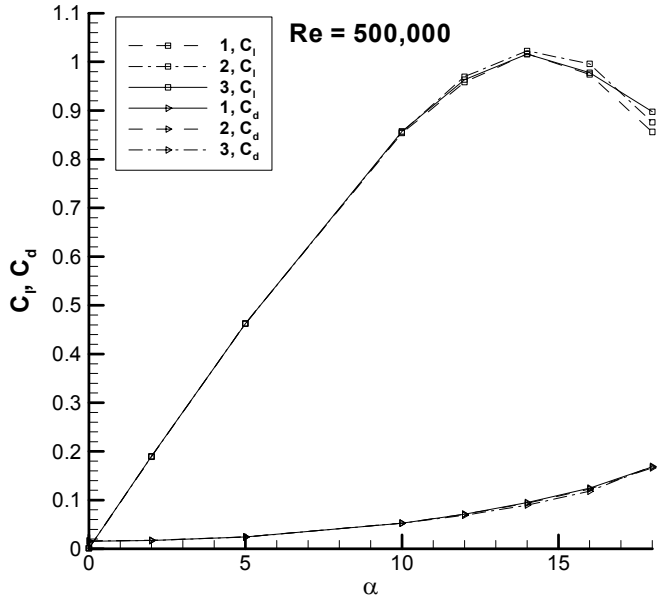

Figure 4.3 Grid independence study of the grids in Table 4.1 under Re=500,000 condition

Even though the current paper mainly focuses on suction and blowing under an angle of attack of 18^0, we do further computation both lower and beyond 18^0 to confirm the

quality of our model. We first compare our computation results at low angle of attack ($\alpha \le 10^0$) with the experimental data ([2][3][4]) in table 4.3. First, it can be seen that the computation results are near the experimental data of E. Jacobs [4]. Second, it can be seen that most of all the experimental data are higher than computation results. The reason can be attributed to the closer wall effects in experiment which lead to the increase of lift.

At higher angle of attack of 20^0, the lift and drag coefficient of computation do not converge to a stable value, hence a time dependent version of GHOST is applied. The results vary periodically, which is similar to the result of Wu et al.[51] for large angle of attack. Therefore, in figure 4.4, computational results above 18^0 are plotted with an upper and lower value boundary; they are also compared to computational results of Wu et al. and three sets of experimental data ([2], [3], [4]), all at Re=500,000.

Table 4.3 Comparison of computation results and experimental at $\alpha \le 10^0$

Angle of Attack α	Computation Results	Experiment Sheldahl [2]	Experiment Critzos [3]	Experiment E. Jacobs[4]
0	0.001325	0	0	0
2	0.189645	0.22	0.23	0.18
5	0.462302	0.55	0.6	0.45
10	0.855687	1.00306	0.95	0.9

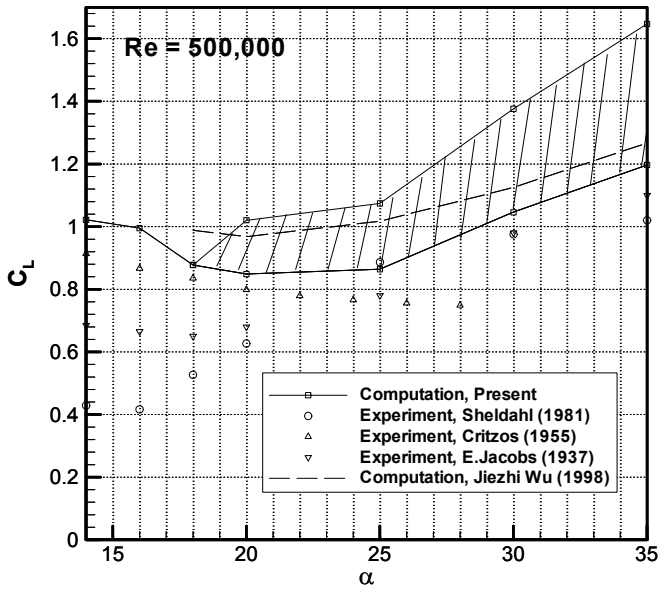

Figure 4.4 Comparison between computation data and experiment data at Re=500,000

It can be seen from the figure that the experimental data from sources 1, 2, and 3 vary widely, implying a large amount of experimental uncertainty. This uncertainty is attributable to several factors. As suggested by numerous researchers, different flow regimes can occur depending on Reynolds number, angle of attack (α), and airfoil geometry. Based on our survey of previous research, for the given NACA0012 airfoil at an angle-of-attack around 14^0 (a starting stall angle) and Reynolds number 500,000, the flow may fall into the low-frequency regime as proposed by Zaman et al. [84] where effects of both angle of attack and Reynolds number are strong. First, in the vicinity of an angle of attack at 14^0 (angles before the deep stall angle 18^0), the flow can naturally switch between stall and non-stall, and between steady attached and steady separated flow. Second, at Re=500,000 the flow regime is one where laminar separation is still possible. Therefore, this flow regime and its vicinity remain a challenge for both experimental measurement and computation prediction.

Given these Reynolds number concerns and assuming no transition, computations have also been performed on both a lower and higher Reynolds number than 500,000. Results at different Reynolds number in figure 4.5 demonstrate that the stall starts consistently around 14^0. The maximum C_l for Re=500,000 and 1,000,000 are consistent with the maximum C_l of NACA, TN-1945 cited by Wu et al.[51]; the C_l for the Re=100,000 case is different from the proposed correlation value, partly because no transition is assumed in the present computation, and partly because of the natural complexities of this regime.

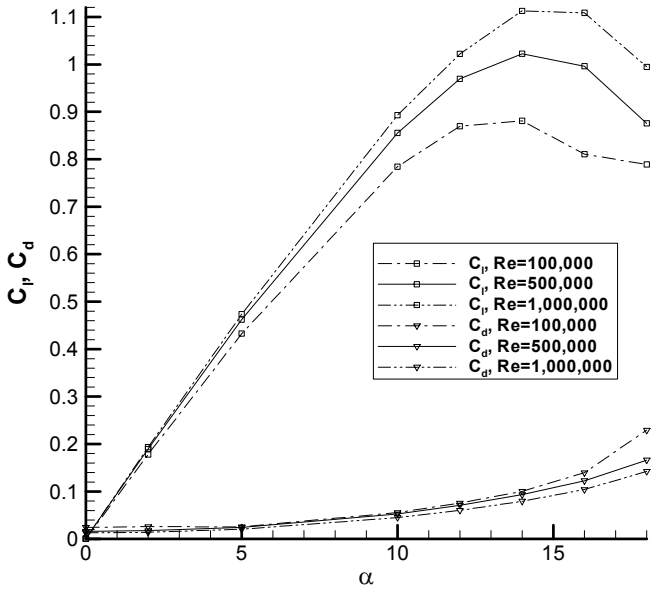

Figure 4.5 Computation results at Re=100,000, 500,000, 1000,000

In addition to the complexities and difficulties of this regime, the differences between the experiment and numerical simulation results over the NACA airfoil can also be attributed to other factors and errors which exist both on the experimental side and the numerical simulation side. On the experimental side, error in airfoil model, installation disturbance of measurement devices, interference between wind-tunnel wall and airfoil body, and

free-stream turbulence and boundary-layer trips effects can create errors in the measurements. On the numerical simulation side, turbulence models, artificial viscosity, grid density, and the limitations of two-dimensional simulation can produce computational inaccuracies. Also, different turbulence models, as well as their different combinations with various numerical schemes, could lead to qualitatively different predictions for separated flows. A detailed explanation of potential experimental errors can be found in the discussion of E. Jacobs et al. [4] and W. J. McCroskey [85], and a heuristic discussion of numerical simulation limitations can be found in Wu et al. [51]. Despite these challenges, present computation results fall within the range of data used in previous published studies; therefore, we argue that these results can at least be used for qualitative understanding of the underlying flow physics and control mechanism.

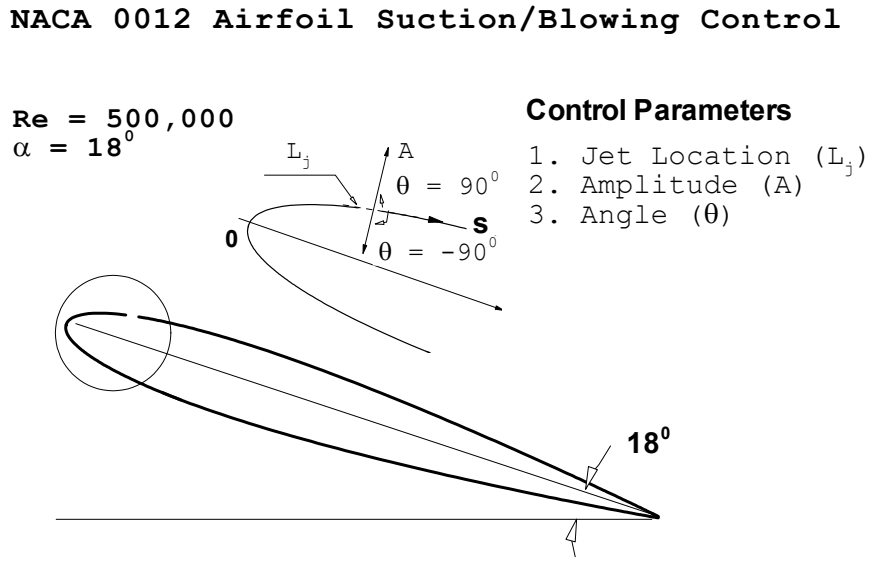

Figure 4.6 Three control parameters: Jet Location (L_j), Amplitude (A), Angle (θ)

4.1.3 Parameter Selection

While most of the previous research has focused on suction or oscillatory blowing on the leading edge, studies about blowing and suction control separately in a wider scope are less frequent. This information is important for understanding the basic control effects. Therefore, a sensitivity study of suction and blowing on the control of a NACA0012 airfoil is performed. Three parameters (figure 4.6) are selected in the current investigation, namely, jet location L_j, suction/blowing amplitude A, and suction/blowing angle θ. The jet width for both suction and blowing is fixed at 2.5% chord length based on a study [30] by Dannenberg, who showed that an increase of suction area beyond 2.5% chord length will not increase lift significantly. For this 2.5% chord length jet, we use 25 grid points along the span as compared to 5 points of Wu et al.'s implementation; we believe the grid density of Wu et al. is not sufficient for such simulation. The reason why the jet width currently chosen is not smaller than 2.5% is because a smaller jet will increase the computation grid size and computation cost and will not give more profits to this control study, which is the first approach to qualitative and systematic study of the blowing and suction control parameters.

In our numerical investigation, the jet entrance velocity is set as

$$u = A \cdot \cos(\theta + \beta)$$

$$v = A \cdot \sin(\theta + \beta)$$

where β is the angle between the free-stream velocity direction and the local jet surface, and θ is the angle between the local jet surface and jet entrance velocity direction. Note

that negative θ represents suction condition and positive θ indicates blowing condition. For perpendicular suction, θ is -90^0 and for a perpendicular blowing, θ is 90^0. The range of jet entrance velocity amplitude is selected to be from 0.01 to 0.5 of free-stream velocity. This range corresponds to a jet momentum coefficient, C_μ,

$$C_\mu = \frac{\rho \cdot h \cdot v_j^{\,2}}{\rho \cdot c \cdot u_\infty^{\,2}} = \frac{h}{c} \cdot A^2 \text{, and } \frac{h}{c} = 0.025$$

of 2.5×10^{-6} to 0.00625. It has been proposed [41] that a jet momentum coefficient C_μ around 0.002 is necessary to have some impact on the flow pattern. The jet location L_j is varied from 3% to 80% of the NACA 0012 airfoil's upper surface. This range covers more of the airfoil length than those used in previous experimental and numerical studies. All cases are under Reynolds number 500,000 and angle of attack 18^0 conditions.

Table 4.4 Parameters of the four series of numerical simulations

	Jet Location L_j	Amplitude A	Angle θ
First Run (64)	0.1, 0.333, 0.567, 0.8	0.01, 0.173, 0.337, 0.5	-90, -30, 30, 90
Second Run (32)	0.05, 0.075, 0.1, 0.125	0.01, 0.073, 0.137, 0.2	-90, -30
Third Run (64)	0.03, 0.04, 0.05, 0.06	0.01, 0.073, 0.137, 0.2	0_+, 30, 60, 90
Fourth Run (128)	0.2, 0.286, 0.371, 0.457, 0.543, 0.629, 0.714, 0.8	0.01, 0.073, 0.137, 0.2	0_+, 30, 60, 90

4.2 Computation Results and Analysis

There are four rounds of numerical simulations performed in current study, and the computations are carried forward according to our target area of interest. The values chosen for each round are given in Table 4.4. In order to address the different mechanisms that govern suction and blowing, computation results for these two alternatives are presented and discussed separately.

4.2.1 Suction Jet Study

In figure 4.7, predicted lift and drag coefficients are compared for $0.01 < A < 0.5$, $0.1 < L_j < 0.8$ and $\theta = -90^0, -30^0$. The lift and drag coefficients are normalized by their corresponding values in the baseline case (no suction or blowing, $C_l = 0.875904$ and $C_d = 0.166208$ at Re=500,000 and $\alpha = 18^0$). It can be concluded from these computation results that: (1) perpendicular suction (-90^0) has the largest impact on the increase of lift coefficient; (2) suction at location 0.1 is better than further downstream; (3) lift increases as suction amplitude increases above an amplitude of 0.01; below 0.01, the flow does not appear to be significantly affected by the suction.

In order to further explore the flow control patterns of different locations, we plot the results for $L_j = 0.1, 0.333$ and 0.567 at $A = 0.173$ and $\theta = -90^0$ in figure 4.8 and compare them with the baseline case. The streamlines of these three cases all clearly demonstrate a smaller separation bubble on the surface of the airfoil than the baseline case. In figure 4.8(a), when suction is applied near the leading edge ($L_j = 0.1$), the separation is most

effectively delayed and hence the separation bubble is much smaller than in the other cases. At $L_j = 0.567$, the only control effect of suction is to break the separation bubble

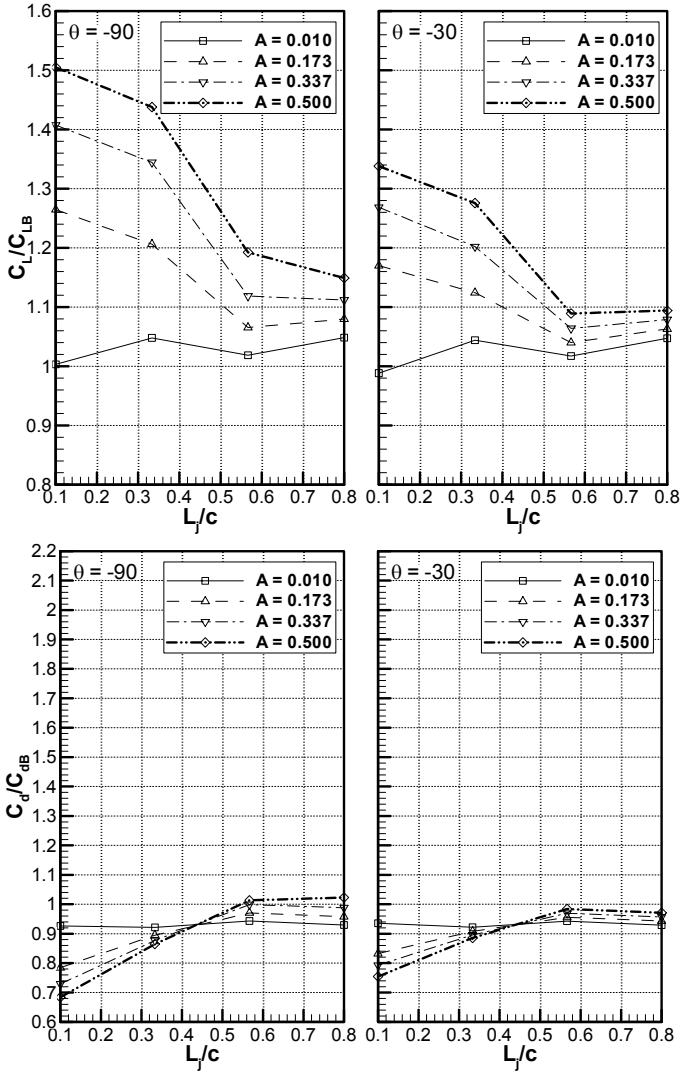

Figure 4.7 Suction computation results of initial single jet study, $0.1 \le L_j \le 0.8$, $0.01 \le A \le 0.5$, $\theta = -90^0, -30^0$

into two smaller separation bubbles, but the lift increase is less than that for suction at location 0.1. It can be observed from figure 4.8(b) that the pressure change near the leading edge area is significant, and leading edge suction changes the upper surface low pressure zone more efficiently than downstream suction. Therefore, a location near the

leading edge is the most effective place for a suction jet to manipulate the boundary layer in order to increase lift.

In figure 4.9, the effects caused by the changes of suction amplitude are investigated. The suction location is fixed at 0.1 and the suction angle is fixed at 90^{o}. As suction amplitude increases from 0.01 to 0.2, the flow becomes more attached to the surface and a larger and lower pressure zone is created at the leading edge. The corresponding separation bubble also continues to decrease to where it is effectively eliminated at amplitude of 0.2. For amplitude greater than 0.2, the separation bubble remains suppressed; further increase in the lift coefficient is due to the continually decreasing pressure zone near the leading edge rather than changes in the downstream flow.

Figure 4.10 mainly focuses on the effects of suction near the leading edge. In this numerical study, the suction amplitude is limited to a smaller range: 0.01 to 0.2. As can be seen from the figure, the increase of lift and drag does not seem to be affected by the location of the suction within this range, from $L_j = 0.05$ to 0.125. These results are consistent with several reported numerical and experimental works which demonstrated the effective control locations on the airfoil for suction jets. For example, Dannenberg et al. [30] studied changing porous area suction located between the leading edge to 0.03 chord length on airfoil upper surface. Weiberg [31] et al. studied changing porous area suction located from 0.02 chord length on the lower surface to 0.07 chord length on the upper surface. Gilarranz et al. [41] studied a synthetic jet which is located at 0.115 chord

length on the upper surface. Hassan et al. [53] studied a synthetic jet located at 0.13 chord length on the upper surface.

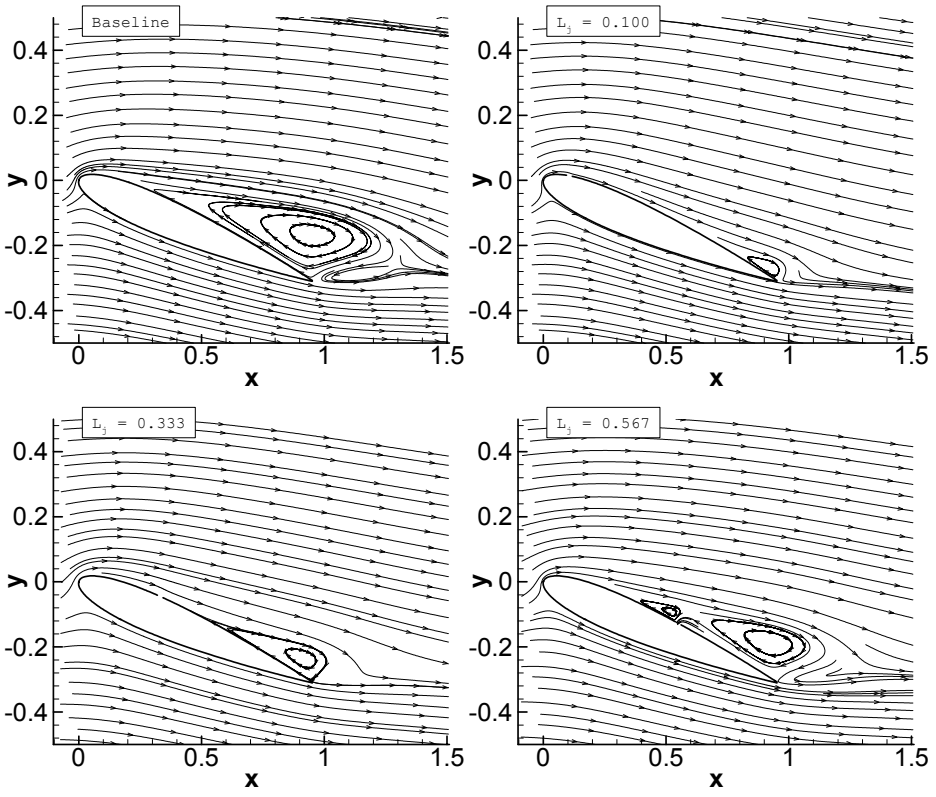

(a)

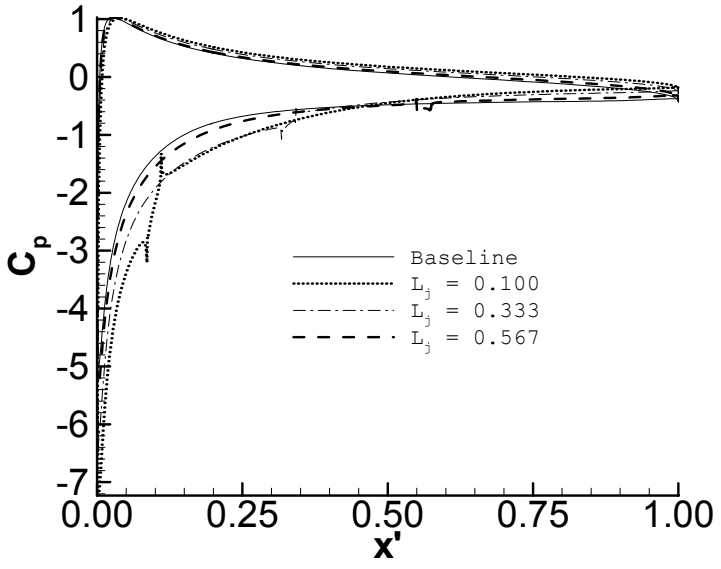

(b)

Figure 4.8 Control effects of suction at different locations , L_j=0.1, 0.333 and 0.567, A=0.173, θ=-90^0

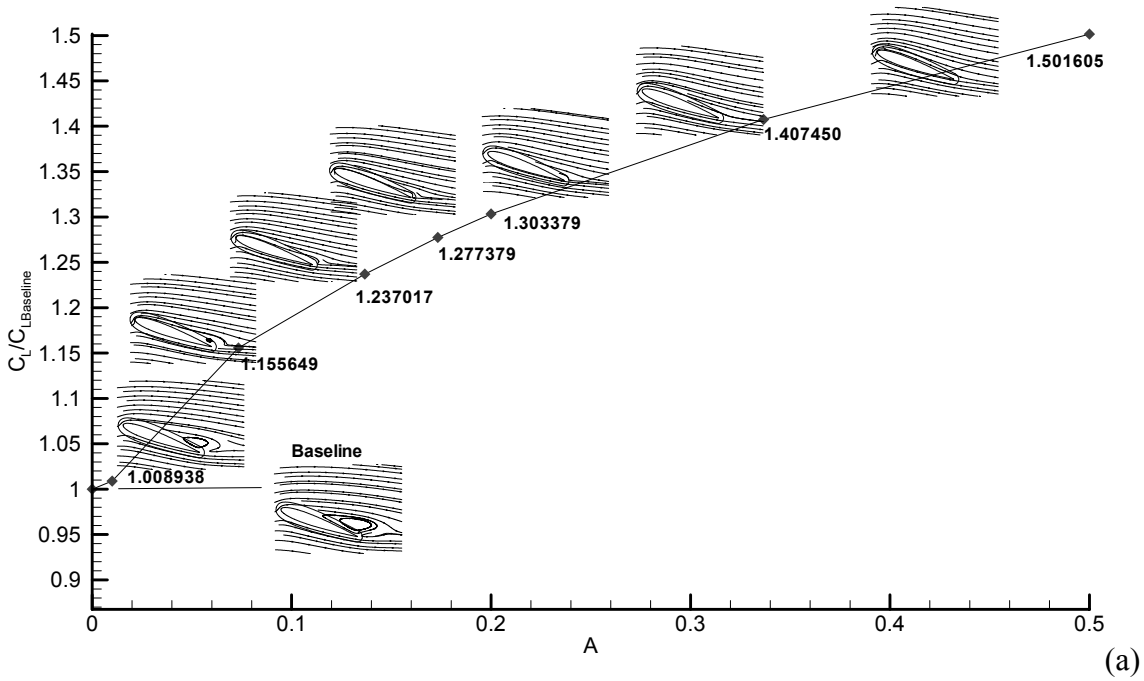

Figure 4.9 Control effects of suction at different amplitudes, L_j=0.1, 0≤A≤0.5, θ=-90^0

4.2.2 Blowing Jet Study

From figure 4.11, the immediate observation regarding blowing effects is that downstream blowing at a smaller angle (30^0) increases the lift and decreases the drag; however, leading edge blowing has the opposite effect, not only decreasing the lift but

also increasing the drag at the same time. Even though leading edge blowing exerts negative effects on the lift and drag coefficients, these effects are much smaller than the favorable effects caused by the jet suction. Therefore, we speculate that for the oscillatory blowing control on the leading edge, such as synthetic jet control, suction period is the dominant factor on increasing the lift and decreasing the drag. Another interesting phenomenon regarding drag is that when blowing amplitude increases near the leading edge, it increases; but downstream, drag decreases with increasing amplitude, although the changes are slight. This observation will be confirmed through further investigation after the blowing location range of interest is narrowed down to the leading edge and downstream region separately.

Blowing control on changing flow patterns at different locations are described in figure 4.12. The results for $L_j = 0.1$, 0.333 and 0.567 are plotted and compared with the baseline case. These cases are all under $A = 0.173$ and $\theta = 90^0$ conditions. It can be observed from figure 4.12(a) that perpendicular blowing at location 0.1 creates a significantly different flow pattern compared with the baseline cases - the separation bubble is significantly larger, and the circulation is larger which makes the pressure after the jet location much lower. It can be correspondingly seen in figure 4.12(b) that the C_p curve with a blowing jet at location 0.1 is different from the baseline case, consistent with the changes of the separation bubble. The C_p value of the upper surface before the blowing jet significantly increases, and although the value after the jet decreases, the end result is a much smaller closed area within the C_p curve. This corresponds to a reduced

lift compared to the baseline case. When blowing is moved downstream to locations 0.333 and 0.567, the separations are more suppressed than leading edge blowing; only far downstream around 0.8 of chord length does blowing have a positive effect on lift as seen in figure 4.11.

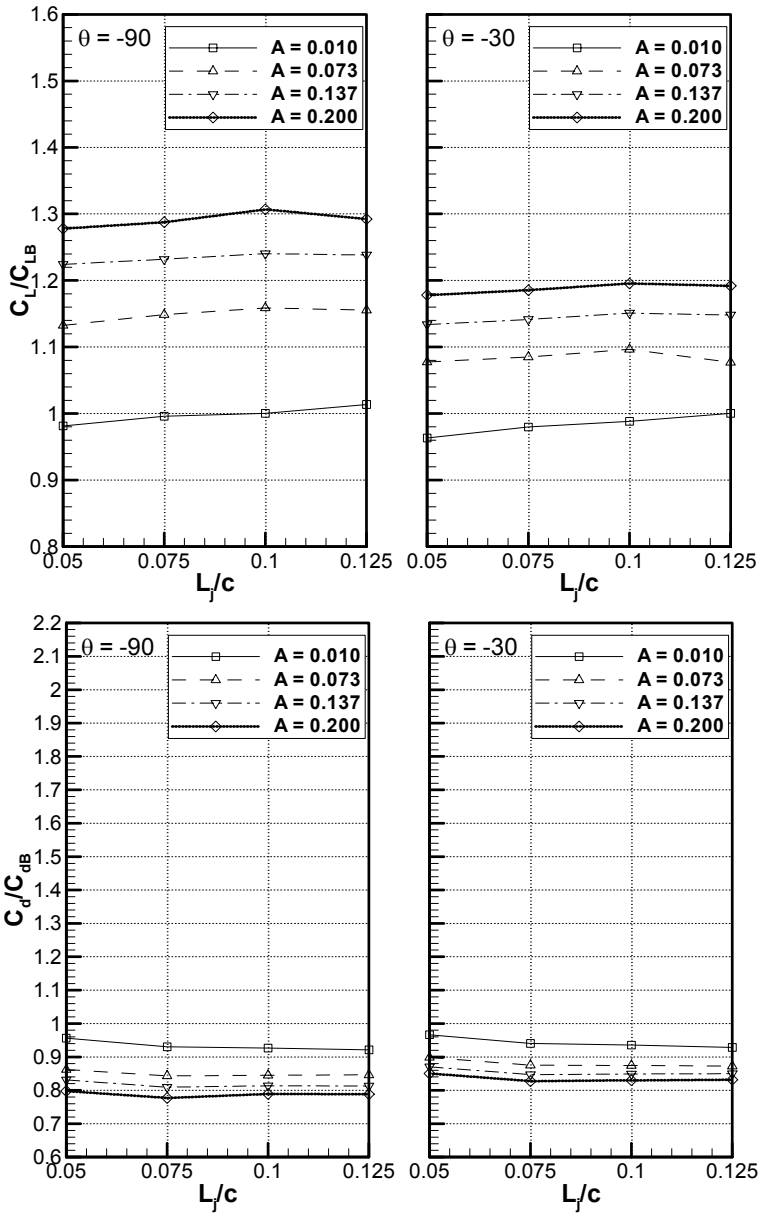

Figure 4.10 Suction computation results on leading edge, $0.05 \le L_j \le 0.125$, $0.01 \le A \le 0.2$, $\theta = -90^0, -30^0$

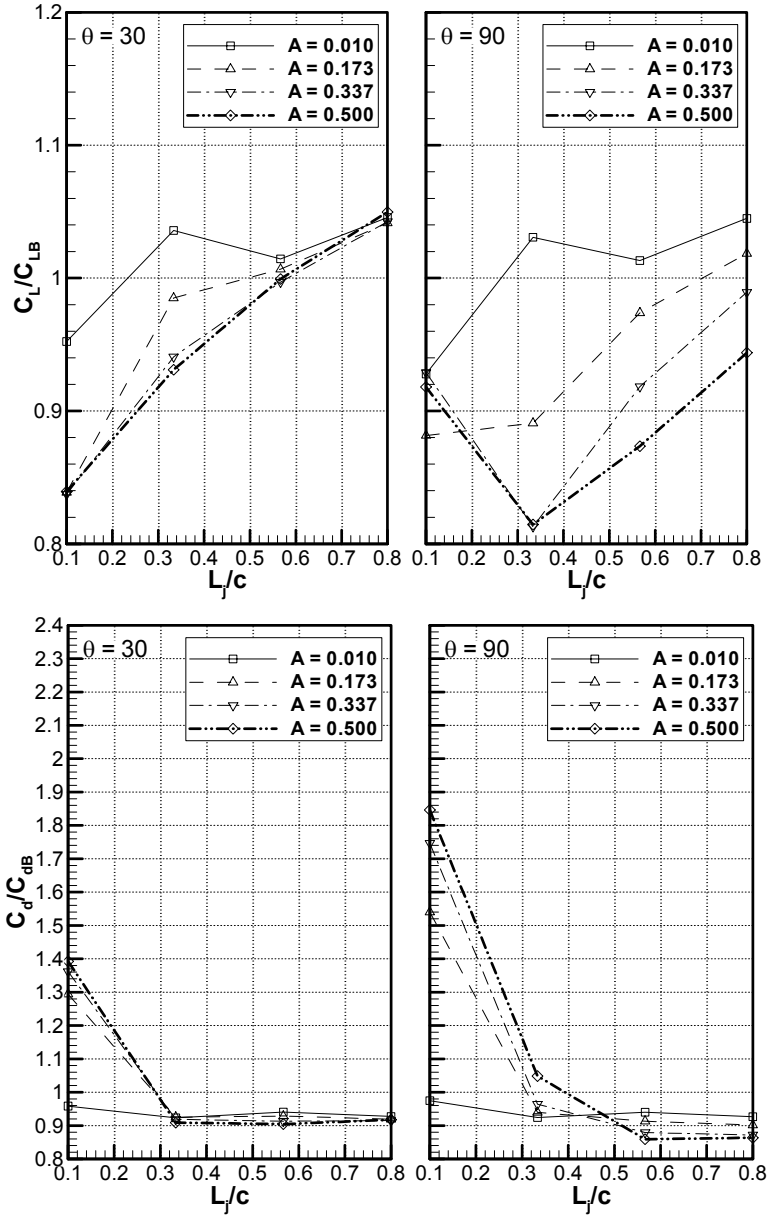

Figure 4.11 Computation results of initial blowing study, $0.1 \le L_j \le 0.8$, $0.01 \le A \le 0.5$, $\theta = 30^0, 90^0$

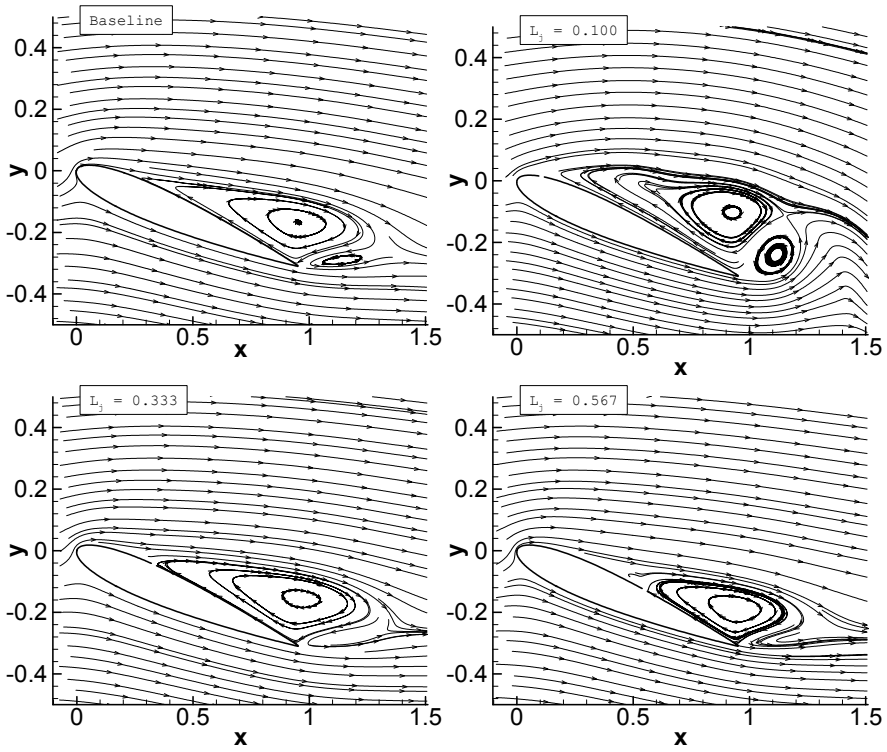

(a)

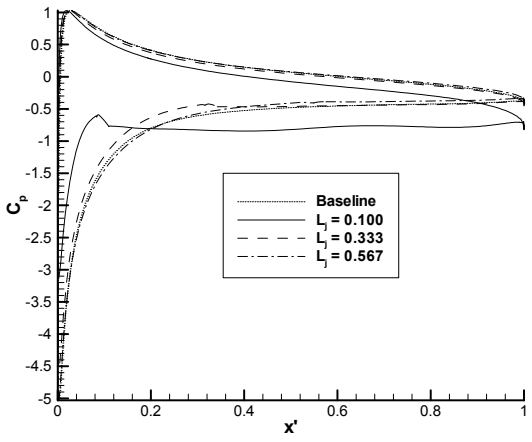

(b)

Figure 4.12 Control effects of blowing at different locations, L_j=0.1, 0.333 and 0.567, A=0.173, θ=90^0

Because we found little discussion of leading edge blowing in previous works, the focus is narrowed down to the effects of blowing near the leading edge in figure 4.13.

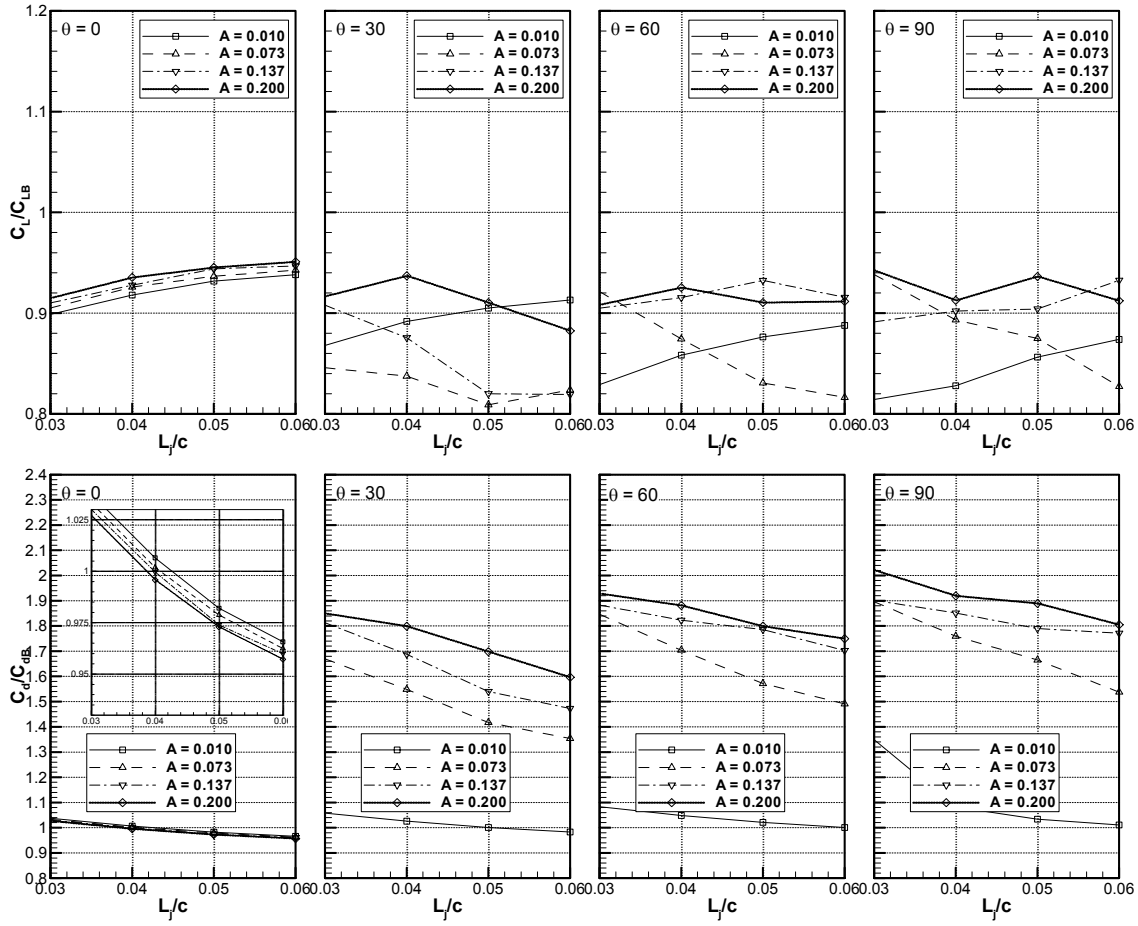

Figure 4.13 Computation results for blowing on the leading edge, $0.2 \le L_j \le 0.8$, $0.01 \le A \le 0.2$, $\theta = 0^0, 30^0, 60^0, 90^0$

It can be easily seen that all of the end results of leading edge blowing control are worse than the baseline cases - all normalized lift values are smaller than 1.0 and most of the normalized drag values are larger than 1.0. There are three driving factors which together explain the lift and drag changes. The first factor is changes in the upper surface pressure (C_p) in the vicinity of the jet due to the direct effect of the blowing. The second factor is increased shear stress near the surface in the vicinity of the jet. The third factor is changes in the overall circulation about the airfoil (Γ) caused by the blowing modifying the flow

around the separation bubble. The first factor increases the pressure on the airfoil upper surface near the leading edge, decreasing the lift and increasing the drag in all of the cases. The second factor increases the drag and decreases the lift due to skin friction. The third factor decreases the airfoil upper surface pressure beneath the separation bubble downstream, increasing lift ($L = -\rho U\Gamma$) when the amplitude increases. Another interesting observation in this figure is that when amplitude increases, the normalized drag of tangential (0^0) blowing decreases slightly (see insert of figure 4.13), but increases in perpendicular (90^0) blowing which is consistent with previous observations in figure 4.11.

To explore the control effects of these driving factors in detail, figure 4.14 illustrates the changes in the flow due to amplitude at the location 0.05 of chord and the angle of 30^0 . It can be seen from the figure that the flow pattern at amplitude 0.01 is essentially the same as the baseline case except that the pressure near the leading edge upper surface is slightly higher due to the blowing; the lift decrease at this point is primarily caused by skin friction effects. When the amplitude goes from 0.01 to 0.073, C_p at the upper surface of leading edge increases dramatically (figure 4.14(b)). Meanwhile the circulation Γ around the separation bubble increases significantly (figure 4.14(c)) which in turn makes the circulation about the airfoil increasingly negative, decreasing the downstream upper surface C_p and thereby increasing the lift. The net effects of these driving factors are that lift decreases and drag increases. For the amplitudes of 0.137 and 0.2, lift increases relative to the 0.073 case. The reason can be found in figure 4.14(b), and 4.14(c). Near

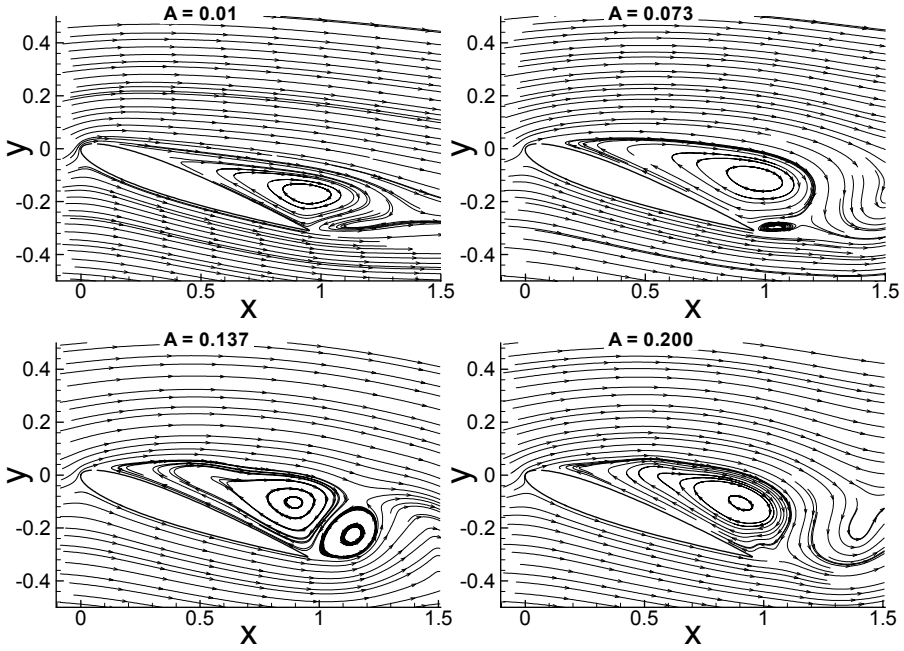

(a)

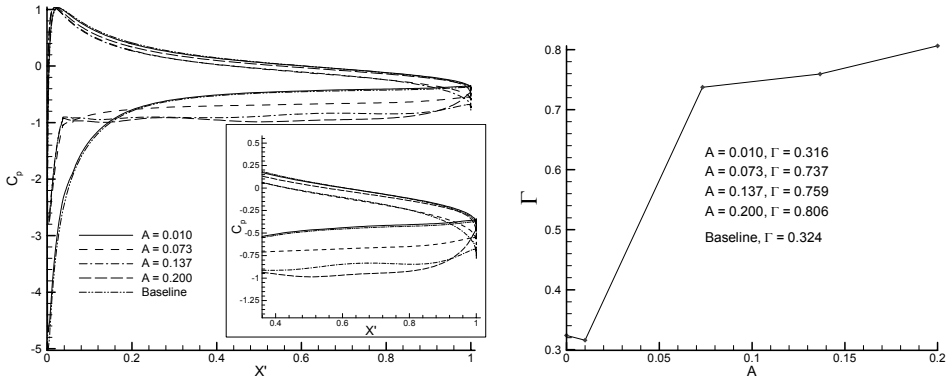

(b) **(c)**

Figure 4.14 Control effects of blowing at different amplitudes, L_j=0.1, 0.01≤A≤0.5, θ=30^0

the leading edge, the upper surface pressure of these three amplitude cases are essentially the same, but the steady increase in circulation about the separation bubble flattens the downstream pressure curve significantly. The gains in lift downstream more than compensate for the loss of lift near the leading edge which means a larger lift. In no case,

however, did the overall lift increase relative to the no-jet baseline due to leading edge blowing.

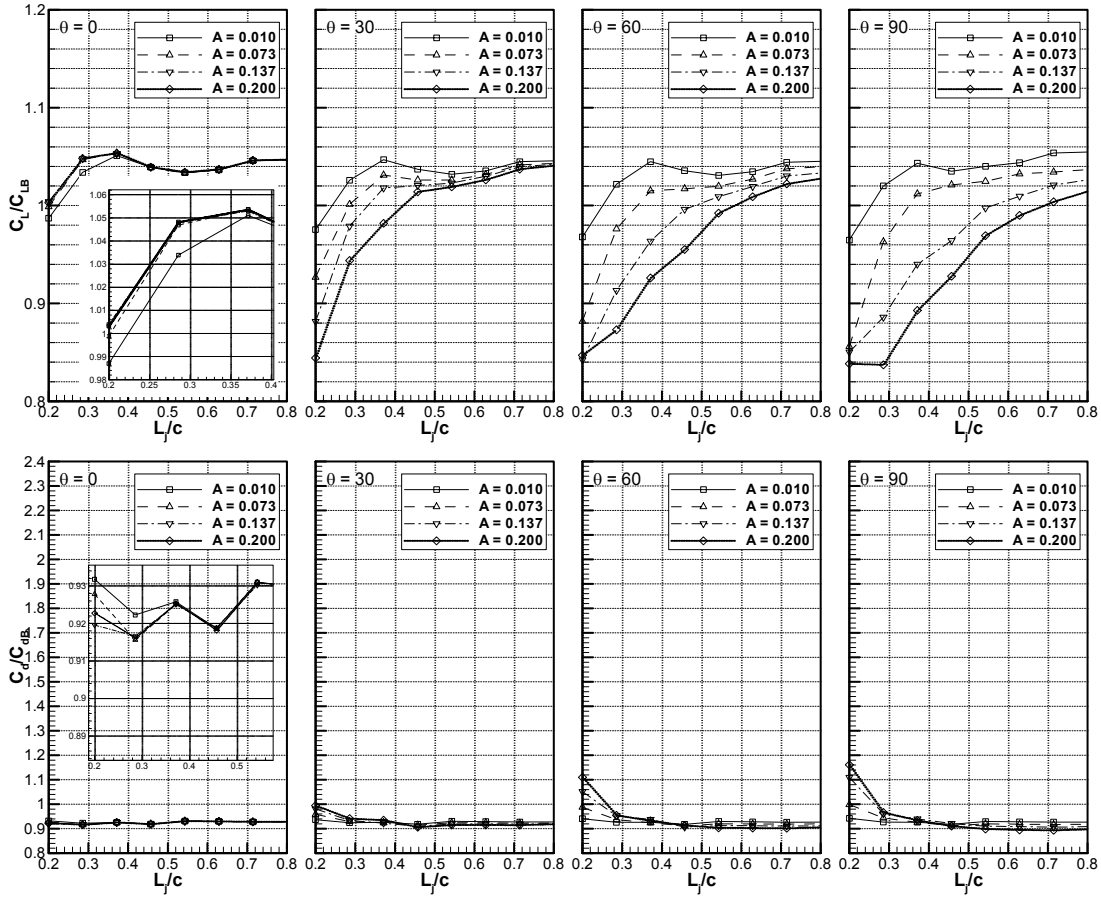

Figure 4.15 Computation results for blowing on downstream, $0.2 \le L_j \le 0.8$, $0.01 \le A \le 0.2$, $\theta = 0^0, 30^0, 60^0, 90^0$

In figure 4.15, the focus is shifted to the effects of blowing downstream, which ranges from 0.2 to 0.8. For downstream blowing, with fixed blowing location and blowing amplitude, tangential blowing is insensitive to amplitude changes and has a larger impact on increasing lift than other angles. These results indicate that there are two locations which are better for increasing the lift, one around 0.371, and the other around 0.8. The first location manipulates the separation bubble; the second location manipulates the

trailing edge vortex circulation. Another important observation in the current figure is that the control effects generated by the smallest blowing amplitude of 0.01 are comparable in terms of drag reduction and generally better in terms of lift enhancement than those of larger amplitudes independent of the blowing angle. Therefore, while at high jet amplitudes, suction is clearly more effective, downstream tangential blowing may be as or more advantageous at a smaller jet amplitude.

4.2.3 Conclusions of Single Suction/Blowing Jet Study

In this chapter, we presented the numerical simulation results of suction and blowing control on a NACA 0012 airfoil at a Reynolds number of 500,000 and an angle of attack of 18^0. By changing three parameters (jet location, amplitude and angle) over a wide range, specific ranges and values of interest have been discovered and analyzed, and the following conclusions have been drawn.

First, from a mechanism perspective, suction is different from blowing. Suction takes the advantage of creating a larger and lower pressure (C_p) zone on the airfoil's upper surface to increase lift, hence the flow is more attached and the profile drag decreases. Blowing is often counter-productive with most control results worse than the baseline case. Leading edge blowing increases lift by generating greater circulation about the separation bubble and about the airfoil, but at the cost of significantly increasing leading edge pressure; therefore, the flow is more detached and the profile drag increases. Downstream blowing can improve lift and drag characteristics, but smaller amplitudes are better than larger amplitudes. Second, from an amplitude perspective, a larger amplitude unsurprisingly

results in a larger impact on the flow field around the airfoil, although for blowing that impact is a negative one in many cases. For perpendicular suction, the optimum control amplitudes range between 0.01 and 0.2—values exceeding 0.2 no longer manipulate the separation bubble for perpendicular suction since the separation bubble is fully suppressed at 0.2. For downstream tangential blowing, smaller blowing amplitudes appear to be the most effective choice. Third, when location and angle considerations are combined, perpendicular suction at leading edge (from 0.075 to 0.125) is better than other suction situations for increasing lift; in the case of blowing, tangential blowing at downstream locations (around 0.371 and 0.8) is better than other blowing situations for increasing lift.

The extensive study presented on the control effects of a single blowing or a single suction jet under different locations, angles and amplitudes. It is not for the purpose of seeding a relative good initial two-jet control generation, rather to apply this knowledge to understanding and examining the final results of the two-jet control system optimization.

Chapter 5

Two Jet System Optimization (I)

5.1 One Suction Jet and One Blowing Jet Case Setup

Our objective in this section is two-fold. First, the optimization process of the two-jet, five-parameter control system is presented and the nature of this optimization process is discussed. Second, the flow properties and physics of the GA-determined optimum results are analyzed and compared with the one-jet suction/blowing results.

5.1.1 Control Parameters Selection

In our previous research on single suction/blowing jet control, three parameters (figure 4.6) are selected in the investigation, namely jet location L_j, suction/blowing amplitude A, and suction/blowing angle θ. The jet width for both suction and blowing is fixed at 2.5% chord length based on a study by Dannenberg [30], who showed that an increase of suction area beyond 2.5% chord length will not increase lift significantly. In the numerical investigation, the jet entrance velocity is set as

$$u = A \cdot \cos(\theta + \beta)$$

$$v = A \cdot \sin(\theta + \beta)$$

where β is the angle between the free-stream velocity direction and the local jet surface, and θ is the angle between the local jet surface and jet entrance velocity direction. Note

that negative θ represents suction condition and positive θ indicates blowing condition. For perpendicular suction, θ is -90^0 and for a perpendicular blowing, θ is 90^0.

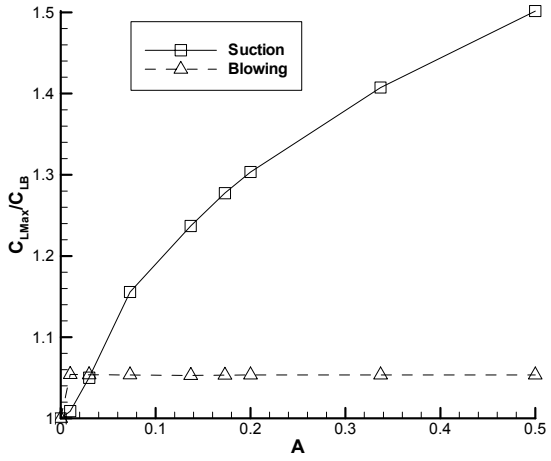

Figure 5.1 Maximum normalized lift at different amplitudes of single suction of single blowing jet control

From the results of previous chapter (figure 5.1), we can see that the maximum normalized lift under different amplitudes between suction and blowing determined from the single jet studies have large differences ─ the control effects of suction are much stronger than blowing. Therefore, in the two-jet control system, we will fix the suction amplitude at 0.03, and let the blowing amplitude change within 0 to 0.2 in order not to have the blowing control effects inundated by the suction control effects. So, for the two-jet control system, the five design parameters and their ranges are chosen as follows:

Suction Location: $0.05 \le L_{jS} \le 0.8$

Suction Angle: $-90^0 \le \theta_S \le 0^0$

Blowing Location: $0.05 \le L_{jB} \le 0.8$

Blowing Angle: $0^0 \le \theta_B \le 90^0$

Blowing Amplitude: $0 \le A_B \le 0.2$

5.1.2 Genetic Algorithm Coefficients and Programming Model

For the optimization of a two-jet control system, the genetic coefficients are chosen as

$NGeneration = 100$,

$NPopSize = 32$,

$NVariable = 5$,

$NUpdate = 8$,

$P_c = 0.2$, $P_m = 0.1$, $s = 1.0$.

The system aggregate fitness function is

$$(Fit_A)_{\max} = a \cdot C_l / C_{lB} + b \cdot C_{dB} / C_d,$$

with $a = 1.0$, $b = 1.0$. Five control parameters – suction location (L_{jS}), suction angle (θ_S), blowing location (L_{jB}), blowing angle (θ_B), and blowing amplitude (A_B), are optimized by the genetic algorithm towards the maximum aggregate fitness value. Of course, the combination of lift and drag effects can be changed by adjusting a and b values to address the different importance of lift and drag for a given search. In the following discussion, "fitness" will refer to "aggregate object fitness".

From figure 5.2, it can be seen that after each new generation is generated on the server, the lift coefficient (C_l) and drag coefficient (C_d) of each individual (candidate solution) is evaluated through the CFD code GHOST (children process) on multiple processors. The main program process uses the "fork()" and "waitpid()" functions to generate and control the children process (evaluating each individual) until the computation of every individual within one generation has finished.

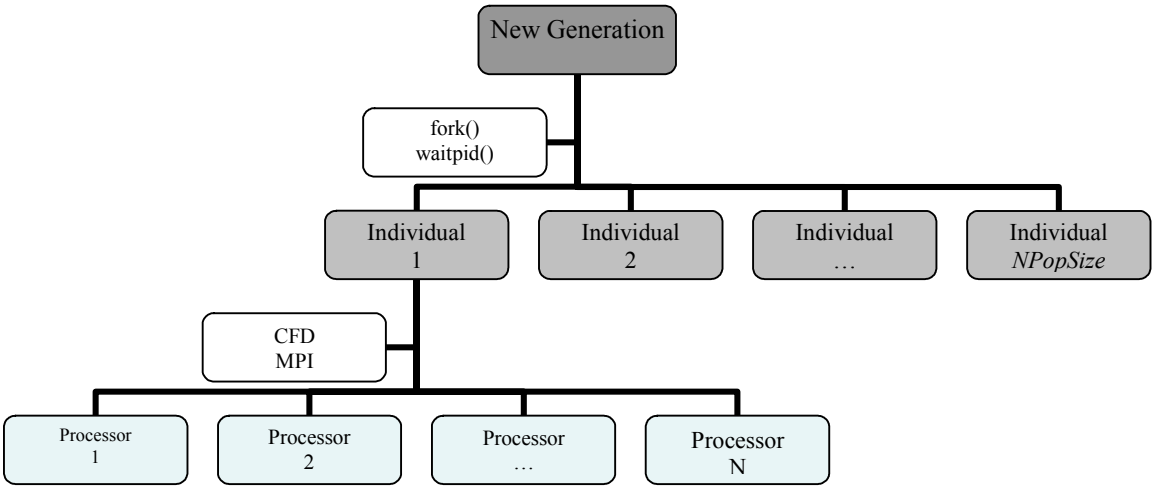

Figure 5.2 Programming Model

5.2 Optimization Process of One Suction Jet and One Blowing Jet System

In this section, we will first present and analyze the two-jet system optimization process using the improved genetic algorithm without diversity control. Then, these results are compared with the results which use the improved genetic algorithm with diversity control; the benefits of diversity control to the improved genetic algorithm can be seen from the comparison.

5.2.1 Understanding of the optimization process

The characteristics of improved genetic algorithm without using the diversity control on optimizing the one suction-jet and one blowing-jet system are shown in figure 5.3, 5.4, and 5.5.

In figure 5.3, both "run-time best fitness" and "offline average fitness" are plotted. Run-time best fitness is defined as the maximum fitness among the fitnesses of all previous and current individuals. Offline average fitness is defined as the average fitness of all previous and current individuals. The 0^{th} generation starts with 32 individuals distributed in an equal space. Within the 0^{th} generation, the average fitness is 1.98 and the maximum fitness is 2.12. Therefore, it can be observed from the figure that offline average fitness curve starts from 1.98 and maximum fitness curve starts from 2.12; the difference between the maximum fitness and the average fitness at the start is 0.14. It can be seen from the run-time best fitness curve that within the first 10 generations, the maximum fitness value rises from 2.12 to about 2.17; from generation 10 to generation 100, the run-time maximum aggregate fitness value rises more slowly, from about 2.17 to about 2.18. The final 90 generations add another 20% improvement compared to the fitness increase in the first 10 generations. Therefore, one might assume that the control parameters do not change much during the last ninety generations. But the continual growth of the offline average fitness indicates that the two-jet control system does undergo notable changes in their control parameter space.

In the current two-jet control system optimization process, after every 8 ($NUpdate$) generations the new generation will be generated according to the best 256 ($NUpdate \cdot NPopSize$) individuals' statistic information; their means (μ) and deviations (σ) are plotted in figure 5.4. Also, in the application, both the lower and upper boundaries are explicitly updated as $[\mu - 5.0\sigma, \mu + 5.0\sigma]$ in every next 8 ($NUpdate$) generations after the 50^{th} generation to trim unnecessary evaluation in not promising

areas. This makes the optimization advance in a more deterministic direction in the second half of the evolution. It can be seen in figure 5.4 that the optimization process before 48th generation and after 48th generation is different. From our previous single jet suction/blowing study, it is known that suction control effects are much stronger than blowing control effects. In figure 5.4, the main efforts of the optimization process before the 48th generation appear to focus on optimizing suction location (L_{jS}) and suction angle (θ_S) to their near optimum position, and the optimization process after the 48th generation shifts to optimizing blowing location (L_{jB}), blowing angle (θ_B) and blowing amplitude(A_B).

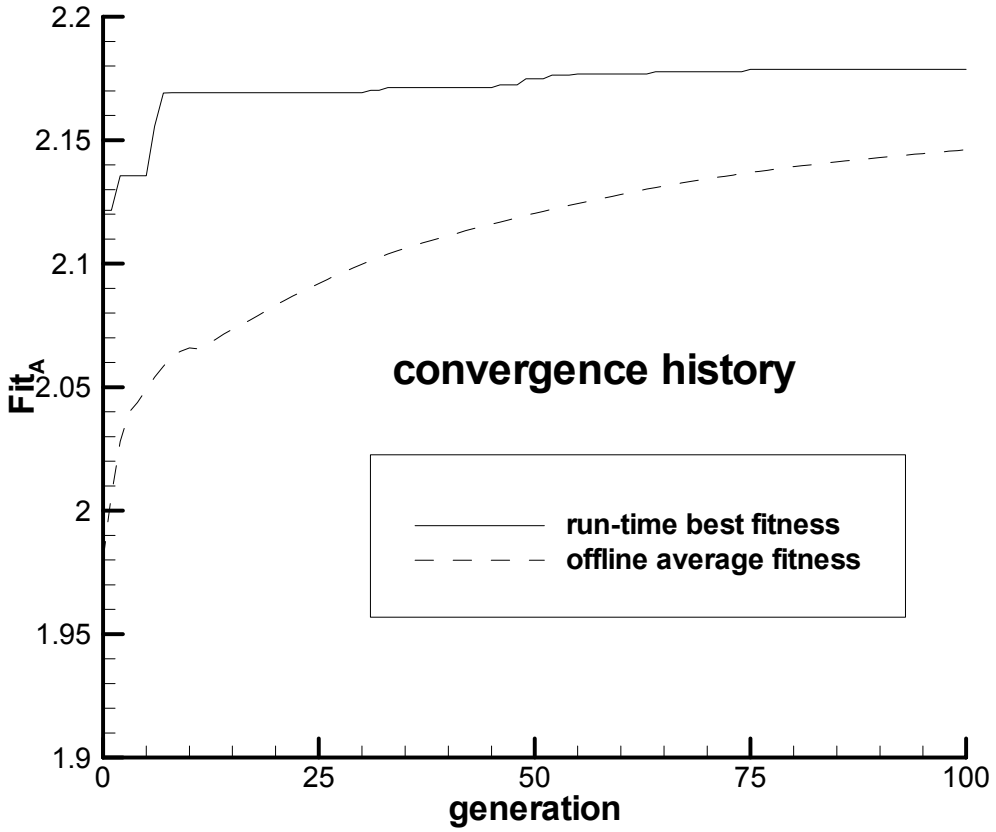

Figure 5.3 Two-jet control system optimization convergence history

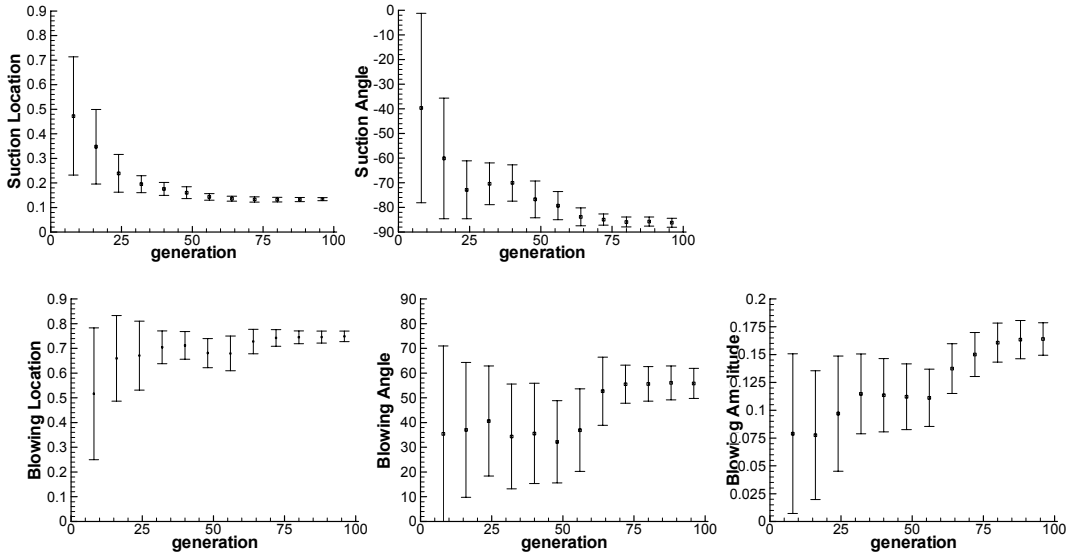

Figure 5.4 Statistic information of optimization process: mean and deviation (error bar) for every eighth generation

Further examining the process before the 48th generation, we can determine that the suction location moves to a near optimum position faster than suction angle, which suggests that suction location is the more sensitive and important parameter. This will be further validated in the upcoming analysis of the suction flow physics. The process after the 48th generation first moves the blowing location to its near optimum value, and then identifies the near optimum values of the blowing angle and blowing amplitude. It can be seen that even at the 96th generation, the deviations of the blowing angle and the blowing amplitude are still very large compared to the other 3 parameters (suction location, suction angle and blowing location). Therefore, we may assume blowing angle and blowing amplitude are the least sensitive and likely least important parameters among the five control parameters being chosen. This assumption will be further confirmed in the upcoming discussion about the flow physics and combination effects of suction plus blowing.

In figure 5.5, the values of five control parameters for the most fit 100 individuals among the 100 generations are plotted in sequence according to their fitness ranking. From this figure, it first can be seen that the solutions scatter in a range instead of converging on some deterministic value, which demonstrate the statistic characteristics of the genetic algorithm. Second, values of suction location, suction angle and blowing location scatter less than blowing angle and blowing amplitude. This also suggests that for the two-jet control system, suction location, suction angle, and blowing position are the dominant factors that maximize the aggregate fitness value.

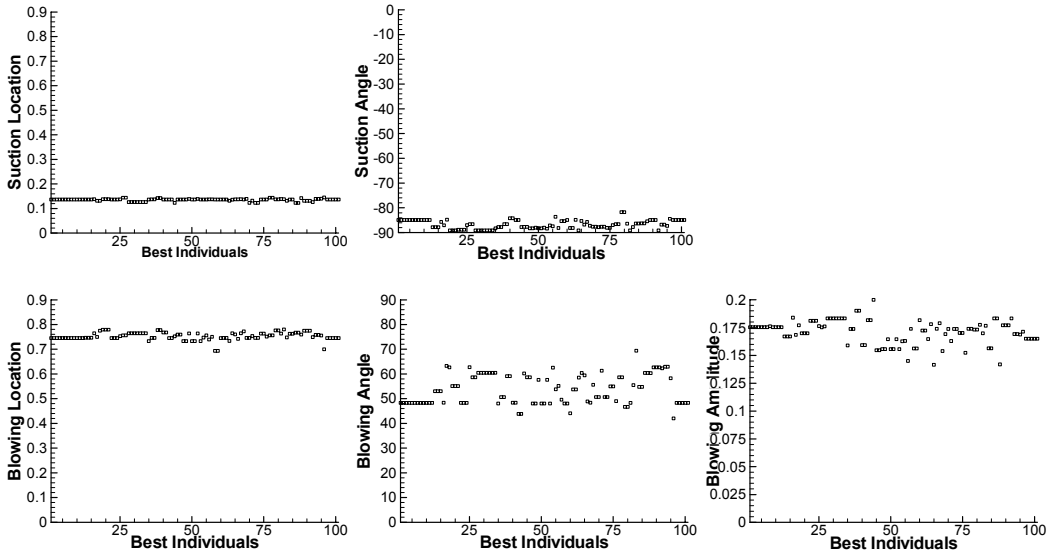

Figure 5.5 Value of five control parameters of the best 100 fit individuals

5.2.2 Improved algorithm with/without diversity control comparison

For the current one suction-jet and one-blowing jet system, the optimization is completed three times. The first and second time, the improved genetic algorithm without diversity control is applied; the third time, the improved genetic algorithm with diversity control is applied.

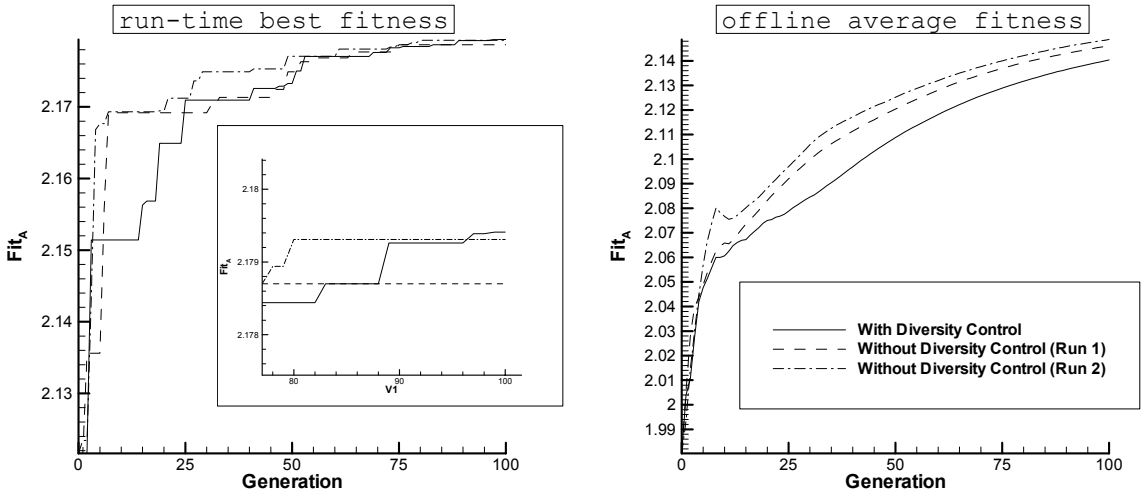

Figure 5.6 Fitness comparison between algorithm without and with diversity control

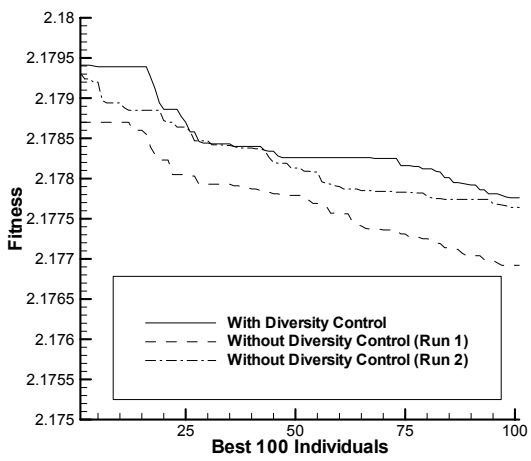

Figure 5.7 Comparison of fitness of the best 100 individuals between the algorithm without diversity control and the algorithm with diversity control

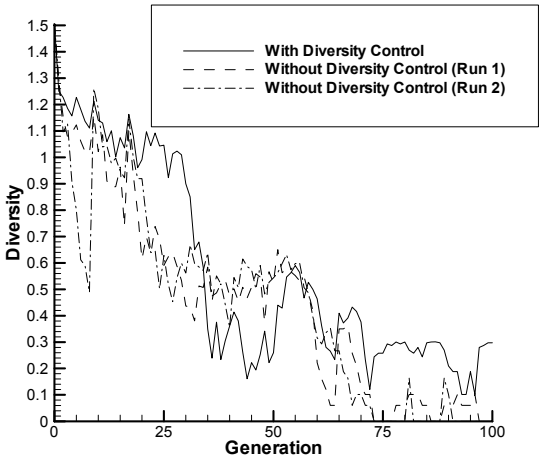

Figure 5.8 Comparison of diversity level between the algorithm with diversity control and the algorithm without diversity control

From figure 5.6, it can be seen that even though the "offline average fitness" of the algorithm with diversity control are lower than that of the algorithm without diversity

control because the super individuals' reproduction has been suppressed during the initial 20% of the optimization process, the end "run-time best fitness" of algorithm with diversity control are better than that of the algorithm without diversity control. This can also be seen in figure 5.7 by comparing the object fitness of the "Best 100 Individuals" between each optimization process with/without diversity control.

In the current optimization, the diversity value of each generation is calculated based on a space classification in which each dimension (parameter) is equally divided. Therefore, for this five-parameter optimization case, the searching space is divided into 32 categories. From figure 5.8, we can see that the diversity level of the algorithm with diversity control maintains in a higher level than the algorithm without diversity control during the initial optimization process. By suppressing the reproduction of super individuals in the initial process, the algorithm with diversity control explores the global searching space more thoroughly than the algorithm without diversity control. This in turn makes the subsequent searching process head in a more deterministic direction. It can be seen in figure 5.8 that the diversity level of algorithm with diversity control drops later and more rapidly than the algorithm without the diversity control. Also, in figure 5.9, the values of five control parameters of the best 100 fit individuals of the algorithm with diversity control cluster more narrowly than the algorithm without diversity control. This same effect can also be seen in figure 5.10. From all these comparison figures, we can draw the conclusion that the diversity control did make the algorithm more robust for finding the global optimum, and at the same time does not compromise the convergence speed.

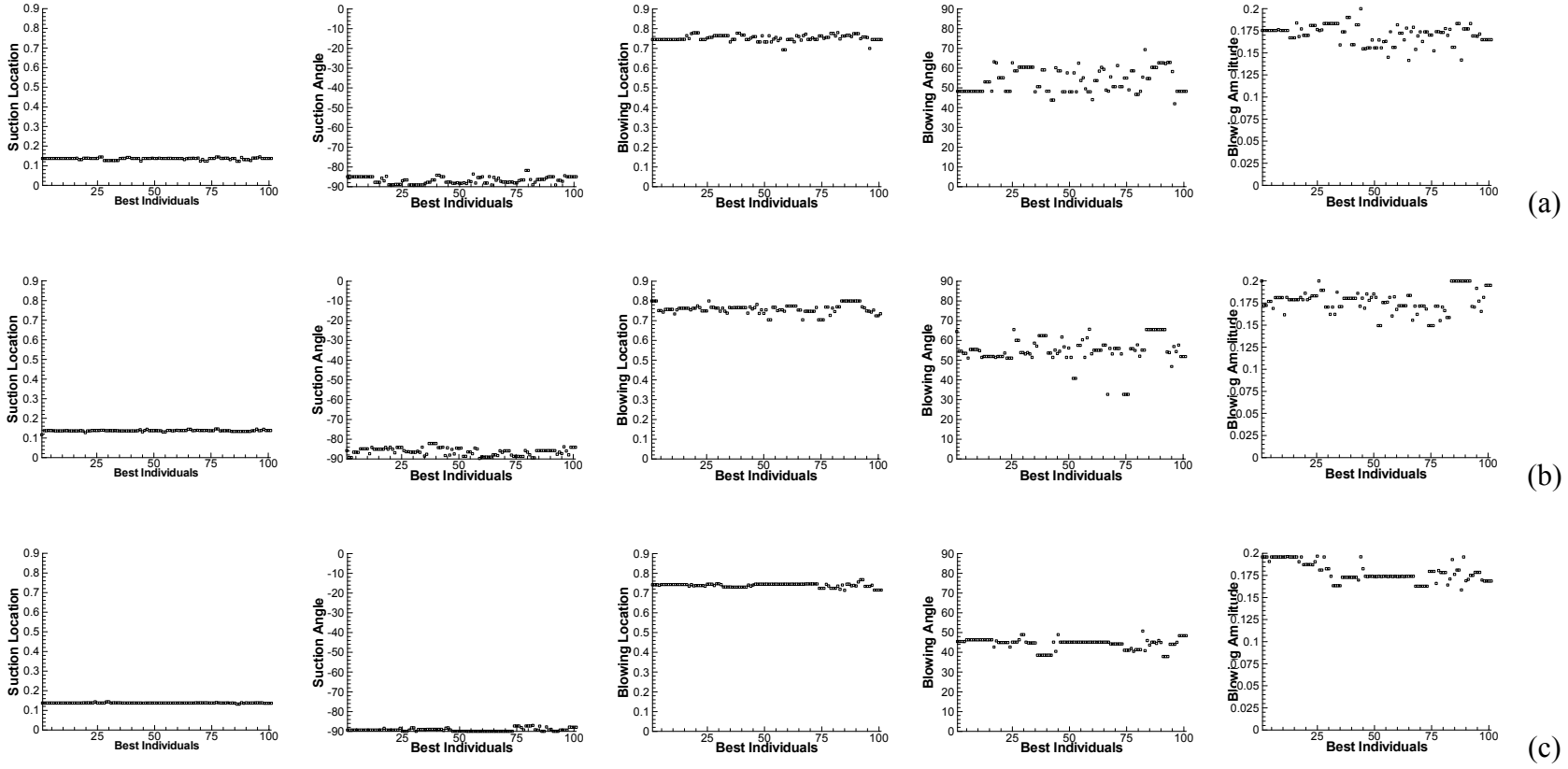

Figure 5.9 Values of design parameters of five control parameters of the best 100 fit individuals: (a) algorithm without diversity control (run 1), (b) algorithm without diversity control (run 2), (c) algorithm with diversity control (run 3)

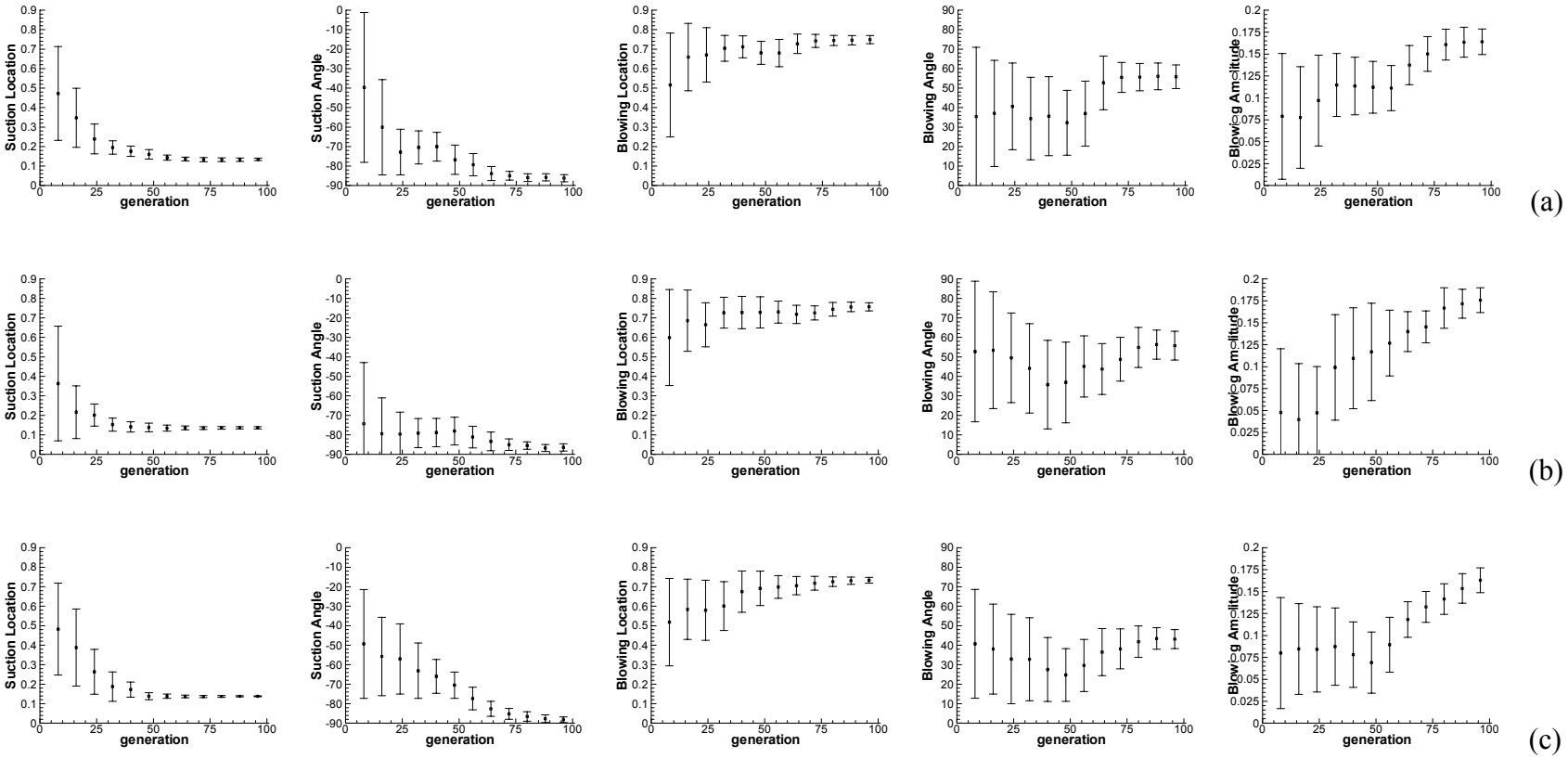

Figure 5.10 Statistics information of optimization process: mean and deviation (error bar) for every eight generation: (a) algorithm without diversity control (run 1), (b) algorithm without diversity control (run 2), (c) algorithm with diversity control (run 3)

5.3 Flow Control Physics

There are three optimization runs for the one suction-jet and one blowing-jet arrangement. The 10 best individuals for each run are listed in table 5.1, 5.2 and 5.3. The first and second run use the improved genetic algorithm without diversity control, the third run uses the improved genetic algorithm with diversity control. It can be seen from the table that the top 10 results of the three runs are almost the same; therefore, we can focus on the flow control physics for the end results of run 1, and discuss issues in runs 2 and 3 if there are notable differences.

Among the 100 generations of run 1, the end optimized best individual with the maximum aggregate fitness is: $L_{jS} = 0.136512$, $\theta_S = -84.9052$, $L_{jB} = 0.745153$, $\theta_B = 48.3057$, $A_B = 0.175368$, with a total fitness of $Fit_A = 2.178696$. First, in order to have better understanding about control physics, the above end results are split into a suction part and a blowing part, and are studied within the single suction control and single blowing control scopes. Second, the parameters' vicinity areas are explored and the combination effects are discussed.

5.3.1 Suction Control

In figure 5-11, under the fixed suction amplitude $A_S = 0.03$ condition, we explored the control effects by changing angle ($\theta_s = -90^0, -84.9052^0, -60^0, -30^0$) and position ($L_{jS} = 0.1, 0.136512, 0.166667, 0.2, 0.333, 0.567, 0.8$), when only suction control is applied to the system. First, considering the suction angle control effects, the

Table 5.1 Run 1 (Without Diversity Control)

Rank	L_{jS}	θ_S	L_{jB}	θ_B	A_B	C_l / C_{lB}	C_d / C_{dB}	Fit_A $C_l / C_{lB} + C_{dB} / C_d$
1	0.136512	-84.9052	0.745153	48.3057	0.175368	1.043814	1.134882	2.178696
2	0.136512	-84.9052	0.745153	48.3057	0.175368	1.043814	1.134882	2.178696
3	0.136512	-84.9052	0.745153	48.3057	0.175368	1.043814	1.134882	2.178696
4	0.136512	-84.9052	0.745153	48.3057	0.175368	1.043814	1.134882	2.178696
5	0.136512	-84.9052	0.745153	48.3057	0.175368	1.043814	1.134882	2.178696
6	0.136512	-84.9052	0.745153	48.3057	0.175368	1.043814	1.134882	2.178696
7	0.136512	-84.9052	0.745153	48.3057	0.175368	1.043814	1.134882	2.178696
8	0.136512	-84.9052	0.745153	48.3057	0.176285	1.043814	1.134882	2.178696
9	0.136512	-84.9052	0.745153	48.3057	0.175368	1.043814	1.134882	2.178696
10	0.136512	-84.9052	0.745153	48.3057	0.175368	1.043814	1.134882	2.178696

Table 5.2 Run 2 (Without Diversity Control)

Rank	L_{jS}	θ_S	L_{jB}	θ_B	A_B	C_l / C_{lB}	C_d / C_{dB}	Fit_A $C_l / C_{lB} + C_{dB} / C_d$
1	0.116531	-85.7663	0.8	64.4686	0.2	1.030962	1.148345	2.179307
2	0.136901	-89.2337	0.8	54.5884	0.172308	1.045234	1.134007	2.179241
3	0.136901	-89.2337	0.8	54.5884	0.172308	1.045234	1.134007	2.179241
4	0.137824	-86.567	0.75085	53.4468	0.176829	1.042347	1.136854	2.179201
5	0.137824	-86.567	0.75085	53.4468	0.176829	1.042347	1.136854	2.179201
6	0.136822	-86.7068	0.743204	51.0672	0.16899	1.043845	1.13513	2.178975
7	0.136357	-84.8461	0.7571	55.4204	0.181229	1.040673	1.138271	2.178944
8	0.136357	-84.8461	0.7571	55.4204	0.181229	1.040673	1.138271	2.178944
9	0.136357	-84.8461	0.7571	55.4204	0.181229	1.040673	1.138271	2.178944
10	0.136357	-84.8461	0.7571	55.4204	0.181229	1.040673	1.138271	2.178944

Table 5.3 Run 3 (With Diversity Control)

Rank	L_{jS}	θ_S	L_{jB}	θ_B	A_B	C_l / C_{lB}	C_d / C_{dB}	$\frac{Fit_A}{C_l / C_{lB} + C_{dB} / C_d}$
1	0.137383	-89.3069	0.741999	45.4739	0.195951	1.04318	1.136224	2.179407
2	0.137383	-89.3069	0.741999	45.4739	0.195951	1.04318	1.136224	2.179407
3	0.137383	-89.3069	0.741999	45.4739	0.195951	1.04318	1.136224	2.179407
4	0.137697	-89.3004	0.739589	45.4457	0.190742	1.04327	1.136131	2.179402
5	0.137383	-89.3069	0.743114	46.3086	0.195951	1.0424	1.136994	2.179390
6	0.137383	-89.3069	0.743114	46.3086	0.195951	1.0424	1.136994	2.179390
7	0.137383	-89.3069	0.743114	46.3086	0.195951	1.0424	1.136994	2.179390
8	0.137383	-89.3069	0.743114	46.3086	0.195951	1.0424	1.136994	2.179390
9	0.137383	-89.3069	0.743114	46.3086	0.195951	1.0424	1.136994	2.179390
10	0.137383	-89.3069	0.743114	46.3086	0.195951	1.0424	1.136994	2.179390

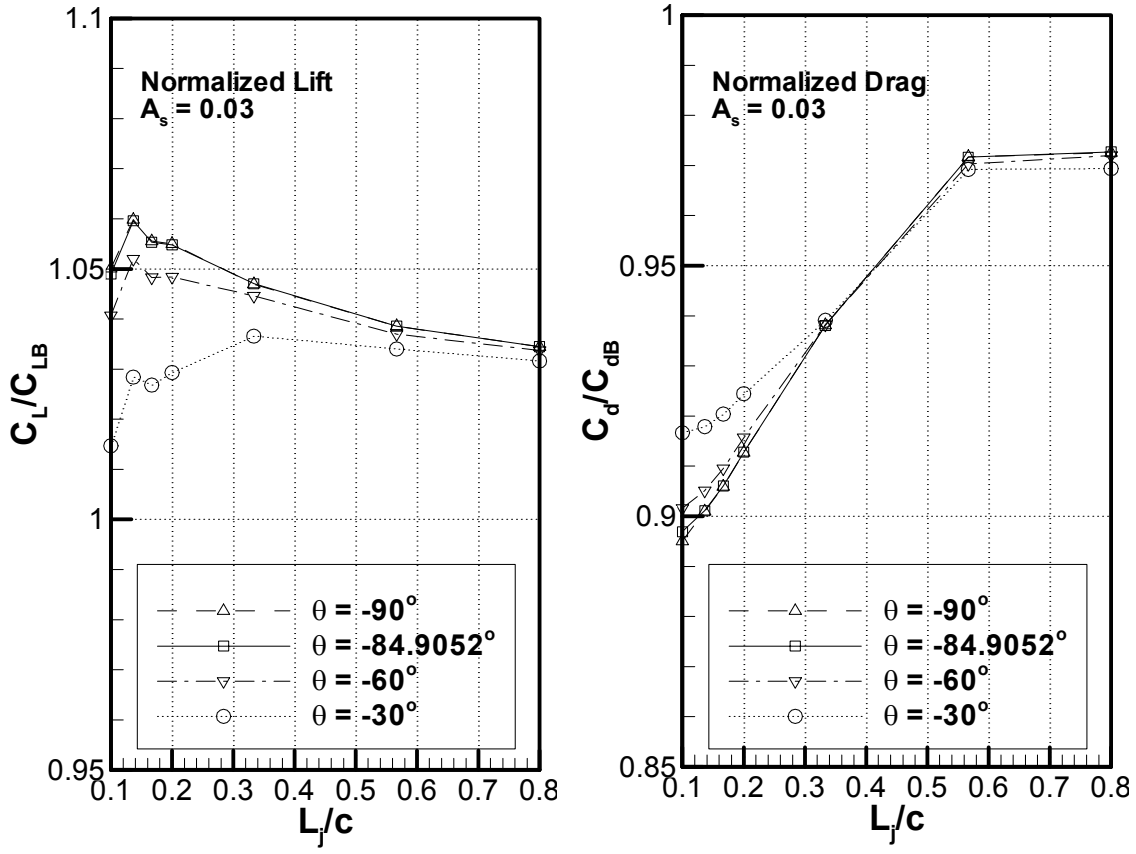

Figure 5.11 Single suction jet study

performance at -90^0 suction and -84.9052^0 suction are almost the same (with -90^0 suction slightly better than -84.9052^0), and both are better than -60^0 and -30^0 suction. It can be seen that the suction angle of the optimized result of run 3 in table 5.3 is -89.3^0 which is closer to the single jet optimum of -90^0. Second, considering the suction location, the control performance for leading edge locations are better than those on the airfoil downstream area, and among the seven suction locations, suction at location 0.136512 is better than all other locations. These two observations are consistent with previous single suction jet study in chapter 4 (reference [86]), where the conclusion

regarding the suction is that under the same suction amplitude, perpendicular (-90^0) suction at the leading edge is most effective. Third, comparing the importance between suction location and suction angle by comparing the changes of normalized lift and normalized drag, suction location causes more changes than suction angle; in other words, the flow is more sensitive to the suction location to the suction angle. This confirms our previous analysis of figure 5.4 and figure 5.5, in which suction location does converge faster and cluster more densely than suction angle.

The critical role of suction location can be further seen in figure 5.12. In this figure the -90^0 suction amplitude is 0.173 (about six time greater than 0.03) in order to more clearly demonstrate the suction control physics. The flow fields are compared with the baseline case (without suction and blowing). The streamlines of these three suction cases all demonstrate a smaller separation bubble on the surface of the airfoil than the baseline case. In figure 5.12(a), when suction is applied near the leading edge ($L_j = 0.1$), the separation is most effectively delayed and hence the separation bubble is much smaller than in the other cases. At $L_j = 0.567$, the only control effect of suction is to break the separation bubble into two smaller separation bubbles, and its lift increase is less than that for suction at location 0.1. It can be observed from figure 5.12(b) that the pressure change near the leading edge area is significant, and leading edge suction changes the upper surface low pressure zone more efficiently than downstream suction. From this figure, it can be seen that the underlying suction control mechanism is the suppression of the separation bubble and the reduction of the airfoil upper surface C_p to increase lift and decrease the profile drag.

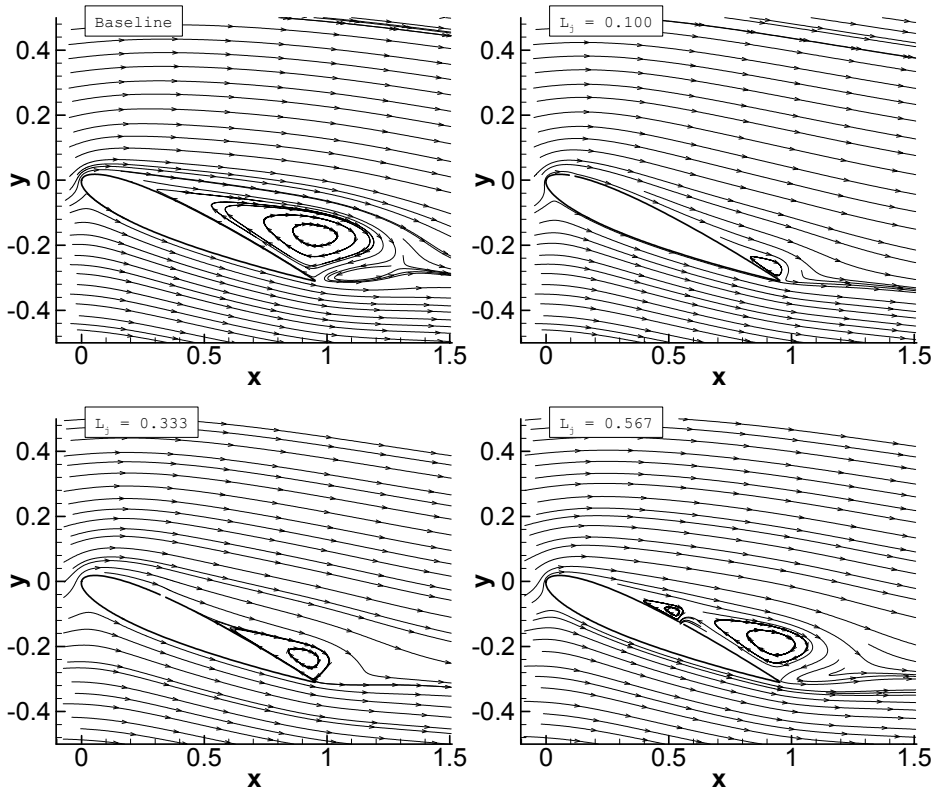

(a)

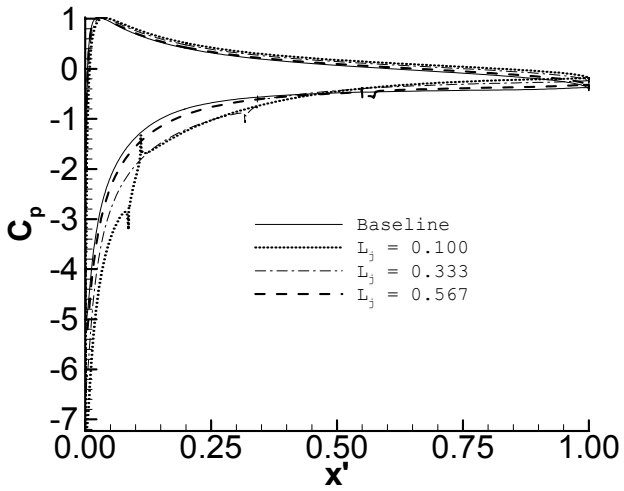

(b)

Figure 5.12 Control effects of suction at different locations , L_j=0.1, 0.333 and 0.567, A=0.173, θ=-90^0

5.3.2 Blowing Control

The blowing control parameters are extracted from the best two-jet solution from run 1, which is $L_{jB} = 0.745153$, $\theta_B = 48.3057$, $A_B = 0.175368$; the control effects of these three blowing parameters are explored and compared with the results of our previous single blowing jet study in figure 5.13. The values of three blowing parameters being explored are $L_{jB} = 0.542857,\ 0.628571,\ 0.745153$ and 0.8; $\theta_B = 0^0$, 48.3057^0 and 90^0 ; $A_B = 0.01,\ 0.073333,\ 0.175368$, and 0.2.

First, from figure 5.13, it can be seen that for downstream blowing, with fixed blowing location and blowing amplitude, tangential blowing is insensitive to amplitude changes and has a larger impact on increasing lift than other angles. Second, the results also indicate that downstream locations, 0.745153 and 0.8, are better for increasing lift. And these two locations are both reflected from the blowing location part of the optimized results in run 1, 2 and 3. Another important observation in the current figure is that the control effects generated by the smallest blowing amplitude of 0.01 are comparable in terms of drag reduction and generally better in terms of lift enhancement than those of larger amplitudes independent of the blowing angle. Downstream tangential (0^0) blowing seems more advantageous at most of the locations with the exception at around 0.8 in terms of increasing lift. Like lift, drag reduction is insensitive to amplitude for tangential blowing, but for larger angles, larger amplitude both decreases drag and increases lift, although not in a simply proportional fashion. As such, the blowing jet configuration of maximum fitness is an intermediate state between that of maximum lift (tangential blowing, low amplitude) and minimum drag (perpendicular blowing, high

amplitude). Drag also exhibits a local minimum around $L_j = 0.74515$ consistently across all angles and amplitudes. Maximum fitness occurs at the downstream locations, but varies in a more complex fashion with blowing angle and amplitude.

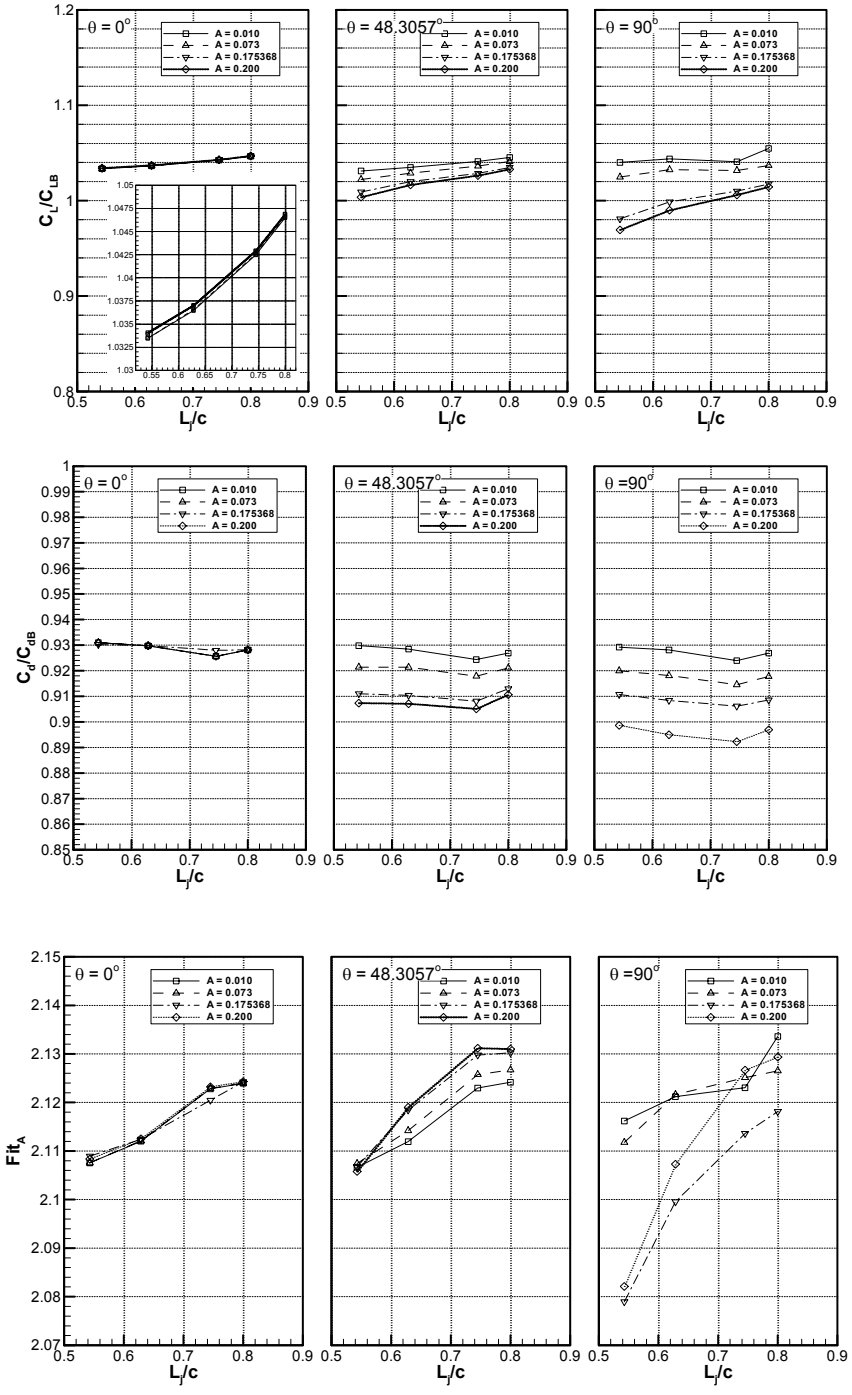

Figure 5.13 Single blowing jet study

5.3.3 Two Jet Control

Because the suction is the dominant control factor, comparing the two-jet optimized results with the single suction/blowing jet results not surprisingly yields the optimized locations in tight region near the leading edge (0.136512 in run 1, 0.116531 and 0.136901 in run 2, and 0.137383 in run 3), and nearly perpendicular suction angles (-84.9052^0 in run 1, -85.7663^0 in run 2, and -89.3069^0 in run 3), both of which are generally consistent with the optimal single-jet results. For the blowing jet, as seen in the single jet results, the GA appears to have selected a configuration that yields optimal fitness between that for maximum lift and that for minimum drag. The optimized blowing locations of 0.74515 in run 1, 0.8 in run 2, and 0.741999 in run 3 are around one of the two optimal locations suggested by single blowing jet studies. The effect of blowing angle and amplitude on fitness is less sharply defined than that of location. As such, the GA is less sensitive to their precise convergence to a local maximum. This is suggested by the relatively small increase in aggregate fitness (only about 20%) in the second half of the evolution.

In order to examine the sensitivity of the two-jet control system to each parameter, different conditions relative to or within the vicinity of the best optimized results are explored, and their normalized lift, normalized drag and aggregate fitness are listed in table 5.4. The representative flow patterns for these cases are shown in figure 5.14(a), and the corresponding pressure coefficients around the airfoil surface are presented in figure 5.14(b). First, from the flow patterns in 5.14(a), comparing the "suction only" case (case 1) to the baseline (no blowing/suction) case, it can be seen that the suction increases lift

and decreases drag by suppressing the separation bubble. Second, comparing the "blowing only" case (case 2) to the baseline case, it is clear that the physical effects are more subtle than those due to suction. Our previous single blowing control study in chapter 4 demonstrates that blowing increases lift and decreases drag through increased circulation, although the control effects are much less than suction given larger amplitude conditions. However, there may be additional physical effects that characterize blowing in this two-jet configuration. Third, comparing the two-jet optimal GA solution (case *) to the baseline case, the separation bubble is reduced by the suction; on the other hand, the circulation about the separation bubble is expected to increase due to the downstream blowing. These changes are reflected in the surface pressure coefficient (C_p) changes in figure 5.14(b).

Further examining table 5.4, it can be seen from the normalized lift and normalized drag changes that the optimized two-jet control system from run 1 (case *) can be imagined as a best single suction system (case 1) combined with an appropriate blowing system (case 2). When blowing effects are stacked on the suction effects, normalized drag decreases more than normalized lift decreases, so the combination of suction and blowing yields a better total aggregate fitness, although the net effect is not large. To investigate the blowing angle parameter, case 3 and 4 in table 1 change only the blowing angle from case *. In both cases, the aggregate fitness is less than the optimized case; second, it can be seen that from the 0^0 blowing angle of case 3 to the 90^0 blowing angle of case 4, both normalized lift and normalized drag decrease. This implies that the optimal solutions of $48^0 \sim 55^0$ over the 3 runs are a compromise between two potential extremes picked out by

the genetic algorithm. Cases 5 and 6 likewise study the sensitivity of the GA. In case 5, the blowing amplitude is increased to the maximum possible value of 0.2; in case 6, the suction angle is decreased to the minimum (and the ideal single-jet value) of -90^0. Both of these cases yield a slightly greater aggregate fitness than case * (optimum result of run 1). Therefore, the optimum result in run 3 is probably closer to the true optimum result which suggests that the improved algorithm with diversity control is better than the improved algorithm without diversity control.

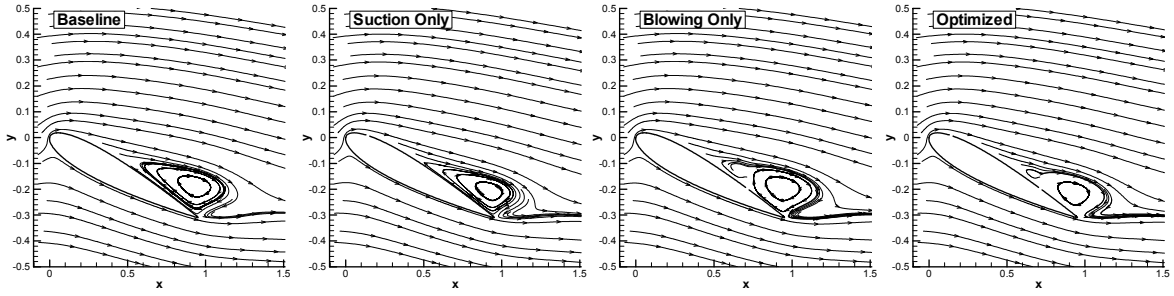

(a)

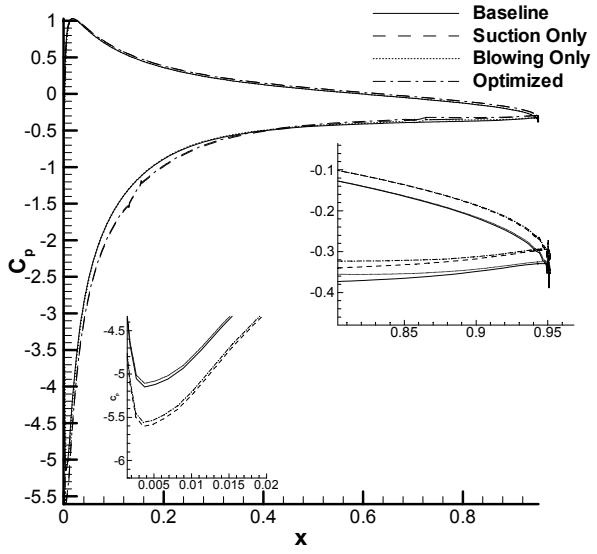

Figure 5.14 Flow field and C_p distribution of "Baseline" case, "Suction Only" case, "Blowing Only" case and "Optimized" case

Table 5.4 Two jet study

Case1	L_{jS}	θ_S	L_{jB}	θ_B	A_B	C_l / C_{lB}	C_d / C_{dB}	Fit_A $C_l / C_{lB} + C_{dB} / C_d$
*	0.136512	-84.9052	0.745153	48.3057	0.175368	1.043814	0.881149	2.178696
1	0.136512	-84.9052				1.059825	0.900979	2.169728
2			0.745153	48.3057	0.175368	1.028564	0.908091	2.129775
3	0.136512	-84.9052	0.745153	0	0.175368	1.058715	0.899530	2.170408
4	0.136512	-84.9052	0.745153	90	0.175368	1.025183	0.870097	2.174480
5	0.136512	-84.9052	0.745153	48.3057	0.2	1.041248	0.878177	2.179974
6	0.136512	-90	0.745153	48.3057	0.175368	1.044024	0.881029	2.179061

Chapter 6

Two Jet System Optimization (II)

6.1 Two Suction Jet Case Setup

The previous chapter investigated a single blowing-jet and single suction-jet control system and our final optimization results demonstrate that the suction jet is the dominant control factor. One question that arises from this finding is that if two suction jets are implemented on to the airfoil, what are their optimum locations and angles? Will these two suction jets merge to become one double width perpendicular suction jet? In order to answer this question, we now test a two suction jet control system.

6.1.1 Control Parameters Selection

As in the present chapter, the suction jet amplitude is fixed at 0.03, and the suction jet location and angle can be changed within a fixed range; therefore, in the current two suction jet study there are only four control parameters:

Suction Location 1: $0.05 \le L_{jS1} \le 0.8$

Suction Angle 1: $-90^0 \le \theta_{S1} \le 0^0$

Suction Location 2: $0.05 \le L_{jS2} \le 0.8$

Suction Angle 2: $-90^0 \le \theta_{S2} \le 0^0$

6.1.2 Genetic Algorithm Coefficients and Programming Model

For the present two suction jet optimization, the genetic coefficients are chosen as

$NGeneration = 100$,

$NPopSize = 16$,

$NVariable = 4$,

$NUpdate = 8$,

$P_c = 0.2$, $P_m = 0.1$, $s = 1.0$.

Table 6.1 Initial Generation (0^{th} Generation)

Rank	L_{jS1}	θ_{S1}	L_{jS2}	θ_{S2}
1	0.360788	-22.6416	0.639440	-43.9780
2	0.473752	-29.1152	0.751893	-47.3836
3	0.094289	-72.1056	0.506930	-72.0196
4	0.709987	-20.6192	0.427522	-63.5856
5	0.317920	-80.6535	0.701861	-57.4387
6	0.775833	-25.7488	0.366217	-81.5335
7	0.529277	-32.6156	0.177573	-55.1679
8	0.348450	-46.4779	0.664641	-16.8915
9	0.224004	-35.5103	0.292755	-18.2693
10	0.261454	-66.6423	0.352892	-59.3108
11	0.393768	-10.8213	0.455580	-59.5495
12	0.537995	-86.0277	0.493874	-89.2902
13	0.160990	-44.9118	0.327259	-79.5812
14	0.171162	-18.7829	0.207377	-13.1474
15	0.371679	-55.8060	0.230706	-15.5845
16	0.697635	-84.5583	0.529367	-81.4034

The system aggregate fitness function is

$$(Fit_A)_{\max} = a \cdot C_l / C_{lB} + b \cdot C_{dB} / C_d ,$$

with $a = 1.0, b = 1.0$. Four control parameters – suction location 1 (L_{jS1}), suction angle 1 (θ_{S1}), suction location 2 (L_{jS2}), and suction angle 2 (θ_{S2}) are optimized by the genetic algorithm towards the maximum aggregate fitness value. The initial generation in this two suction jet system is generated randomly as listed in Table 6.1.

6.2 Optimization Process of Two Suction Jets System

Because of the better performance of the improved algorithm with diversity control as demonstrated both in chapter 3 and chapter 5, the present optimization only uses the improved algorithm with diversity control method.

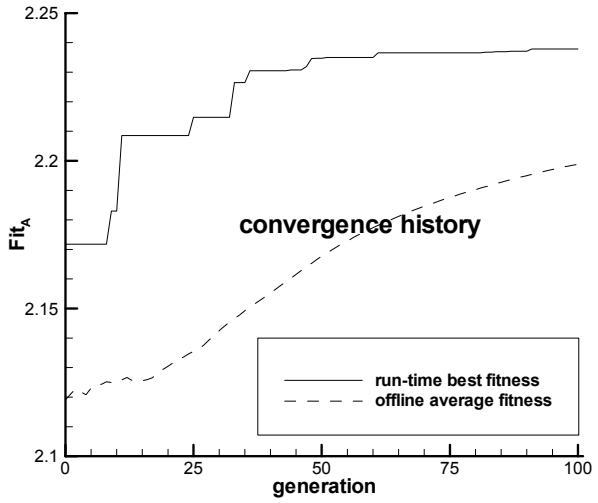

Figure 6.1 Two Suction Jet Control System Optimization Convergence History

In figure 6.1, both "run-time best fitness" and "offline average fitness" are plotted. The 0^{th} generation starts with 16 individuals randomly distributed in the searching space. Within the 0^{th} generation, the average fitness is 2.12 and the maximum fitness is 2.17. Therefore, it can be observed from the figure that offline average fitness curve starts from

2.12 and maximum fitness curve starts from around 2.17; the difference between the maximum fitness and the average fitness at the start is 0.05. After 60 generations, the best fitness value is nearly constant which indicates that the near optimum condition is reached. But the continual growth of the offline average fitness indicates that the two suction jet control system still undergoes notable changes in the control parameters' space in the final 40 generations.

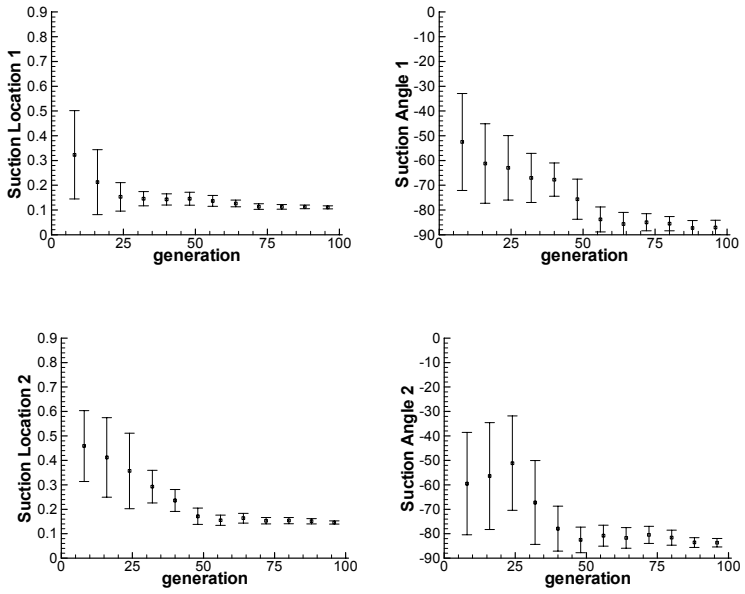

Figure 6.2 Statistic information of optimization process: mean and deviation (error bar) for every eighth generation.

In this two suction jet control system optimization process, every 8 (*NUpdate*) generations the new generation will be generated according to the best 128 ($NUpdate \cdot NPopSize$) individuals' statistic information; their means (μ) and deviations (σ) are plotted in figure 6.2. No surprise, it can be seen in the figure that at 48^{th} generation, both suction jets are located to the leading edge. After 48^{th} generation, the

algorithm locates the first jet forward of the second jet. This is not forced ─ the second jet can be in front of the first. This result does reflect that during the optimization process, there are a few more better-fit individuals whose first suction location values are smaller than the second suction jet location values than the opposite. Over time, the gradually increasing selection pressure (preference) continually magnifies this difference. For suction jet 1 and 2, their angles both approach perpendicular at the final stage.

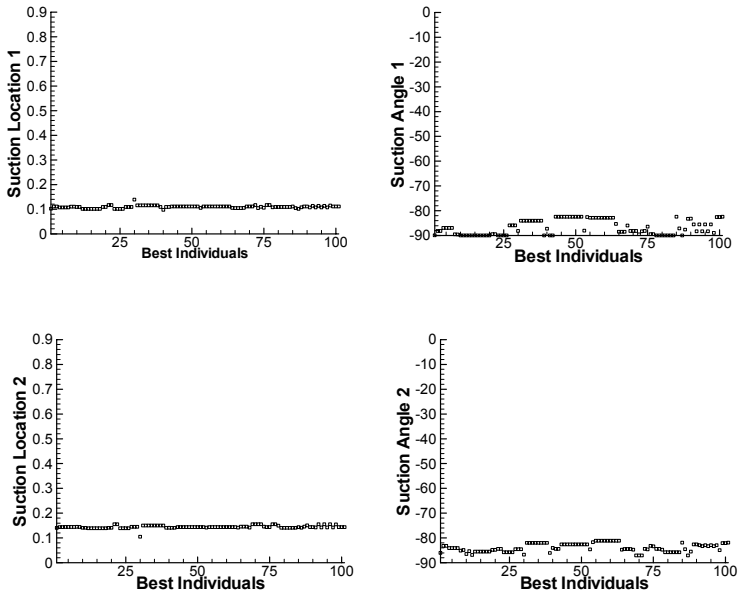

Figure 6.3 Value of four control parameters of the best 100 fit individuals

In figure 6.3, the values of five control parameters for the most fit 100 individuals among the 100 generations are plotted in sequence according to their fitness ranking. No surprise, all these individuals' location are on the leading edge and their suction angle are close to the ideal -90^0. Of the most fit 100 individuals, suction location 1 are located ahead of the suction location 2 with one exception (rank 29 with $L_{jS1} = 0.139350$,

$\theta_{S1} = -88.1884^0$, $L_{jS2} = 0.105072$, $\theta_{S2} = -86.7513^0$). This observation is consistent with our discussion in the previous paragraph.

6.3 Discussion of Optimized Results

The 10 best fit individuals for current two suction jets optimization are listed in table 6.1. First, it can be seen that both first and second suction jet location of each individual are close to each other and are located within the 0.1-0.145 range on the leading edge. From the suction (amplitude at 0.03) study in figure 5.11, it can be seen that this range is located within the optimum suction range. Therefore, suction locations of these best fit individuals do hit the optimum range. Second, from the suction angle perspective, both first and second suction jet angles are close to ideal -90^0, although the first suction jet angles are closer. In table 6.2, in case 1, we demonstrate that ideal -90^0 angle of two suction jets will yield a better result than case * ─ the current rank 1 optimized result.

From the locations of best fit results in table 6.1, it can be seen that during the final convergence stage, the two suction jets are closer to each other on the leading edge. Consider case *, the optimized results, two suction jets are only 0.01318 (=0.140014-0.101834-0.025) away from each other. Therefore, it naturally leads us to test whether a double width suction jet is better (under the current aggregate fitness definition) than two suction jets separated with some distance. From the results of case 2 in table 6.2, comparing with the optimized case * and 1, it can be seen that the double width suction jet decreases both lift and drag a little, and its aggregate fitness is smaller than both case*

and 1. It can be seen from the C_p curve in figure 6.4 that the reason for the decreasing lift is because the loss of a small amount of the lower pressure area on the upper surface. Hence, under the current definition of better (aggregate fitness), two suction jets separated by a small distance is better than a double width suction jet. And it can be seen from table 6.1 that this separation distance depends on the jet locations on the leading edge.

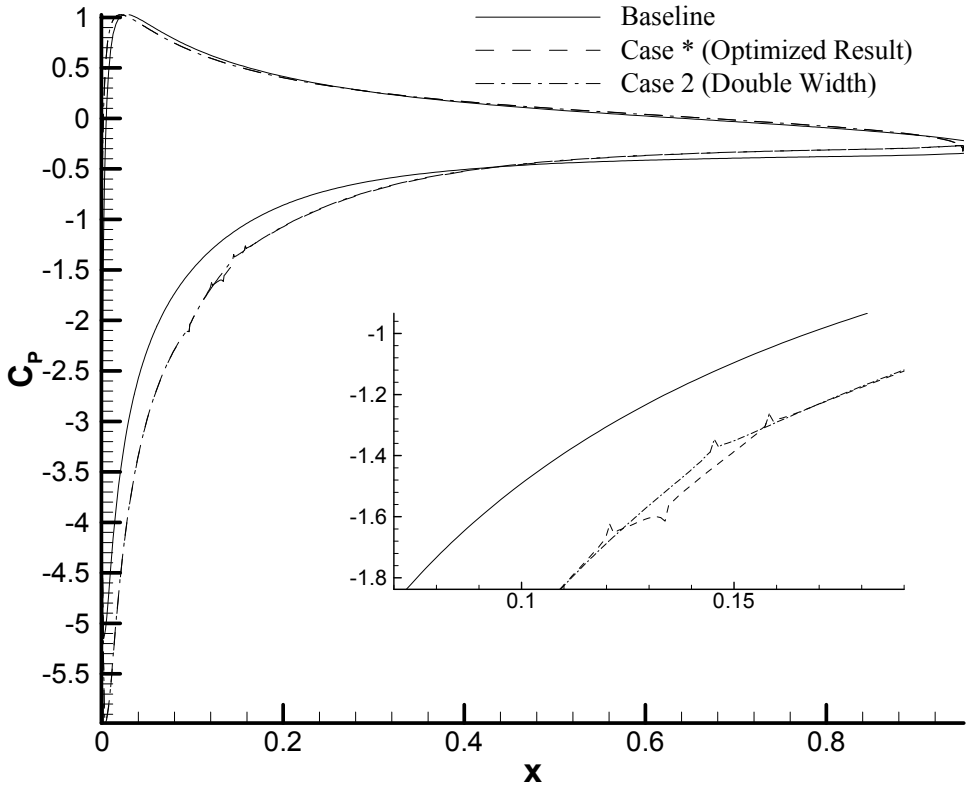

Figure 6.4 C_p distribution of "case *" and "case 2"

Table 6.1 10 best fit individuals of two suction jets system

Rank	L_{jS1}	θ_{S1}	L_{jS2}	θ_{S2}	C_l	C_d	C_l / C_{lB}	C_{dB} / C_d	$\frac{Fit_A}{C_l / C_{lB} + C_{dB} / C_d}$
1	0.101834	-89.9168	0.140014	-86.0520	0.966284	0.146477	1.10318	1.13470	2.23789
2	0.111014	-88.1602	0.143712	-83.1392	0.965479	0.146391	1.10227	1.13537	2.23764
3	0.111014	-88.1602	0.143712	-83.1392	0.965479	0.146391	1.10227	1.13537	2.23764
4	0.107174	-86.9535	0.144685	-84.0549	0.971018	0.147236	1.10859	1.12885	2.23744
5	0.107174	-86.9535	0.144685	-84.0549	0.971018	0.147236	1.10859	1.12885	2.23744
6	0.107174	-86.9535	0.144685	-84.0549	0.971018	0.147236	1.10859	1.12885	2.23744
7	0.107174	-86.9535	0.144685	-84.0549	0.971018	0.147236	1.10859	1.12885	2.23744
8	0.110159	-89.5160	0.144871	-85.1201	0.971030	0.147275	1.10860	1.12856	2.23716
9	0.110159	-89.5884	0.144703	-84.8953	0.971401	0.147337	1.10903	1.12808	2.23711
10	0.109148	-90.0000	0.140574	-86.4329	0.965752	0.146499	1.10258	1.13453	2.23711

Table 6.2 Comparison between different cases

Case	L_{jS1}	θ_{S1}	L_{jS2}	θ_{S2}	C_l	C_d	C_l / C_{lB}	C_{dB} / C_d	$\frac{Fit_A}{C_l / C_{lB} + C_{dB} / C_d}$
*	0.101834	-89.9168	0.140014	-86.0520	0.966284	0.146477	1.10318	1.13470	2.23789
1	0.101834	-90.0000	0.140014	-90.0000	0.966381	0.146474	1.10330	1.13473	2.23802
2	0.101834	-90.0000	Double Width Jet		0.961617	0.145928	1.09786	1.13897	2.23683

Chapter 7

Conclusions and Discussions

7.1 Genetic Algorithm in current work

From our two-jet optimization results, it can be seen that the EARND (Explicit Adaptive Range Normal Distribution) improved algorithm with diversity control is designed to identify and optimize important control factors in sequence. This algorithm yields greater efficiency and robustness over the other tested algorithms in all test cases and proved to be a successful approach to investigating the two-jet system.

Two main challenges faced by the Genetic Algorithm have been solved by the proposed algorithms. Regarding the convergence speed, the current algorithm regenerates and normally distributes the children generation according to the best individuals' statistical information, and further changes the boundary ranges of the control parameters to gain the fast fine-grain searching ability during the last 50% of the evolution. Regarding the prevention of preliminary convergence to local optima, the current proposed algorithm maintains a high diversity level by suppressing the similar super fit individuals as a reproductive group in the selection process during the initial 20% evolution.

In the current two-jet optimization study, the information of the single jet study is used for understanding the flow control physics, but it is not used to seed the initial generation.

But for solving a real engineering problem in a limited time frame, problem-specific knowledge can be used to generate a desirable initial generation and promote faster searching and learning.

7.2 Conclusions of Blowing and Suction Jet Control

Analyzing the single blowing jet and single suction jet system GA optimization solution in detail reveals that the suction jet is dominant; the blowing jet is secondary to the overall fitness improvement. This is consistent with the studies of the single-jet flow physics in chapter 4. Based on the results, the most important and fastest converging parameters are the suction location and angle. The blowing location is of secondary importance, while the blowing angle and blowing amplitude are the parameters least well-constrained and least critical to the overall performance of the one blowing jet and one suction jet system.

Analyzing two suction jets system optimization study reveals that, under the current aggregate fitness definition ($Fit_{Agg} = C_l / C_{lB} + C_{dB} / C_d$), a double width suction jet on an optimum location is not better than two suction jets locate on the optimum location with certain separated distance, but the difference is small. If this can be further validated by experimental data, this information will be useful for the arrangement of jet arrays on the airfoil.

7.3 Future Work and Other Potential Applications

Current successful application of the Genetic Algorithm on a two static (non-forcing) jet system can naturally extend to a multiple jet (non-forcing/forcing) control system as

computing power increases as Moore's law. In reality, manufacture of a micro-jet array as a flow control device is a mature technique, but the full implementation to a real environment needs an efficient and robust searching algorithm to locate the best place and control its real-time working conditions. Hence, the studies of multiple micro-jets or even jet array control optimization will have their realistic applications. At the same time, the static (non-forcing) jet control study will advance to the oscillatory (forcing) jet control study as the computing power increases.

Outside the jet control area, there are numerous other flow control problems which can be studied by using Computational Fluid Dynamics and optimized by using a Genetic Algorithm, such as in-land vehicle body design (Mechanical Engineering), metropolitan housing development (Civil Engineering), artificial organ (heart, lung, kidney) design (Biomedical Engineering), and spray painting (Chemical Engineering). All these promising research areas require multi-disciplinary knowledge which interweaves the technology and advancement in Flow Control, Computational Fluid Dynamics and Genetic Optimization Algorithms.

References

1. Mohamed Gad-el-Hak, “Introduction to Flow Control”, *Flow Control, Fundamentals and Practices*, Springer, 1998, pp. 12-13
2. Sheldahl, R. E. and Klimas, “Aerodynamic Characteristics of Seven Airfoil Sections Through 180 Degrees Angle of Attack For Use In Aerodynamic Analysis Of Vertical Axis Wind Turbines”, SAND80-2114, Sandia National Laboratories, Albuquerque, New Mexico, March 1981
3. Chris C. Critzos, Harry H. Heyson and Robert W. Boswinkle Jr., “Aerodynamic Characteristics of NACA0012 Airfoil Section at Angles of Attack from 0^0 to 180^0 ”, NACA TN 3361, 1955
4. E. Jacobs, A. Sherman, “Airfoil Section Characteristics As Affected By Variations Of the Reynolds Number”, NACA Report#586,231, 1937
5. T. Hauser, T.I. Mattox, R.P. LeBeau, H.G. Dietz, and P.G. Huang, "High-cost CFD on Low-cost PC clusters," in Proceedings of ACM/IEEE SC2000, Dallas, Texas, Nov, 2000
6. J. H. Holland, “Adaptation in Natural and Artificial Systems”, University of Michigan Press, Ann Arbor, 1975
7. B. Thwaites, “Approximate calculation of the laminar boundary layer”, *Aeronautical Quarterly*, Vol. 1, 1949, pp. 245-280
8. B. S. Stratford, “The Prediction of Separation of the Turbulent Boundary Layer”, *Journal Fluid Mechanics*, Vol. 5, 1959, pp. 1–16

9. M. J. Lighthill, “On Boundary Layers and Upstream Influence. I, A comparison between subsonic and supersonic flows”, *Proceedings of Royal Society* A, Vol. 217, pp. 344-367
10. N. Curle and S. Skan, “Approximate Methods for Predicting Properties of Laminar Boundary Layers”, *Aeronautical Quarterly*, Vol. 8, 1957, pp. 257-268
11. L. Crabtree, “Prediction of Transition in the Boundary Layer of An Aerofoil”, *Journal of Royal Aeronautical Society*, Vol. 62, 1958, pp. 525-537
12. B. Thwaites, “Incompressible Aerodynamics”, Oxford University Press, 1959
13. E. C. Maskell, “Approximate Calculation of the Turbulent Boundary Layer In Two Dimensional Incompressible Flow”, M. O. S. Report, 1958
14. Jack D. Brewer and Josephine F. Polhamus, “Wind-tunnel investigation of the boundary layer on an NACA 0009 airfoil having 0.25 and 0.50 airfoil chord plain sealed flaps”, NACA TN-1574, Langley Memorial Aeronautical Laboratory, April 1948
15. Eli Reshotko and Maurice Tucker, “Approximate calculation of the compressible turbulent boundary layer with heat transfer and arbitrary pressure gradient”, NACA TN-4154, Lewis Flight Propulsion Laboratory, December 1957
16. Julian Nitzberg Allen, and E. Gerald, “The effect of compressibility on the growth of the laminar boundary layer on low-drag wings and bodies”, NACA TN-1255, July 1947
17. John Stack, “Tests of airfoils designed to delay the compressibility burble”, NACA TN-976, Langley Memorial Aeronautical Laboratory, Langley Field, VA, December 1944

18. L. J. Runyan, L. L. Steers, "Boundary Layer Stability Analysis of a Natural Laminar Flow glove on the F-111 TACT Airplane", *Progress in Astronautics & Aeronautics*, Vol. 72, pp. 17-32, 1980
19. D. M. Bushnell, "Applications and Suggestioned Directions of Transition Research", Fourth Symposium on Numerical and Physical Aspects of Aerodynamic Flows, Long Beach, CA, January 1989, pp. 16-19
20. G. B. Schubauer, W. G. Spangenberg, "Forced Mixing in Boundary Layers", *Journal of Fluid Mechanics*, Vol. 8, 1960, pp. 10-32
21. A.M.O. Smith, "Stratford' Turbulent Separation Criterion for Axially Symmetric Flows", Journal of Applied Math & Physics, Vol. 28, 1977, pp. 929-939
22. A.M.O. Smith, T. R. Stokes, R.S. Lee Jr., "Optimum Tail Shapes for Bodies of Revolution", *Journal of Hydronautics*, Vol. 15, 1981, pp. 67-73
23. L. Bahi, J.M. Ross and H.T. Nagamatsu, "Passive Shock Wave/Boundary Layer Control for Transonic Airfoil Drag Reduction", AIAA Paper 1983-0137, 1983
24. G. Savu and O. Trifu, "Porous Airfoils in Transonic Flow", *AIAA Journal*, Vol. 22, 1984, pp. 989-991
25. H. D. Taylor, "Application of Vortex Generator Mixing Principles to Diffusers", Research Department Concluding Report No. R-15064-5, United Aircraft Corporation, East Hartford, 1948.
26. H. H. Pearcey, "Shock Induced Separation and Its Prevention by Design and Boundary Layer Control", Boundary layer and Flow Control, Vol. 2, Pergamon Press, Oxford, England, 1961, pp. 1166-1344

27. J. D. Nickerson, “A Study of Vortex Generators at Low Reynolds Numbers”, AIAA Paper 1986-0155, 1986

28. M.B. Bragg and G.M. Gregorek, “Experimental Study of Airfoil Performance with Vortex Generators”, *Journal of Aircraft*, Vol. 24, 1987, pp. 305-309

29. P. A. Hunter and H. I. Johnson, “A Flight Investigation of the Practical Problems Associated with Leading-Edge Suction”, NACA TN-3062, Washington, D.C., 1954

30. Robert E. Dannenberg and James A. Weiberg, “Section Characteristics Of A 10.5-Percent Thick Airfoil With Area Suction As Affected By Chordwise Distribution Of Permeability”, NASA Technical Note 2847, Ames Aeronautical Laboratory, Moffett Field, CA, Dec. 1952

31. James A. Weiberg and Robert E. Dannenberg, “Section Characteristics Of An NACA 0006 Airfoil With Area Suction Near The Leading Edge”, NASA Technical Note 3285, Ames Aeronautical Laboratory, Moffett Field, CA, Sep. 1954

32. S.C. Purohit, “Effect of Vectored Suction on a Shock-Induced Separation”, *AIAA Journal*, Vol. 25, 1987, pp. 759-760

33. J. Williams and A. J. Alexander, “Pressure-plotting measurements on an 8 percent thick aerofoil with trailing edge flap blowing. A. R. C., R. & M. No. 3087

34. J. Williams and A. J. Alexander. Wind-tunnel investigation of trailing flap blowing on a 5 per cent thick 60^0 delta wing. Unpublished N.P.L. Paper, 1957

35. S. F. J. Butler and M. B. Guyett, “Low-speed wind-tunnel tests on the De Havilland Sea Venom with blowing over the flaps”, A.R.C., R. & M. No. 3129, 1957

36. H. B. Squire, “Jet flow and its effects on aircraft”, *Aircraft Engineering*, Vol. 22, March, 1957

37. A. Glezer, M. G. Allen, D. J. Coe, S. L. Barton, M. A. Trautman and J. W. Wiltse, “Synthetic Jet Actuator and Applications Thereof”, U.S. Patent 5,758,823, June 2, 1998

38. Barton L. Smith and A. Glezer, “The Formation and Evolution of Synthetic Jets”, *Physics of Fluids*, Vol. 10, No. 9, Sep 1998, pp. 2281- 2297

39. A. Glezer, “Shear Flow Control Using Fluidic Actuator Technology”, *Proceedings of the 1st Symposium on Smart Control of Turbulence*, Tokyo, Japan, 1999

40. D. C. McCormick, S. Lozyniak, D. G. MacMartin, and P. F. Lorber, “Compact High Power Boundary Layer Separation Control Actuation Development”, ASME Fluids Engineering Division Summer Meeting, New Orleans, ASME FEDSM2001-18279, May 2001

41. J. L Gilarranz and O.K. Rediniotis, “Compact, High-Power Synthetic Jet Actuators for Flow Separation Control”, 39th AIAA Aerospace Sciences Meeting and Exhibit, AIAA Paper 2001-0737, 2001

42. J. L. Gilarranz, X. Yue, and O. K. Rediniotis, "PIV Measurements and Modeling of Synthetic Jet Actuators for Flow Control," Proceedings of FEDSM'98, ASME Fluids Engineering Meeting, 1998

43. B. L. Smith, M. A. Trautman, and A. Glezer, "Controlled Interactions of Synthetic Jets," AIAA 37th Aerospace Sciences Meeting, AIAA Paper 1999-0669, 1999

44. B. L. Smith and G. W. Swift, "Synthetic jets at high Reynolds number and comparison to continuous jets," 31st AIAA Fluid Dynamics Conference paper AIAA Paper 2001-3030, 2001

45. M. Amitay, B. L. Smith, and A. Glezer, "Aerodynamic flow control using synthetic jet technology," 36th AIAA Fluid Dynamics Conference, AIAA Paper 1998-0208, 1997

46. B. D. Ritchie, D.R. Mujumdar and J.M. Seitzman, “Mixing in Coaxial Jets Using Synthetic Jet Acutators”, 38th AIAA Aerospace Sciences Meeting and Exhibit, AIAA Paper 2001-0737, 2001

47. Naoki Kurimoto, Yuji Suzuki and Kasagi, “Mixing Enhancement of Coaxial Jet with Arrayed Flap Actuators for Active Control of Combustion Field”, Proceedings of the 2nd Symposium on Smart Control of Turbulence, Tokyo, Japan, March 4-6, 2001

48. L. D. Kral, J. F. Donovan, A. B. Cain, and A. W. Cary, "Numerical Simulation of Synthetic Jet Actuators," AIAA 28th Fluid Dynamics Conference, AIAA Paper 1997-1824, 1997

49. D. P. Rizzetta, M. R. Visbal, and M. J. Stanek, "Numerical Investigation of Synthetic Jet Flowfields," *AIAA Journal*, Vol. 37, No. 8, August 1999

50. C.Y. Lee and D.B. Goldstein, "Two-Dimensional Synthetic Jet Simulation," 38th AIAA Aerospace Sciences Meeting and Exhibit, AIAA Paper 2000-0406, 2000

51. Jie-Zhi Wu, Xi-Yun Lu, Andrew G. Denny, Meng Fan and Jain-Ming Wu, “Post-stall Flow Control On An Airfoil By Local Unsteady Forcing”, *Journal of Fluid Mechanics*, Vol. 371, 1998, pp. 21-58
52. Catalin Nae, “Synthetic Jets Influence on NACA 0012 Airfoil at High, Angles of Attack”, AIAA Atmospheric Flight Mechanics Conference and Exhibit, Boston, Massachusetts, August 10-12, 1998
53. A. Hassan, and R. D. Janakiram, "Effects of Zero-Mass Synthetic Jets on the Aerodynamics of the NACA 0012 Airfoil", Journal of the American Helicopter Society, Vol. 43, No. 4, Oct, 1998
54. A. Dasdan and K. Oflazer, “Genetic Synthesis of Unsupervised Learning Algorithms”, Proc. 2nd Turkish Conf. Artificial Intelligence and Neural Networks, pp. 213-20, June 1993
55. Olivier V. Pictet, Michel M. Dacorogna, Rakhal D. Dave, Bastien Chopard, Roberto Schirru and Marco Tomassini, “Genetic Algorithms with collective sharing for Robust Optimization in Financial Applications”, Olsen and Associates, Working Papers 1995-02-06
56. E. K. Burke, D.G. Elliman and R.F. Weare, “A Genetic Algorithm for University Timetabling”, AISB Workshop on Evolutionary Computing, Leeds, 1994
57. Robert J. Collins and D. R. Jefferson, “AntFarm: Towards Simulated Evolution”, Artificial Life II, Addison-Wesley, 1991
58. C. Z. Janikow and Z. Michalewicz, “An Experimental Comparison of Binary and Floating Point Representations in Genetic Algorithms”, Proceedings of the Fourth

International conference on Genetic Algorithms, Morgan Kaufmann Publishers, San Mateo, CA, 1991, pp. 31-36

59. A. H. Wright, "Genetic Algorithms for Real Parameter Optimization", Foundations of Genetic Algorithms, Morgan Kaufmann Publishers, San Mateo, CA, 1991, pp.205-218
60. D. E. Goldberg, "Genetic Algorithm in Search, Optimization and Machine Learning", Addison-Wesley Publishing Company, Reading, MA, 1989
61. Z. Michalewicz, "Genetic Algorithms + Data Structures = Evolution Programs", Springer-Verlag. Berlin, 1996
62. D. E. Goldberg and K. Deb, "A comparative analysis of selection schemes used in genetic algorithms", Foundations of Genetic Algorithms, Morgan Kaufmann Publishers, San Mateo, CA, 1991, pp. 69-93
63. L. B. Booker, "Improving Search in Genetic Algorithms", Genetic Algorithms and Simulated Annealing, Morgan Kaufmann Publishers, San Mateo, CA, 1987, pp.61-73
64. K. Deb and M. Goyal, "A robust optimization procedure for mechanical component design based on genetic adaptive search", Transactions of the ASME: Journal of Mechanical Design, Vol. 120, No. 2, 1998, pp. 162-164
65. Mitsuo Gen and Runwei Cheng, "Algorithms & Engineering Design", Wiley-Interscience Publication, ISBN: 0-471-12741-8, 1996
66. R. M. Hicks and P. A. Henne, "Wing Design by Numerical Optimization", *Journal of Aircraft*, Vol. 15, 1978, pp. 407-412

67. O. Baysal and M. E. Eleshaky, “Aerodynamic Design Optimization Using Sensitivity Analysis and Computational Fluid Dynamics”, *AIAA Journal*, Vol. 30, No. 3, 1992, pp. 718725
68. J. J. Reuther and A. Jameson, “Supersonic Wing and Wing-body Shape Optimization Using An Adjoin Formulation”, Technical Report, The Forum on CFD for Design and Optimization, IMECE95, San Francisco, CA, Nov, 1995
69. M. F. Bramlette and R. Cusic, “A Comparative Evaluation of Search Methods Applied to the Parametric Design of Aircraft”, Proceedings of the Third International Conference on Genetic Algorithms, Morgan Kaufmann Publishers, San Mateo, CA 1989, pp. 213-218
70. I. C. Parmee and A. H. Watson, “Preliminary Airframe Design Using Co-Evolutionary Multi-objective Genetic Algorithms”, Proceedings of the Genetic and Evolutionary Computation Conference, Vol. 2, Morgan Kaufmann Publisher, San Mateo, CA 1999, pp. 1657 -1671
71. D. J. Powell, S. S. Tong and M. M. Sholbick, “EnGENEous Domain Independent, Machine Learning for Design Optimization”, Proceedings of the Third International Conference on Genetic Algorithms, Morgan Kaufmann Publishers, San Mateo, CA 1989, pp. 151-159
72. D. Quagliarella and A. D. Cioppa, “Genetic Algorithms Applied to the Aerodynamic Design of Transonic Airfoils”, AIAA Paper 1994-1896, June 1994
73. K. Yamamoto and O. Inoue, “Application of Genetic Algorithm to Aerodynamic Shape Optimization”, AIAA Paper 1995-1650, June 1995

74. S. Obayashi and A. Oyama, “Three-Dimensional Aerodynamic Optimization with Genetic Algorithms”, Proceedings of the Third ECCOMAS Computational Fluid Dynamics Conference, John Wiley & Sons, U.K., 1996, pp. 420-424

75. Terry L. Holst and Thomas H. Pulliam, “Aerodynamic Shape Optimization Using a Real-Number-Encoded Genetic Algorithm”, AIAA Paper 2001-2473, 2001

76. William H. Press, Saul A. Teukolsky, William T. Vetterling and Brian P. Flannery, “Golden Section Search in One Dimension”, *Numerical Recipes in Fortran*, Cambridge University Press, Second Edition, 1992, pp. 390-395

77. A. Oyama, S. Obayashi, K. Nakahashi, “Real-Coded Adaptive Range Genetic Algorithm and Its Application to Aerodynamic Design,” JSME International Journal, Series A, Vol. 43, No. 2, pp. 124-129, February 2000

78. William H. Press, Saul A. Teukolsky, William T. Vetterling and Brian P. Flannery, “Incomplete Gamma Function, Error Function, Chi-Square Probability Function, Cumulative Poisson Function”, *Numerical Recipes in Fortran*, Cambridge University Press, Second Edition, 1992, pp. 209-215

79. Y. B. Suzen, P. G. Huang, "Numerical Simulation of Wake Passing on Turbine Cascades", AIAA Paper 2003-1256, 41st Aerospace Sciences Meeting and Exhibit, January 2003

80. Y. B. Suzen, P.G. Huang, R. J. Volino, T. C. Corke, F. O. Thomas, J. Huang, J. P. Lake and P. I. King, “A Comprehensive CFD Study of Transitional Flows In Low-Pressure Turbines Under a Wide Range of Operation Conditions”, 33rd AIAA Fluid Dynamic Conference, AIAA Paper 2003-3591, June 2003

81. Y. B. Suzen and P. G. Huang, "Predictions of Separated and Transitional Boundary Layers Under Low-Pressure Turbine Airfoil Conditions Using an Intermittency Transport Equation", *Journal of Turbomachinery*, Vol. 125, No.3, July 2003, pp. 455-464

82. F. R. Menter, "Two-Equation Eddy-Viscosity Turbulence Models For Engineering Applications", *AIAA Journal*, Vol. 32, No. 8, August 1994, pp. 1598-1605

83. Bardina, J. E., P. G. Huang and T. J. Coakley, "Turbulence Modeling Validation, Testing and Development", NASA TM-110446, April 1997

84. K. B. M. Q. Zaman, D. J. McKinzie, and C. L. Rumsey, "A natural low-frequency oscillation of the flow over an airfoil near stalling conditions", *Journal of Fluid Mechanics*, Vol. 202, 1989, pp. 403-442

85. W. J. McCroskey, "A Critical Assessment Of Wind Tunnel Results For The NACA0012 Airfoil", NASA Technical Memorandum 100019, Ames Research Center, Moffett Field, CA, October 1987

86. L. Huang, P.G. Huang, R.P. LeBeau and Th. Hauser, "Numerical Study of Blowing and Suction Control Mechanism on NACA 0012 Airfoil", *Journal of Aircraft*, 2004 (In press)

Vita

The author was born on Nov 6, 1975 in Nanchang, JiangXi Province, P. R. China. He enrolled in Tsinghua University, Beijing, P.R. China, in September 1994 and received his Bachelor degree in Engineering from Tsinghua University in June 1998. After that, he continued his graduate studies at the graduate school of Tsinghua University and earned his Master degree in June 2000. Two months after graduation, he came to the United States to pursue his doctorate degree in the Department of Mechanical Engineering, University of Kentucky. The author had published 4 books and 3 conference and journal papers.

Liang Huang

April 28, 2004